# Mid-IR Supercontinuum Generation in Microstructured Optical Fibers

**Ph. D. Thesis**

Submitted by

**SANDEEP VYAS**
(College ID:- 2012REC9015)

Under Supervision of

**Dr. GHANSHYAM SINGH**
Associate Professor, Department of ECE, MNIT Jaipur

&

**Dr. MANISH TIWARI (External)**
Professor, Department of ECE, Manipal University Jaipur


**DEPARTMENT OF ELECTRONICS AND COMMUNICATION ENGINEERING**

**MALAVIYA NATIONAL INSTITUTE OF TECHNOLOGY JAIPUR**
**(JUNE, 2017)**

# Mid-IR Supercontinuum Generation in Microstructured Optical Fibers

**Ph. D. Thesis**

Submitted by

**SANDEEP VYAS**
(College ID:- 2012REC9015)

Under Supervision of

**Dr. GHANSHYAM SINGH**
Associate Professor, Department of ECE, MNIT Jaipur

&

**Dr. MANISH TIWARI (External)**
Professor, Department of ECE, Manipal University Jaipur

Submitted as a partial fulfillment of the degree of Doctor of Philosophy
in


**DEPARTMENT OF ELECTRONICS AND COMMUNICATION ENGINEERING**

**MALAVIYA NATIONAL INSTITUTE OF TECHNOLOGY JAIPUR**
**(JUNE, 2017)**

# Certificate

It is certified that:

- The thesis has not been submitted in part or full to any other University or Institute for award of any degree.
- I have fulfilled all the requirements for submission of the thesis.

SANDEEP VYAS
ID: 2012REC9015

This is to certify that the thesis entitled **"Mid-IR Supercontinuum Generation in Microstructured Optical Fibers"**, being submitted by **Sandeep Vyas** to the Department of Electronics and Communication Engineering, Malaviya National Institute of Technology, Jaipur, for the award of the degree of **Doctor of Philosophy**, is a bonafide research work carried out by him under my supervision and guidance. The results obtained in this thesis have not been submitted to any other university or institute for the award of any other Degree.

(Dr. Ghanshyam Singh)
**Associate Professor**
Department of ECE
Malaviya National Institute of Technology,
Jaipur.

(Dr. Manish Tiwari)
**Professor**
Department of ECE
Manipal University, Jaipur.

Thesis was examined and approved for award of degree of Doctor of Philosophy.

_____
_____
_____

External Examiner

# DECLARATION OF AUTHORSHIP

I, Sandeep Vyas, declare that this thesis titled, '**Mid-IR Supercontinuum Generation in Microstructured Optical Fibers**' and the work presented in it are my own. I confirm that:

- This work was done wholly or mainly while in candidature for a Ph.D. degree at MNIT.
- Where any part of this thesis has previously been submitted for a degree or any other qualification at MNIT Jaipur or any other institution, this has been clearly stated.
- Where I have consulted the published work of others, this is always clearly attributed.
- Where I have quoted from the work of others, the source is always given. With the exception of such quotations, this thesis is entirely my own work.
- I have acknowledged all main sources of help.
- Where the thesis is based on work done by myself jointly with others, I have made clear exactly what was done by others and what I have contributed myself.

Signed:_____

Date:_____

# Acknowledgement

My long journey in obtaining my doctorate degree in Electronics and Communication Engineering comes to an end with the completion of this thesis. It is an outcome of several years of work, survey, reading, understanding and bewilderment. This thesis would not have come out in its present form without the kind help and support of the following individuals and organizations. Hence, to extend my appreciation and gratitude, I take up this opportunity to recognize and acknowledge all the people who have help me in some way or other throughout the research work that has made this thesis possible.

First and foremost, I thank my Ph.D. supervisors, **Dr. Ghanshyam Singh** and **Dr. Manish Tiwari** for granting me opportunity to work in the area which had always motivated me to pursue my research. I could not have ever imagined having a better supervisors, advisors and mentors for my Ph.D., and without their knowledge, vision and problem-solving attitude, I would never have concluded my thesis.

It is difficult for me to express my heartfelt gratitude to my guide **Dr. Ghanshyam Singh**. He has always been an everlasting source of motivation, encouragement, advice, learning and ideas. I would have reached nowhere without his guidance. He always provided his timely, invaluable comments whenever they were most needed.

I am also grateful to my co supervisor **Dr. Manish Tiwari** who has been always present in every way as a resource, be it scholarly, administratively, socially or emotionally. I owe gratitude to him for his remarkable patience to put me back on track whenever I was confused.

I would also like to thank other faculty members at MNIT Jaipur for their kind support, especially Dr. K.K. Sharma, Head of the ECE Department, Dr. Vijay Janyani, Dr. Ritu Sharma, Dr. Ravi Maddila and faculty fraternity of the department.

During my research work, I was fortunate enough to be associated with INDIA–JAPAN COOPERATIVE SCIENCE PROGRAMME awarded jointly to MNIT Jaipur and KEIO University, Hiyoshi Campus, Japan (Project sanction number: DST/INT/JSPS/P-180/2014). I am gratefull to **Dr. Takasumi Tanabe** and Dr. Ghanshyam Singh who give me opportunity to work in this project. Dr. Takasumi

Tanabe, Department of EEE, Keio University, Keio, Japan was always a great support with his valuable expertise.

I am indebted to Ms. Shruti Kalra, Mr. Mukesh Gupta, Mr. Sourabh Sahu and Mr. Vinay Kanungo for their great support, guidance and fruitful discussions during my thesis work.

Lastly, and most importantly, I extend my gratitude to my parents especially my father Sh. Ramesh Chandra Vyas who raised me, taught me, supported me and loved me. He always motivated me to take admission in Ph.D. programme. I am heartly indebted to my mother Smt. Krishna Vyas who has always been understanding, encouraging, loving, caring and supporting since my birth and helped me in overcoming through bad times. I am forever indebted to my parents for their understanding, endless patience and encouragement when it was most required. I dedicate this thesis to my parents.

Last, but not the least, I specially thank my wife Babita for always being so understanding, caring, helping, supporting and loving. I thank my loving daughters Saumya and Trisha for all their love and care.

(**Sandeep Vyas)**

# Abstract

This Ph.D.-project presents the numerical simulations of supercontinuum generation (SCG) in microstructured optical fiber based on $Ge_{11.5}As_{24}Se_{64.5}$ chalcogenide (ChG) material and $As_2S_3$ based multi-material photonic crystal fiber structure. To achieve supercontinumm generation in microstuctured optical fiber we thoroughly studied and developed understanding about the characteristics and parameters responsible for supercontinuum generation. The methods and numerical simulations were understood, practised and carried out with finite-difference-time-domain (FDTD) method and split-step Fourier method (SSFM) in order to understand and characterize the generated supercontinuum (SC) in the photonic crystal fibers. With rigorous literature survey we shortlisted designs matching our interest. The selected designs were verified and further optimized for higher nonlinearity, minimized effective area, and anomalous dispersion curve to generate a broad spectra supercontinuum with low input power. The design parameters and dispersion of different $Ge_{11.5}As_{24}Se_{64.5}$ based chalcogenide microstructured optical fibers were tailored to identify the most promising design that can be employed for spanning supercontinuum up to 15 $\mu$m bandwidth pumped at 3.1 $\mu$m with the low input peak power of 3 kW. After obtaining satisfactory results with $Ge_{11.5}As_{24}Se_{64.5}$ based design, we investigated multi-material photonic crystal fibers for supercontinuum generation. In the proposed multi-material design, $As_2S_3$ based photonic crystal fiber doped with borosilicate glass was investigated to generate supercontinuum. The dispersion tailored design resulted a flat anomalous dispersion curve with two zero dispersion wavelength (ZDW) at 2.27 µm and 3.3 µm. Supercontinuum spectra ranging from 1.6 µm to 4.2 µm was observed with pump energy of 350 W at wavelength 2.5 µm. The satisfactory results motivated us to explore new potential materials in Chalcogenide group for supercontinuum generation. With this idea lithium ternary compounds chalcogenide PCFs such as $LiGaSe_2$, $LiGaS_2$ and LiGISe ($LiGa_{0.5}In_{0.5}Se_2$) were carefully investigated in our research work. The desired dispersion curves for generation of supercontinuum were observed with lithium ternary compounds. These results motivate us to continue our research in this new avenue in future.

**List of figures**

**List of tables**

**List of Acronyms**

| | |
|---|---|
| **ChG** | chalcogenide |
| **CW** | continues wave |
| **DWDM** | density diversion division multiplexing |
| **EDFA** | erbium doped fiber amplifier |
| **EM** | electromagnetic |
| **ES** | equiangular spiral |
| **FCA** | free-carrier absorption |
| **FDTD** | finite-difference time-domain |
| **FFT** | fast Fourier transform |
| **FT** | fourier transform |
| **FWHM** | full-width-at-half-maximum |
| **FWM** | four-wave mixing |
| **GNLSE** | generalized nonlinear Shrödinger equation |
| **GVD** | group-velocity dispersion |
| **HOD** | higher order dispersion |
| **IFFT** | inverse fast Fourier transform |
| **IR** | infrared |
| **MCN** | mean coordination number |
| **MF** | microstructured fiber |
| **MI** | modulation instability |
| **MIR** | mid-infrared |
| **MPB** | MIT Photonic-Bands |
| **NIR** | near infrared |

| | |
|---|---|
| **NSR** | nonsolitonic radiation |
| **OCT** | optical coherence tomography |
| **PBG** | photonic bandgap |
| **PCF** | photonic crystal fiber |
| **SC** | supercontinuum |
| **SCG** | supercontinuum generation |
| **S** | sulphur |
| **SBS** | stimulated Brillouin scattering |
| **Se** | selenium |
| **Si** | silicon |
| **SS** | self-steepening |
| **SIF** | step-index fiber |
| **SOI** | silicon-on-insulator |
| **SPM** | self-phase modulation |
| **SRS** | stimulated Raman scattering |
| **SSFM** | split-step Fourier method |
| **SSFS** | soliton self-frequency shift |
| **TC** | triangular core |
| **THG** | third-harmonic generation |
| **TOD** | third-order dispersion |
| **TPA** | two-photon absorption |
| **UV** | ultraviolet |
| **XPM** | cross-phase modulation |
| **ZBLAN** | ZrF4 BaF2 LaF3 AlF3 NaF |
| **ZDW** | zero-dispersion wavelength |

**List of Symbols**

| | |
|---|---|
| $A_{eff}$ | effective mode area |
| $\beta$ | propagation constant |
| $\beta_m$ | higher-order dispersion parameter |
| $C$ | velocity of light in vacuum |
| $K$ | wavenumber |
| $n_{eff}$ | effective mode index |
| $T_g$ | transition temperatures |
| E | permittivity |
| $\Lambda$ | wavelength |
| $\mu_o$ | vacuum permeability |
| $\phi_{NL}$ | nonlinear phase shift |
| X | nonlinear susceptibility |
| $\Omega$ | angular frequency |
| $\omega_p$ | pump frequency |
| $\omega_o$ | central frequency |
| $n_2$ | nonlinear refractive index |
| A | linear propagation loss |
| $h_R(t)$ | temporal Raman response |
| $D$ | air-hole diameter |
| $\Lambda$ | pitch |
| $v_g$ | group velocity |
| **P** | polarization |

| | |
|---|---|
| **B** | magnetic flux density |
| **D** | electric flux density |
| **H** | magnetic field intensity |
| **E** | electric field intensity |
| **Jf** | electric current density |
| **M** | magnetization |
| P | dielectric charge density |
| *P* | penalty factor |
| Γ | nonlinear coefficient |
| L | waveguide length |
| $P_0$ | input power |
| $P_T$ | transmitted power |

## Motivation & Thesis layout

The research described in this thesis concerns Mid-infrared (MIR) supercontinuum generation (SCG). Supercontinuum generation that deals with non-linear effects of the optical fiber has been an area of significant interest for past 20 years. Supercontinuum (SC) is an optical source with special features such as large bandwidth, high brightness and high coherence. While the optical pulses propagating through a highly non-linear fiber, their temporal and spectral escalation are influenced not only because of the predominance of non-linear effects, but also because of the dispersive properties of optical fiber. Each non-linear process is responsible for generating new frequencies in the spectrum of pulses [1]. With sufficiently intense pulse, the spectrum becomes enormous broader. It can extend over a range of frequencies more than 100 THz [2]. Supercontinuum is a phenomenon due to which the pulse undergoes a extreme broadening and it was in 1970, when Alfano and Shapiro firstly reported SC generation in the bulk BK7 glass [3]. Later in 2000 Ranka *et al.* [5] achieved spectral spreading more than one octave in a newly invented photonic crystal fiber (PCF) [4]. Later in the MIR region different types of photonic crystal fibers [6] [7] [8], tapered fibers [9] [10] [11] and planar waveguides [12] have shown enormous potential as supercontinuum light sources. SC light source finds their applications in various different fields like telecommunication bio-imaging, spectroscopy, optical sensing, pulse compression and OCT (optical coherence tomography)[13]. All these applications are the strong motivation to design a photonic crystal fiber to achieve the broadber spectrum in MIR. The highly nonlinear microstructured fiber (MF) or photonic crystal fiber incorporation with the mode-locked laser is employed to generate a broad spectrum called supercontinuum generation. The concept of SCG in MOFs/PCFs is presented by various researchers. The efficient supercontinuum generation is communal interplay of multitudinous nonlinear effects namely self-phase modulation (SPM), cross-phase modulation (XPM), soliton dynamics, Raman scattering, and four-wave mixing (FWM). In addition to nonlinear effects the photonic crystal fiber design has to be tailored to obtain zero-dispersion wavelength (ZDW) close to the central wavelength of the pump sources along with appropriate group

velocity dispersion (GVD) to obtain supercontinuum generation as desired [14] [15] [16].

Initially, researchers focused on fused silica PCFs for supercontinuum generation from ultra-violet to mid-infrared region.The escalation of supercontinuum generation beyond 2.5 μm is a challenging task with fused silica due to its intrinsic transmission window [17]. In view of this limitation researchers successively have move to other types of materials which can offer transmission windows transparency in the region of longer wavelengths. To achieve supercontinuum expansion beyond 2.5 μm, other nonlinear materials such as ZBLAN, tellurite, and chalcogenide (ChG) have been investigated by researchers. Silicon (Si) has good Kerr nonlinearity and its desirable material for SCG using silicon-on-insulator (SOI) nanowires [18]. However, silicon is the lowest loss material in near infrared (NIR) but it has few drawbacks to be used in the telecommunication field. In existing telecommunication system where operating band is centered at 1.55 μm using silica fiber, its functioning is limited mainly due to absorption. The two-photon and free-carrier absorption becomes significant at 1.55 μm and due to which the spectral broadening of supercontinuum is clamped, limiting the expected bandwidth [19]. The heavy metal fluoride based fibers (ZBLAN) exhibits almost similar nonlinear properties like silica though tellurite has nonlinearity approximately 30 times higher than silica. Further the chalcogenide can offer thousand times higher nonlinearity than silica [20].

In last few decades chalcogenide materials have emerged as promising nonlinear glasses for the MIR region escalation from 1 to 20 μm. Chalcogenide glasses have several incomparable properties making them preferable and suitable for fabricating optical fibers, with low nonlinear absorption, low two-photon absorption, without free-carrier absorption and fast response time due to the absence of free-carrier effects [21] [22] [23] [24]. Chalcogenide glasses are composite material consisting of one or more chalcogen elements (S, Se, Te excluding Oxygen) from group 16 of the periodic table covalently bonded with As, P, Ga, Sb, Si and Ge etc. Its composition has comparatively weak bond with heavy elements makes them identical with special optical and physical properties. The weak energy bond is responsible for optical gaps in the visible and the near infrared along with less energy to *Tg*, moderate glass transition temperatures which varies from 100°C to 400°C. The optical transparency is expanded to near about 8 micron for sulphides, more than 14 micron for selenides and above 20 micron for tellurites due to low vibrational energies of the bonds.

Chalcogenide glasses have high refractive index in range of 2 to 3, wide transparency ranging from 1 to 20 micron making them the best choice for the waveguide fabrication for their application in the area of optical sensing, telecommunications, and mid-infrared sciences [25] [26]. Another advantage with ChG glasses is its third-order high ultrafast nonlinearity. The ChG glasses are immensely suitable for designing both active and passive compact devices for nonlinear applications in mid-infrared regime [27] [28]. $As_2S_3$, $As_2Se_3$, $Ge_{11.5}As_{24}S_{64.5}$ and $Ge_{11.5}As_{24}Se_{64.5}$ chalcogenide glasses are example of most suitable material for making MIR region applications devices. Among all the $Ge_{11.5}As_{24}Se_{64.5}$ glass has high optical and thermal stability under intense illumination along with excellent film-forming properties [29]. All these significant and remarkable properties of $Ge_{11.5}As_{24}Se_{64.5}$ chalcogenide glass attracted researchers to design a photonic crystal fiber for mid-infrared supercontinuum generation. A broad SC can be achieved by tailoring dispersion of the PCF close to the zero-dispersion wavelength which should be close to the pump sources central wavelength.

The work presented in this dissertation is inspired by the requisite to investigate theoretical fundamentals of PCFs and optimitize the designs for SCG in the mid-infrared region by employing the nonlinear and dispersive properties of the PCFs. We have rigorously analysed and optimized the design of photonic crystal fibers. Here, we have used finite-difference time-domain (FDTD) method for numerical modelling. The study of supercontinuum generation in the fiber was carried out by simulations. Thus spilt-step Fourier method was used to solve generalized non-linear Schrodinger equation (GNLSE) for an optical pulse escalation along the length of the fiber. We have methodically and carefully analysed supercontinuum with $Ge_{11.5}As_{24}Se_{64.5}$ chalcogenide glasses in the mid-infrared region by rigorous numerical simulations through dispersion tailoring of the PCFs.

The anothology of the thesis is hereunder:

Chapter 1 introduces detailed concepts of nonlinear optics and expounds the several important linear and nonlinear spectral escalation procedures which are responsible for the generation of supercontinuum spectra. The evolution of optical signal inside a fiber can be modelled by the Maxwell's equation and pulse propagation along the fiber length is modelled with generalized nonlinear Schrödinger equation (GNLSE) which helps understanding the process.In waveguides propagation loss and dispersion are incurred due to linear effects and the nonlinear effects helps generating

processes like SPM, soliton dynamics, XPM, FWM, stimulated Raman scattering (SRS). All these phenomena are discussed in detail.

Chapter 2 gives the overview of the two numerical methods applied in this research work. The first one is finite-difference time-domain (FDTD) method which is used to simulate the light guidance in the waveguide. Another one is the split-step Fourier method (SSFM), used for SCG numerical calculation by GNLSE equation using SSFM. Both the methods are explained as per their role in simulations realted to our research work.

Chapter 3 discusses the fundamentals of SCG in the starting. With research and developments with time SC has emerged as one of the most promising research field. With published research work on SC we have made an attempt to describe different nonlinear materials which can be used to design optical fibers and waveguides as a SC source. There are enormous possibilities of research in this field as there are variety of optical fiber, waveguides with different feasible designs and different materials. Further the careful selection of design and material for a optical fiber and waveguide is helpful in potential applications in diverse fields. There are enormous applications, but few important applications are discussed for our understanding.

Chapter 4 presents the results of the supercontinuum generation in chalcogenide photonic crystal fibers with delve investigation. Here, we investigated different geometries of $Ge_{11.5}As_{24}Se_{64.5}$ chalcogenide glasses PCFs and tailored the dispersion curve according to the requirement of efficient SCG by FDTD method. With the help of varying pitch, air hole diameter in hexagonal photonic crystal fiber dispersion curves were optimized. In this chapter supercontinuum calculations have been made, including the higher dispersion coefficient along with other pulse parameter for each proposed PCF. We have demonstrated an increase in SC bandwidth in the MID-infrared region by changing design parameter of PCF.

Chapter 5 demonstrates a improved design for supercontinuum generation. Here we are using multi-material photonic crystal fiber to have better control of refractive index and dispersion characteristics. With the help of two different materials and the perfect combination of air-holes geometry we have achieved a mid-IR supercontinuum. Here, $As_2S_3$ is used as background material and few air-holes in hexagonal PCF structure have been replaced by the borosilicate glass rod helping us to create some unique properties.

Chapter 6 try to explore new materials for future work of supercontinuum generation with improved results. Here, we introduced a new Li-containing ternary compounds chalcogenide material for mid-IR supercontinuum generation. We have tailored dispersion curve according to our requirement by carefully choosing the dimensions of air holes and pitch.

At last in Chapter 7 we concluded the thesis and have summarised all results with discussion and possibilities for the future work.

# Chapter 1

**Nonlinear Fiber Optics**

The medium in which the electromagnetic wave propagates plays a vital role in its propagation. The pulse remains unchanged during its propagation in the vacuum. The pulse traversing through the medium experiences loss and dispersion due its interaction with the atoms of the medium. In a medium with linear response, these effects are incurred due to the pulse travelling with different velocities and the wavelengths being function of the refractive index of the medium. With the high intensity of the pulse the medium depicts a nonlinear response. The nonlinear response at high intensity is mainly due to Kerr effect, where the photons interact with phonons due to high molecular vibrations. In the case of linear optics, the signal can be attenuated or amplified keeping frequency unchanged. In the nonlinear optics, the spectrum of the laser pulse undergoes different reforms with generation of new frequencies while propagating along the fiber length. Such phenomenon was first time reported by Alfano and Shapiro in 1970 in bulk BK7 glass where the spectral change is referred to as SCG [30]. The spectral broadening is depending on several effects which will be discussed farther in this chapter.

This chapter gives an overview of basic concept to perceive the simulation work done and results presented in the thesis. The Section 1.1 covers the review of fundamental equations used for modelling pulse propagation in the fiber, like generalized nonlinear Schrödinger equation (GNLSE) and Maxwell's equations. In Section 1.2 we explain the linear effects occurring during pulse propagation in the fiber. Section 1.3 introduces several mechanisms responsible for spectral broadening and SCG at the fiber output.

## 1.1 Wave propagation in optical fiber

For understanding the nonlinear effects in supercontinuum generation, firstly we review the concepts of electromagnetic wave propagating in the fiber. In this section we also review the Maxwell's equations used in derivation of wave equation along with nonlinear pulse propagation equation.

### 1.1.1 Maxwell's equations

The Maxwell's equations are used to express the propagation of electromagnetic fields in the optical fiber. The interaction between electric and magnetic fields varying in space is expressed in time-dependent manner using these equations.The generalized Maxwell's equations for the homogeneous, lossless dielectric medium are expressed as [31].

$$\nabla \times \mathbf{E} = -\frac{\partial \mathrm{B}}{\partial \mathrm{t}} \tag{1.1}$$

$$\nabla \times \mathbf{H} = -\frac{\partial \mathrm{D}}{\partial \mathrm{t}} + \mathbf{J}_f \tag{1.2}$$

$$\nabla . \mathbf{D} = \rho \tag{1.3}$$

$$\nabla . \mathbf{B} = 0 \tag{1.4}$$

Where, **E** denotes the electric field, **H** denotes the magnetic field, **D** denotes the electric field displacement, **B** denotes the magnetic flux density, $\mathbf{J}_f$ denotes the current density, and **ρ** denotes the density of free charges. The electromagnetic fields in the underlined equations are suitable for arbitrary media and related by the under mentioned macroscopic equations

$$\mathbf{D} = \varepsilon_o \mathbf{E} + \mathbf{P} \tag{1.5}$$

$$\mathbf{B} = \mu_o \mathbf{H} + \mathbf{M} \tag{1.6}$$

Where, $\varepsilon_o$ denotes the vacuum permittivity, $\mu_o$ denotes the vacuum permeability, P denotes electric polarization, and **M** denotes magnetization.

**Boundary conditions**

Firstly Equations (1.1) to (1.4) are solved for optical media. Optical medium generally has one or more materials forming different number of boundaries between the different media. To obtain continuity of electric field and magnetic field inside the

fiber it is necessary to include the proper boundary conditions. Since the fibers with a dielectric medium do not conduct current and depict no magnetism, **M** = **J** = 0 further the surface charges is assumed as $\rho = 0$.

1) Tangential integrant of the electric field is

$$n \times (\mathbf{E}_1 - \mathbf{E}_2) = 0 \qquad \therefore \ \mathbf{E}_{t1} = \mathbf{E}_{t2} \tag{1.7}$$

2) Tangential integrant of the magnetic field is

$$n \times (\mathbf{H}_1 - \mathbf{H}_2) = 0 \qquad \therefore \ \mathbf{H}_{t1} = \mathbf{H}_{t2} \tag{1.8}$$

3) Normal integrant of the electric flux density is

$$n.(\mathbf{D}_1 - \mathbf{D}_2) = 0 \qquad \therefore \ \mathbf{D}_{n1} = \mathbf{D}_{n2} \tag{1.9}$$

$$\therefore \ \varepsilon_1 \mathbf{E}_{n1} = \varepsilon_2 \mathbf{E}_{n2} \Rightarrow \mathbf{E}_{n1} \neq \mathbf{E}_{n2} \tag{1.10}$$

where, medium one and two permittivity is $\varepsilon_1$ and $\varepsilon_2$, here $\varepsilon 1 \neq \varepsilon 2$

4) Normal integrant of the magnetic flux density is

$$\mathbf{n}.(\mathbf{B}_1 - \mathbf{B}_2) = 0 \qquad \therefore \ \mathbf{B}_{n1} = \mathbf{B}_{n2} \qquad \therefore \ \mu_1 \mathbf{H}_{n1} = \mu_2 \mathbf{H}_{n2} \tag{1.11}$$

where, medium one and two relative permeability is $\mu_1$ and $\mu_2$, here $\mu_1 = \mu_2 = 1$

$$\therefore \ \mathbf{H}_{n1} = \mathbf{H}_{n2} \tag{1.12}$$

The symmetry of the magnetic field vectors of normal component at the boundary is expressed by the above equation (1.12).

In some conditions out of two media one is considered as a perfect electric or magnetic conductor. With an assumption that one of the media to be a perfect electric conductor, the transformed boundary condition is expressed below

$$\mathbf{n} \times \mathbf{E} = 0 \qquad \text{or} \qquad \mathbf{n}.\mathbf{H} = 0 \tag{1.13}$$

The case above ascertains that the electric field vector (E) expresses continuity while the magnetic field vector (H) vanishes at the wall boundary.

In the condition that one of the two media is a perfect electric conductor the transformed boundary condition can be expressed as underlined

$$\mathbf{n} \times \mathbf{H} = 0 \qquad \text{or} \qquad \mathbf{n}.\mathbf{E} = 0 \tag{1.14}$$

In this case the continuity at the boundary both of the electric field vector (E) and the magnetic field vector (H) disappear.

If the close surface is under consideration then additional boundary conditions are taken into account. The natural boundary conditions can be ignored as in this case the field decays at the boundary. Instead of natural conditions we can have forced boundary conditions, which take the advantage of fiber symmetry to minimize elements in FDTD method. Above mentioned boundary conditions can be symbolized as underneath [32].

Homogenous Dirichlet $\qquad ø = 0 \qquad (1.15)$

Inhomogenous Dirichlet $\qquad ø = k \qquad (1.16)$

Homogenous Neumann $\qquad {\partial ø}/{\partial \mathbf{n}} = 0 \qquad (1.17)$

Here, ø represents the specific component of the electric/magnetic field vector, unit vector normal to the surface is denoted by n and *k* is a constant.

On using the curl operator both the part of Equations (1.1 & 1.2) and putting Equations (1.5 & 1.6) in the final result, following equations are achieved.

$$\nabla^2 \mathrm{E} = \varepsilon_o \mu \frac{\partial^2 \mathrm{E}}{\partial t^2} + \mu \frac{\partial^2 \mathrm{P}}{\partial t^2} \tag{1.18}$$

$$\nabla^2 \mathrm{H} = \varepsilon\mu \frac{\partial^2 \mathrm{H}}{\partial t^2} \tag{1.19}$$

On neglecting all higher order nonlinearity susceptibility, linear susceptibility $\chi^{(1)}$ dominates and relates to the electric polarization (P) along with the electric field (E) as follows [2]

$$P = (\chi^{(1)}.E) \tag{1.20}$$

The frequency doamin expressions for Equations (1.18 & 1.19) can be obtained by replacing the time derivative $\partial/\partial \mathbf{t}$ by $j\omega$ and can be illustrated as follows

$$\nabla^2 E + \omega^2 \varepsilon \mu E = 0 \tag{1.21}$$

$$\nabla^2 H + \omega^2 \varepsilon \mu H = 0 \tag{1.22}$$

The above equations (1.21 & 1.22) are analogous depicting the scalar wave equation of electric and magnetic components of electromagnetic field. In solutions of the equations the field components are orthogonal and dissociated with each other, due to this condition the longitudinal components can be ignored. On the fulfilment of of these conditions every orthogonal component of the field can be used to study the evolution of one component as each of them satisfies the scalar wave equation separately. The numerical analysis for modal solution will be explored in detail later in Chapter 2.

### 1.1.2 Equations for nonlinear pulse propagation

The linear effects generated from the motion of bounded electrons in the material that are proportional to the applied field but this concept is applicable to low-intensity light. In the case of high-intensity light sources like ultra-short laser pulse, the material depicts a nonlinear behaviour, as the electron displacement is no longer proportional to the optical field. This phenomenon is responsible for the generation of new frequencies and is called nonlinear optics.

This chapter gives a description of nonlinear effects, focusing on the nonlinear optics involved in supercontinuum generation. In general Supercontinuum generation is a collection of many nonlinear effects appearing simultaneously.

A linearly polarised pulse with reference to x- axis propagating in fundamental mode in an optical fiber is examined, and then the electric field of the pulse can be represented as [2]

$$\boldsymbol{E}_A(\boldsymbol{r},t) = \hat{x}F(x,y)A(z,t)\exp[j(\beta_0 z - \omega_0 t)] \tag{1.23}$$

In above expression r = (*x*, *y*, *z*), $\hat{x}$ denotes the polarisation unit vector in x axis direction, the pulse envelope is represented by *A*(*z*, *t*), *F*(*x*, *y*) is the transverse field distribution, and $\beta_0$ is the mode propagation constant of $\beta(\omega)$ with the pulse operating at the centre angular frequency $\omega_0$ . $\boldsymbol{E}_A$ is the electric field $\boldsymbol{E}$ [V/m] here $\boldsymbol{E}_A = \sqrt{\frac{1}{2}\,\varepsilon_0 cnE}$ where *c* is light speed in vacuum, n is the refractive index of the medium and $\varepsilon_0$ is the permittivity in vacuum. Generalised nonlinear Schrödinger equation (GNLSE) is used to study the changes in pulse envelope (*A*) during pulse propagation along the fiber length in z-axis [2]

$$\frac{\partial A}{\partial z} = -\frac{\alpha(\omega)}{2}A + \sum_{m\geq 2}\frac{\beta_m}{m!}[\omega-\omega_0]^m A + j\gamma(\omega)\left(1+\frac{\omega-\omega_0}{\omega_0}\right)\times \mathfrak{F}\left(A(z,T)\int_{-\infty}^{\infty}R(T)|A(z,T-T')|^2 dT'\right) \tag{1.24}$$

In the above equation the $\mathfrak{F}$ represents the Fourier transform (FT), also the Fourier Transform of *A*(*z*, *t*) is *A*(z,ω) and can be expressed as below

$$\mathfrak{F}\{A(z,t)\} = A(z,\omega) = \int_{-\infty}^{\infty} A(z,t)\exp[j(\omega-\omega_0)t]\,dt \tag{1.25}$$

*A*(*z*,*T*) is the envelope of the pulse moving along the group velocity $1/\beta_1$ at the carrier frequency is analysed in a retarded time frame $T = t - \beta_1 z$ .The dispersion coefficients $\beta_2$, $\beta_3$, $\beta_4$ ....., are defined by the Taylor series expansion of the mode propagation constant (ω) [2]

$$(\omega) = \beta_0 + \beta_1(\omega-\omega_0) + 1/2\,\beta_2(\omega-\omega_0)^2 + 1/6\,\beta_3\,(\omega-\omega_0)^3 + \ldots\ldots \tag{1.26}$$

where

$$\beta_m(\omega_0) = \left(\frac{d^m}{d\omega_m}\right)_{\omega=\omega_0} \qquad m = 0,1,2,3.... \tag{1.27}$$

In equation (1.24) includes both linear and nonlinear propagation loss, where α(ω) denotes the linear propagation loss and the nonlinear parameter can be expressed as $\gamma(\omega)= n_2\omega_0/[cA_{eff}(\omega)]$, and $A_{eff}$ is the effective mode area as expressed below [2]

$$A_{eff}(\omega) = \frac{\left[\iint_{-\infty}^{\infty}|F(x,y,\omega)|^2 dxdy\right]^2}{\iint_{-\infty}^{\infty}|F(x,y,\omega)|^4 dxdy} \tag{1.28}$$

The smaller value of $A_{eff}$ is responsible for enhancing the nonlinearity when the value of $A_{eff}$ is decreased significantly nonlinear parameter (γ) is increased due to the tight confinement of the field in the central core region.

The intensity dependence of the group velocity results in self-steepening effect expressed as the component $\left[1 + \frac{\omega-\omega_0}{\omega_0}\right]$ in the Equation (1.24) [2].

On neglecting linear propagation loss and frequency dependence of nonlinear components, the propagation Equation (1.24) in the time domain is expressed as follows [2]

$$\frac{\partial}{\partial z}A(z,T) = -\frac{\alpha}{2} + \sum_{m\geq 2}\frac{j^{m+1}}{m!}\beta_m\frac{\partial^m A}{\partial T^m} + j\left(\gamma + j\frac{\alpha_2}{2A_{eff}}\right)\left(1 + \frac{j}{\omega_0}\frac{\partial}{\partial T}\right)\times$$
$$\left(A(z,T)\int_{-\infty}^{\infty}R(T)\left|A(z,T-T'\right|^2 dT'\right) \tag{1.29}$$

The Raman response function of material including the instantaneous electronic and vibrational Raman contributions is described by [2]

$$R(t) = (1 - f_r)\delta(t) + f_r h_R(t) \tag{1.30}$$

As we know that the optical properties of the chalcogenide materials are governed by the photoinduced effects namely photodarkening and photoinduced anisotropy. Thereby, the response time and third order susceptibility ($\chi^{(3)}$) change [33]. The temporal Raman response ($h_R(t)$) depends on the Raman gain spectrum and can be expressed as [34]

$$g_R(f) = \frac{2\omega_p}{c} n_2 f_r Im[H_R(f)] \tag{1.31}$$

where pump frequency is $\omega_p$, $Im[H_R(f)]$ is imaginary part of the Fourier transform of $h_R(t)$ [35], $h_R(t)$is calculated as

$$h_R(t) = \frac{\tau_1^2 + \tau_2^2}{\tau_1 \tau_2^2} \exp\left(-\frac{t}{\tau_2}\right) \sin\left(\frac{t}{\tau_1}\right) \tag{1.32}$$

where, $\tau_1$= 15.5 fs and $\tau_2$ = 230.5 fs for $Ge_{11.5}As_{24}Se_{64.5}$ based glasses. These values are selected as they provide a good fit with the lorentzian spectral profile. We can calculate fraction $f_r$ by *Kramers-Kroning* relation [34].The calculated value is 0.031 [35]. *Kramers-Kroning* relation can be expressed as

$$f_r = \frac{\lambda}{2\pi^2 n_2} \int_0^\infty \frac{g_R(f)}{f} df \tag{1.33}$$

## 1.2 Linear effects in optical fibers

This section gives a brief overview of various physical linear effects that appear within the optical fiber as the light propagates along the fiber length.

### 1.2.1 Losses

As the wave propagates through the fiber length it undergoes various changes due to various factors. One of the important waveguide parameter is losses (attenuation). It is a measure of power loss of a signal as it transverses along the length and is expressed as

$$\alpha\left[\frac{dB}{m}\right] = -\frac{10}{L}\log_{10}\left(\frac{P_T}{P_0}\right) \tag{1.34}$$

where, $P_0$ denotes the power launched at the input, $L$ denotes fiber length and $P_T$ denotes the transmitted power.

In the standard waveguide spectra loss mainly depends on material absorption and Rayleigh scattering [2]. On use of photonic crystal fiber the additional losses incurred are mainly bend loss and confinement loss [36] [37]. The finite number of air holes in the cladding of photonic crystal fiber makes guided mode as leaky modes

resulting in confinement losses [38]. The ratio between the diameter of the air holes and the pitch (Λ) for the particular design of the photonic crystal fiber determines the amount of light escaping from the center of the core to the cladding. The lower values of the ratio lead to increased losses. The confinement loss depends on the geometry of the photonic crystal fiber. It has been observed that with increase in number of rings in fiber, the losses can be reduced with improvement in mode confinement in PCF .The confinement loss can also be reduced by including an additional ring of air holes during the design of the photonic crystal fiber. The confinement loss can be controlled and also minimised with careful design of PCF.

The bend loss is due to the bends and curves in the waveguide. It occurs when the internal light signal travelling in the fiber makes the angle greater than the critical angle for total internal reflection depending on the wavelength [39]. The bending in photonic crystal fiber are broadly classified as macro and micro bending. Among these two macro-bending is large scale bending and can be observed with the naked eye when the bend is obtruded on the optical fiber. The area under strain in the fiber influences both acceptance angle and refractive index of the optical ray. Micro-bending is too small to be seen with the naked eye and occurs when pressure is applied to the surface of a microstructure fiber. The applied pressure results in the deformation of the core and cladding interface. Micro-bending affects the index of refraction and thus the optical ray is refracted out from the fiber resulting in the loss [38].

### 1.2.2 Dispersion

Dispersion is the phenomenon in which light wave propagating along the length of the fiber spreads. The dispersion originates due to the frequency dependence of the refractive index of the dielectric medium. Sometimes it's called "chromatic dispersion" in order to differentiate it from intermodal dispersion or polarisation mode dispersion. As per basic principle, the chromatic dispersion is related to frequency and material absorption. To elaborate the evolution of dispersion, the absorption of electromagnetic radiations due to oscillations of bound electrons are absorbed by the material at characteristic resonance frequency. The sellmeier equation is used to well estimate refractive index for medium resonances.

The dispersion has a vital role in the propagation of short optical pulses because the pulse consists of various spectral components travelling at different velocities.

Even that time, non-linear effects are not significant, dispersion induced spreading of optical pulses can be pernicious for the optical communication system. In the case of the non-linear regime, the combination of dispersion and non-linearity can lead to qualitatively different behaviour. The central frequency ($\omega_0$) of the pulse with respect to the extension of a Taylor series in the mode propagation constant ($\beta$) effects and dispersion are expressed in mathematical terms

$$\beta(\omega) = n_{eff}\frac{\omega}{c} = \beta_0 + \beta_1(\omega-\omega_0) + \frac{1}{2}\beta_2(\omega-\omega_0)^2 + \frac{1}{6}\beta_3(\omega-\omega_0)^3 + \cdots \quad (1.35)$$

and

$$\beta_m = \left(\frac{d^m\beta}{d\omega_m}\right)_{\omega=\omega_0} \qquad m = 0,1,2,3... \quad (1.36)$$

here, the $\beta_1 = 1/v_g$ is the envelope of the pulse moves at group velocity ($v_g$), $\beta_2$ denotes the group velocity dispersion (GVD). The GVD is responsible for the spreading of the pulse, while the third order dispersion coefficient (TOD) is denoted by $\beta_3$. Usually it is more convenient to work in the frequency domain. The dispersion for a pulse can be related to group velocity dispersion and propagation constant ($\beta_2$) as

$$D[\text{ps/nm/km}] = \frac{d\beta_1}{d\lambda} = -\frac{2\pi c}{\lambda}\beta_2 = -\frac{\lambda}{c}\frac{d^2n}{d\lambda^2} \quad (1.37)$$

The nonlinear effects depending on the group velocity dispersion can reveal qualitatively different behaviour in the fiber. The sign of dispersion parameter D has a great significance, if the sign is negative ($\beta_2 > 0$) the dispersion lies in normal region and the red components of pulse travels faster than the blue component of the pulse resulting in positive chirp. Accordingly if the sign is positive ($\beta_2 < 0$), dispersion falls in anomalous region and in this situation the blue components of the pulse travel faster than the red components resulting in negative chirp. In case the dispersion parameter D = 0, the zero dispersion wavelength corresponds to the same speed (minimum order) to travel on all pulse frequency components and the pulse retains its actual form. The nonlinear effects in the anomalous dispersion region are of special interest as, in this region the solitons can be obtained in optical fiber with a balance between the nonlinear and dispersive effects.

The total dispersion or chromatic dispersion ($D_c$) is the addition of waveguide dispersion ($D_W$) and material dispersion ($D_M$) i.e. $D_c\ (\lambda) = D_M\ (\lambda) + D_W\ (\lambda)$. The dispersion ($D_W$) in a waveguide or a fiber is significantly related to geometry of waveguide specifically if dimensions are smaller than the wavelength. The chromatic dispersion in photonic crystal fiber is mainly due to the geoemtry design and is engineered by careful selection of dimension of air-hole diameter (d) and pitch ($\Lambda$). For instance, on increasing the pitch value ($\Lambda$) keeping air-hole diameter (d) intact results in decrease in the value of $d/\Lambda$ and the ZDW starts shifting in the mid-infrared region [40]. The dispersion slope and nonlinearity can be controlled by varying the air-hole diameter (d) and the hole-to-hole spacing ($\Lambda$). With this controllability, we can achieve many important and practical applications in optical communication systems, dispersion compensation, nonlinear optics which are difficult to be achieved with conventional optical fibers. With the photonic crystal fibers, we can also achieve ultra-flattened chromatic dispersion and zero dispersion wavelength (ZDW) shifted in the near-IR or visible region [41].

## 1.3 Nonlinearity in optical fibers

The linear effects originate in fiber from the anharmonic motion of bound electrons in the material which is directly proportional to the electromagnetic field. However, this concept only applies for the low-intensity light propagation. In the case of high-intensity light like ultra-short laser pulses, the material starts behaving in a non-linear way so the electron displacement is ceases in response proportional to the electromagnetic field. This response of electromagnetic wave is known as nonlinear optics and it is responsible for the generation of new frequencies. Resultant, the polarization P is an addition of related electric field E is shown in Equation (1.38) in respect to higher-order nonlinear susceptibility is given as [2]

$$\mathbf{P} = \varepsilon_0(\chi^{(1)}.\mathbf{E} + \chi^{(2)}.\mathbf{EE} + \chi^{(3)}.\mathbf{EEE} + \cdots) \tag{1.38}$$

The $n^{th}$ order susceptibility is $\chi^{(n)}$. The linear susceptibility is $\chi^{(1)}$, that represents the linear optical effects such as linear refractive index and absorption. The $2^{nd}$ order susceptibility is $\chi^{(2)}$ which is responsible for nonlinear effects accompanied second harmonic generation. Although, $\chi^{(2)} = 0$ when materials have inversion symmetry at

the molecular level (as silica). Accordingly, most of the nonlinear effects in silica glass engender from the 3rd order susceptibility ($\chi^{(3)}$) which include Kerr nonlinearity, and Raman scattering.

In the optical fiber the lowest order nonlinear effects arise due to the 3rd order susceptibility, namely: four-wave mixing (FWM), third-harmonic generation (THG) and nonlinear refraction. The phase matching is essential condition for both four-wave mixing (FWM) and third-harmonic generation (THG) processes, else both the process are not effective and can be generally ignored. The nonlinear refraction originates with the reason that refractive index is intensity dependent and is expressed as below

$$\tilde{n}(\omega, I) = n(\omega) + n_2 I = n + n_2 |\mathbf{E}|^2 \tag{1.39}$$

where the linear part is $n(\omega)$ which can be calculated by the Sellmeier equation, the optical intensity is $I$ related to the electromagnetic field ($E$). The coefficient of nonlinear index $n_2$ is related to higher order susceptibility $\chi^{(3)}$ and is expressed as below

$$n_2 = \frac{3}{8n} Re(\chi^{(3)}_{XXXX}) \tag{1.40}$$

Assuming the optical field to be polarized linearly, the refractive index is effected by only fourth-rank tensor of $\chi^{(3)}_{XXXX}$. The most of the nonlinear effects are generated due to nonlinear refraction as it is constantly phase matched.

The nonlinear refraction contributes to nonlinear effects like cross phase modulation (XPM) and self-phase modulation (SPM). The nonlinear effects discussed are categorized as elastic, because during the process the dielectric medium and the electromagnetic field don't exchange any energy. The nonlinear effects like stimulated Brillouin scattering (SBS) and stimulated Raman scattering (SRS) are inelastic as they occur due to exchange of energy between the medium and the electromagnetic field. The SRS and SBS process can be distinguished on the basis that in stimulated Raman scattering the optical phonons participate and acoustic phonons participate in stimulated Brillouin scattering.

### 1.3.1 Self-phase modulation

The first non-linear effect is describe as self-phase modulation (SPM), in which a pulse changes its phase because of the non-linear refractive index ($n_2$) of the optical fiber material. It is because of the refractive index of a nonlinear medium depending on the optical intensity or Kerr effect, it is represented in equation (1.39). The complex amplitude representation of the electric field is

$$A(t) = A_0 \exp(-j\phi(t)) \tag{1.41}$$

here $A_0$ denotes the peak intensity.

The optical field phase changes by

$$\phi = (n+n_2|A|^2)k_0L \tag{1.42}$$

The nonlinear phase shift $\phi_{NL}(t)$ which is intensity dependent is expressed as

$$\phi_{NL}(t) = \frac{2\pi}{\lambda} n_2 |A|^2 L \tag{1.43}$$

where, the propagation distance is $L$. SPM originates new frequencies that are responsible for the spectral spreading of pulses that generates because of time dependence of the nonlinear phase shift $\phi_{NL}$, according to that the instantaneous optical frequency changes across the pulse.

The equation of nonlinear pulse propagation with inclusion of only self-phase modulation (SPM) and ignoring all other nonlinear effects can be expressed as [2]

$$\frac{\partial A}{\partial z} = j\gamma |A|^2 A \tag{1.44}$$

here, dispersive effects are also neglected. The above mentioned expression is calculated by assuming a purely instantaneous response and ignoring the frequency dependence of $n_{eff}$ and $A_{eff}$ , optical shock and losses.

The power $P = |A|^2$ is approximated with the help of taking product of the ($A$*) the complex conjugate and addition of result obtained from the complex conjugate. The results show that the power is constant with respect to $z$, and solution for the electric field envelope can be given as

$$A(z,T) = A(0,T)\exp(j\gamma |A(0,T)|^2 z) = A(0,T)\exp[j\phi(z,T)] \quad (1.45)$$

It is observed from the equation that the shape of the temporal pulse $|A|^2$ remains unaffected during time of transverse. The pulse frequency chirp $\delta\omega(T) = -\partial\phi/\partial T$ is generated due to phase shift time-dependent $\phi(z,T)$. The pulse frequency chirp is negative around leading edge representing red shift and positive around the trailing edge [2] representing a blue shift. Usually in initial phase of supercontinuum generation SPM can be observed.

### 1.3.2 Solitons

As mentioned in section (1.3.1) that due to SPM leading edge of the pulse undergoes red shifts and at the trailing edge of the pulse there is blue shift. The red-shifted part of the pulse propagates faster than the blue-shifted part of the pulse due to the presence of normal dispersion [2]. This explains the pulse broadening would have been more rapid with time when only dispersion was present. Due to the anomalous dispersion region, the red-shifted pulse gets delayed and the blue-shifted pulse moves faster. In the anomalous dispersion regime, the delay in the broadening of a pulse propagating is due to the SPM.

With a condition that SPM and group-velocity dispersion (GVD) substantially balance each other, there is a possibility that pulse propagates unchanged. Including the GVD in equation (1.44) of SPM , the changeless NLSE can be expressed as

$$\frac{\partial A}{\partial z} = -j\frac{\beta_2}{2}\frac{\partial^2 A}{\partial T^2} + j\gamma|A|^2 A \quad (1.46)$$

On solving the above equation, we obtain a solution in the pulse does not change its form during its propagation. This unchanged pulse propagation is known as fundamental soliton and can be obtained directly from a solution of $A(z,T) = V(T)\exp[j\phi(z,T)]$ which is pulse shape preserving. On substituting it into the expression (1.46) [2] the possible solution is given below

$$A(z,T) = \sqrt{P_0}\,sech\left(\frac{T}{T_0}\right)\exp\left[\frac{j|\beta_2|}{2T_0^2}\,z\right] \quad (1.47)$$

To obtain the anomalous dispersion pulse width ($T_0$) and the peak power ($P_0$) is so adjusted that $P_0 = |\beta_2|/(\gamma T_0^2)$, and $\beta_2 < 0$ (or $D > 0$). The resulting value of Equation (1.45) is known as fundamental soliton. As during the process GVD and SPM balance each other the power distribution $|A(T)|^2$ does not change with propagation of the pulse.

There are infinite number of solutions of Equation (1.24) [1] and characterized by the soliton number (N) as given below, the fundamental soliton being one of the solutions

$$N = \sqrt{\frac{L_D}{L_{NL}}} = \sqrt{\frac{\gamma P_0 T_0^2}{|\beta_2|}} \tag{1.48}$$

here, the dispersion length is $L_D = T_0^2/|\beta_2|$ and the nonlinear length is $L_{NL} = 1/(\gamma P_0)$. The nonlinear effects is dominate in propagation when $L_D \gg L_{NL}$, while linear dispersive effects dominate when $L_{NL} \gg L_D$. In case of fundamental soliton, the pulse width and peak power is adjusted that's why $N = 1$ and to excite the higher order solitons the values are so adjusted so that $N \geq 2$. Unlike fundamental solitons higher order solitons undergo change in the shape during their propagation, but in the ideal case, as dispicted in Equation (1.24), the higher order undergo shape change in a periodic manner , thus they recover their original shape once in each period. The periodic dynamics is lost during the generation of SC, even though the GNLSE is used for calculating the supercontinuum generation. Initially in anomalous dispersion regime with an energetic seed laser pulse a large soliton number is obtained. The corresponding spectrum develops through pulse breaking up into several fundamental solitons which can be individually distinguished in a well developed supercontinuum spectrum [13] [42].

### 1.3.3 Cross-phase modulation

Kerr nonlinearity also leads to another phenomenon cross-phase modulation (XPM) in the optical fiber. The refractive index (*n)*, here $n = n_0 + n_2 (|E_1|^2 + |E_2|^2)$, is intensity dependent which results in XPM. In the process of XPM, two optical pulses at dissimilar wavelengths can couple without energy exchange between them. XPM is identical to SPM but the spectral spreading is generated when two different optical fields of different wavelengths interact mutually. Other nonlinear effects arise due to XPM in the fiber. The XPM results in modulation instability in a normally dispersive

fibre tailored for flattened dispersion. Pulse compression, optical switching are few important applications of XPM modulation [2].

In generation of supercontinuum (SC) spectrum in the optical fibers with high nonlinearity, XPM plays a vital role. To deeply understand the effect of XPM, it is important to note that, even though the spectra of dispersive waves and Raman solitons are broadly separated, but there is a possibility that they overlap in the time domain. The XPM leads to the temporal interaction of a Raman soliton and the dispersive wave. All these nonlinear interactions can initiate novel spectral components and helps the spectrum of dispersive waves to broaden in an asymmetric manner, resulting the broadening of the supercontinuum (SC) on the short wavelength side of the input spectrum [2].

### 1.3.4 Four-wave mixing

Four-wave mixing (FWM) is a nonlinear process, as the name suggests it is an interplay of four optical waves due to effects of the susceptibility $\chi^{(3)}$ of third order. As this modulates the refractive index it is named as parametric process. The nonlinear reaction of bound electrons of a material or glass to an electromagnetic field is reason of four-wave mixing (FWM) generation [2].

FWM process is a nonlinear interplay of four optical waves vibrating at four different frequencies $\omega_1$, $\omega_2$, $\omega_3$, and $\omega_4$ respectively. In general, FWM process is classified into two categories. In the first category, all the three photons collectively transfer over their energy to one particular photon at the frequency $\omega_4 = \omega_1 + \omega_2 + \omega_3$. In the case of the second category two photons at frequency $\omega_1$ and $\omega_2$ are exterminated and two photons at frequencies $\omega_3$ and $\omega_4$ are generated at the same time so that $\omega_3 + \omega_4 = \omega_1 + \omega_2$. The competency of FWM is primarily strongly relies on phase compatibility and matching of the frequency components and therefore is related to dispersive characteristics of the fiber. The essential phase matching is satisfied on matching of wave vectors $(\Delta k) = 0$. The degenerate case where $\omega_1 = \omega_2$, is of great interest as in this case one input signal can be employed to instigate four wave mixing (FWM) i.e. to create both the types of photons, stokes and anti-stokes

$$2\omega_p = \omega_s + \omega_{as} \tag{1.49}$$

where, $\omega_p$ is the pump frequency, $\omega_s$ is denotes the wave frequency of the stoke and $\omega_{as}$ denotes the wave frequency of anti-stoke.

For this condition, the expression of phase-matching is written as given below

$$\Delta k = (2n_p\omega_p - n_s\omega_s - n_{as}\omega_{as}) /c = 0 \quad (1.50)$$

where $c$ is the speed of light and $n$ denotes the effective mode index at the frequency $\omega$. It is possible in case the dispersion $n_p \neq n_s$ so FWM generally is not phase-matched.

The process of FWM can be employed to transform the input light signal into a light signal at one or other dissimilar frequencies [43] in a way similar to stimulated raman scattering. When compared to SRS, frequency transformation with parametric process is more helpful as with this process it possible to have both up and down-conversion for a broader range frequencies. Since the coefficient of gain of FWM is higher in value compared to SRS [2] and it can be anticipated that FWM consistently predominate over SRS when it is phase-matched.

Degenerate FWM depicts special characteristics, in anomalous dispersion region the gain bands are wide and are continuously connected to the pump pulse whereas the gain band are compressed and separated if the pump pulse is in the normal dispersion region [13]. As the pulse develops in time frame, the FWM itself exhibit instability in amplitude power distribution. The time domain analogue to FWM is termed as modulation instability (MI).

### 1.3.5 Self-steepening

The phenomenon of self-steeping(SS) is a higher order nonlinaer effects which results due to intsensity dependence of group velocity. Due this effect, SPM broadens spectra of ultra short pulse in an asymmetrical manner, as the wings of the pulse transverses at a faster speed than the pulse [2]. Accordingly, as the pulse transverses within the fiber, the trailing edge get sharpen with increasing distance due to shifting of the peak in the direction of the trailing edge and Self-steepening is only significant for optical shock generation for the impulse pulses.

### 1.3.6 Stimulated Raman scattering

A stimulated inelastic scattering phenomenon is a nonlinear effect resulting to Raman scattering. As per fundamental principle, a molecule in the higher energy vibrational

state, scatter one photon to a lower frequency photon. In order to conserve both energy and momentum, on the extermination of the photon of incident field (pump) a photon at a lower frequency i.e. Stokes wave and a phonon with appropriate energy and momentum are generated [2]. SRS is outcome of both stimulated emission and Raman scattering,which further leads to Raman amplification. In a single mode optical fiber the stimulated inelastic scattering (SRS) is bidirectional process. The stokes wave equation for inceptive growth can be described as below

$$\frac{dI_s}{dz} = g_R I_p I_s \tag{1.51}$$

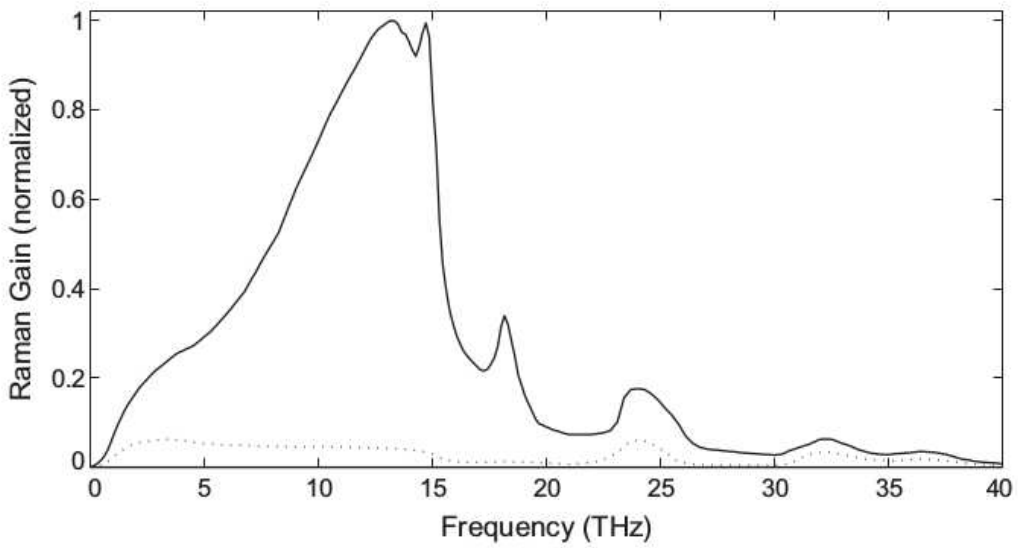


Figure 1.1 Raman gain for silica ($SiO_2$). (Reproduced from [2]).

where, $g_R$ denotes the Raman gain coefficient, $I_s$ denotes the stokes intensity is and $I_p$ is the intensity of pump pulse.

As depicted in Figure 1.1 the Raman gain spectrum for the fused silica, $g_R(\Omega)$ is very broad spreading up to 40 THz with a peak obtained approximately near 13 THz, in $g_R(\Omega)$ , $\Omega$ denotes the frequency difference of the pump and stokes waves [43]. The beam introduced in the optical waveguide input undergoes amplification due to Raman gain as long as the frequency difference $\Omega$ lies inside the bandwidth of the Raman gain spectrum. In silica fiber the maximum gain achieved is for the downshift of frequency component through approximately 13 THz from the pump signal frequency. The maximum pump energy is converted to stokes energy if the pump intensity is more than the threshold level, this depicts the SRS threshold behaviour.

The SRS threshold pump intensity for a single mode fiber can be expressed as below with assumption considering Lorentzian shape approximation for the Raman gain spectrum.

$$I_P^{th} = 16\frac{A_{eff}}{g_R L_{eff}} \tag{1.52}$$

From the equation (1.52) we can interpret that the pump intensity ($I_P$) (threshold) is related to the effective length of fiber ($L_{eff}$), raman gain and affective area. It is inversely proportional to effective length of the fiber. The Raman effect amplifies a weak signal in optical fiber, on introducing a weak signal with an energetic pump signal and the frequency difference between the signals falls in bandwidth of Raman gain spectrum [44].The fused silica ($SiO_2$) has a very short Raman response time in range of 60 to 70 fs. As the pulse propagates along the fiber, due to the Raman effect the spectrum shifts in the direction of the low-frequency resulting to Raman-effect induced frequency shift [2]. The frequency shift becomes very large for the short pulses as it increases linearly along the fiber.

### 1.3.7 Dispersive waves

The generation of fundamental solitons in the fiber is generally assisted with a temporal pedestal of short amplitude which travels along the linear region [45]. With its sensitive response of fundamental solitons towards the perturbations mainly the dispersion of higher order (HOD) results in instability of nonsolitonic radiation (NSR) at a specific frequency [46]. The resonant state involving dispersion of higher order (HOD) play a vital role and due to phase-matching conditions the nonsolitonic radiation (NSR) are coherently enhancement at a narrow band of frequencies. This enhanced spectral constituent is well known as the Cherenkov radiation or the soliton induced resonant emission as it occurs in region of normal dispersion. In reference to particle physics Cherenkov radiation appears in a medium when a particle moves with greater velocity than the phase velocity of light [47]. The similar effect which occurs in optical channel is the reverberation condition between the pulse, travelling with group velocity, and the dispersive wave. This result to transfer of energy from soliton to the dispersive wave at a suitable frequency evolved with phase-matching condition.

The frequency of dispersive wave frequency which originates consequently due to radiation emitted by the perturbed soliton can be achieved by phase-matching such that the dispersive wave propagates moves with phase velocity same as that of the soliton. The two phases at a distance $z$ after a delay $t = z/v_g$ can be expressed as below, where $\omega$ is the frequency of dispersive wave and $\omega_s$ is soliton frequency [2].

$$\phi(\omega) = \beta(\omega)z - \omega(z/v_g) \tag{1.53}$$

$$\phi(\omega_s)=\beta(\omega_s)z - \omega_s(z/v_g) + ½(\gamma P_s z) \tag{1.54}$$

here the group velocity of the soliton is denoted by $v_g$. The last term in Equation (1.54) represents the nonlinear phase shift of the solitons. The phase difference is zero in case of phase matching condition.

$$(\omega) = (\omega_s) + \beta_1(\omega - \omega_s) + ½(\gamma P_s) \tag{1.55}$$

here, on substituting the value of $v_g$ equal to $1/\beta_1$ as one of the solutions obtained from solving the equation, the frequency of one or many other dispersive waves generated due to perturbation initiated in solitons can be easily determined.

As the dispersive waves formation due to soliton fission is susceptible to smallest detail of the dispersion ($\omega$) relation of the fiber, so it becomes necessary to include higher order dispersion terms of order four. With the aid of numerical approach we observed that all the terms with odd-order depending upon the sign of dispersion parameter generate one NSR peak on the blue/red side of the carrier frequency of the pulse [2]. On the other end two NSR peaks on opposite sides of the carrier frequency are generated with the dispersion terms with positive sign and even order [2].

## 1.4 Summary

The complete chapter presents the conceptual description of the fundamental principles related to the generation of supercontinuum required to build the understanding about the work shown in this thesis. The study of Maxwell's equations

and the generalized nonlinear Schrödinger equation (GNLSE) which governs the propagation of optical pulse is very essential as they help understanding both the linear and the nonlinear phenomena along with their effects during the pulse propagation within the fiber. The mathematical steps of derivation of equations related to wave equations and the generalized nonlinear Schrödinger equation (GNLSE) are very well explained. The end section of the chapter reviews the important nonlinear phenomena and principles responsible for propagation dynamics of generation of supercontinuum.

# Chapter 2

**Fundamentals of optical waveguides and numerical methods**

This chapter introduces the basic designs of optical waveguides and the numerical methods for studying their properties. The solutions of generalized nonlinear Schrödinger equation and Maxwell's equations as discussed in Chapter 1 are used in majority of numerical methods to study the properties of optical waveguides. Firstly we briefly analyse the light guidance mechanisms of optical fibers in section 2.1. The linear properties are studied using the finite-difference-time-domain (FDTD) method which is explained in detail in section 2.2. The end section 2.3 characterizes the method used in our research work to estimate generalized nonlinear Schrödinger equation, for estimating the pulse propagation dynamics of the output pulse through supercontinuum generation in waveguide. Split-step Fourier method (SSFM) was employed to estimate generalized nonlinear Schrödinger equation (GNLSE) for our simulation work.

## 2.1 Optical waveguides

Before we start building the fundamentals of numerical methods used, it is important to understand the guiding properties of optical waveguide with aid of few examples. With the enhancements in technology many types of optical waveguides are available for various commercial applications in different fields. On the basis of guiding mechanism the waveguides are classified as index guiding waveguides and photonic bandgap waveguides well known as PBG. The standard step-index fiber (SIF) [48] and microstructured fiber (MF) or photonic crystal fiber (PCF) [49] are widely used as index guiding waveguides and photonic band gap waveguides respectively. The waveguides with cobweb lattice [50], suspended core [51] and wagon-wheel [52] are few other types of fibers available. With the advent of technologies the planar geometry structure (channel/rib) are widely employed as index guided waveguides to generate supercontinuum with advantages of low-cost fabrication, scalability and suitability for integrated optical chip solutions [53]. The hollow core fibers under the category of photonic bandgap guiding (PBG) waveguides are widely used for supercontinuum generation [54].

The structure of ideal step-index fiber (SIF) consists of a cylindrical glass core surrounded by a lower refractive index material forming the cladding as shown in Fig. 2.1(a) [2]. On the similar idea a planar geometry structure (channel/rib) waveguide has a square/rectangular core surrounded by a lower refractive index material in comparison to that of the core forms the cladding, as shown in Fig. 2.1(b). The total internal reflection confines the light in fiber [55]. The PCF structure offers modified total internal reflection guiding mechanism due to the difference in effective index between solid core and the microstructured air-hole cladding [49] as shown in Fig. 2.1(c). The light guiding mechanism is entirely different in photonic band gap guiding waveguides, which enables light guidance in hollow air-core surrounded by microstructured air-hole cladding, as shown in Fig. 2.1(d) [56].

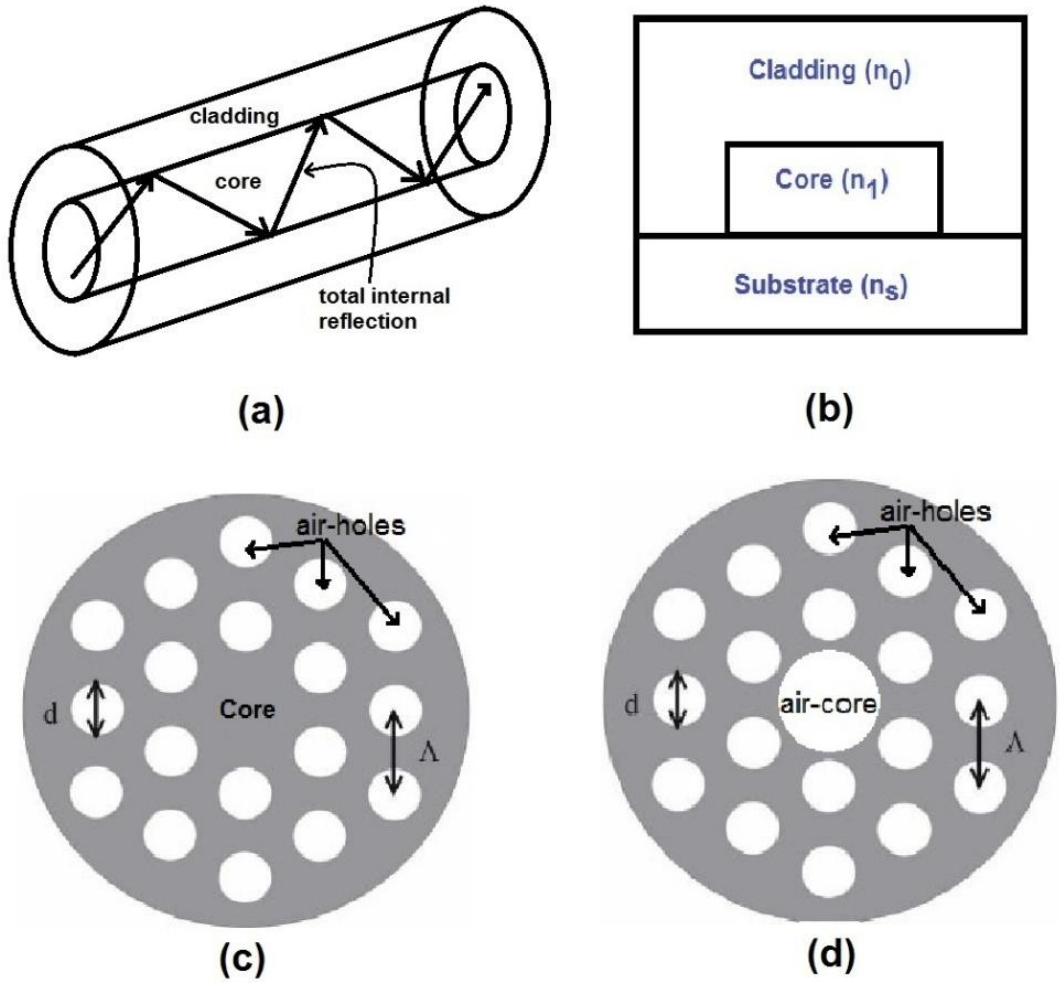


Figure 2.1 Schematics of (a) convection optical fiber (b) planar (channel) waveguide (c) solid core PCF and (d) air-hole core PCF. (Reproduced from [2] [48] [49] [56]).

The analysis of optical waveguides investigations involves the estimation of wave propagation constants ($\beta_0$) and also the mode field profiles of all the supported modes in the optical fiber. The solutions of Maxwell's equations with suitable boundary conditions are used to calculate the propagation constant of the optical waveguide. Solving the Maxwell's equations for analysis and calculations may not be a simple thing, further the accurate analysis is not only time consuming but difficult work due to arbitrary refractive index distribution such as graded-index profiles of optical waveguides or photonic crystal fibers, complex designs, and materials with anisotropic and nonlinear refractive indices, with different and complex refractive index of semiconductor and metals. The various methods developed for analysis of optical waveguide analyses have helped to overcome these difficulties. These methods generally classified as methodical approximation solutions and the numerical solutions. The solution for a two dimensional step-index optical waveguides such as planar waveguides and step-index fiber (SIF) can be obtained by accurate methodical approximations. It is difficult to obtain exact solutions for fibers with an arbitrary refractive index distribution like photonic crystal fibers and graded-index fibers. Our research work also uses the photonic crystal fibers which don't have exact analytical solution so finite-difference-time-domain (FDTD) based numerical method is used for analyzing all optical fibers proposed.

In order to analyze the transverse feild distribution of optical fibers , the wave equations derived from elementary Maxwell's equations discussed in previous Chapter are estimated by finite-difference-time-domain (FDTD) method. The electromagnetic fields evolved in the fiber are linearly guided in medium and can be studied with these equations. The dynamical part of propagation of the complex electric field envelope developed can be studied by solving the generalized nonlinear Schrödinger equation (GNLSE) by split-step Fourier method. The finite difference-time-domain numerical method is employed to analyze the properties of photonic crystal fiber (PCF) and split-step Fourier method is used to study the nonlinear medium GeAsSe, $As_2Se_3$ multi-material, and Li-containing ternary compounds based photonic crystal fibers used for designing broadband supercontinuum laser sources for mid-infrared region.

## 2.2 FDTD modeling of photonic crystal fibers

Photonic crystals have attracted much attention in the field of optics since last few years. The permittivity in a photonic crystal structure is spatially periodic. Analogous to formation of electronic bands with electronic states in a sold crystal, the optical modes of photonic crystal falls in discrete bands. Photonic crystals exhibit band gaps identical to electronic states in solids, prohibiting the propagation of light in the band gaps. It is feasible to tailor the band structure of the photonic crystal by careful selection of geometry and by using the appropriate materials can customize the optical properties [57].

Photonic crystal fibers which evolve as a category of photonic crystals are of special interest due to some of its unique properties. The structure of photonic crystal fiber (PCF) is so designed that it exhibits periodicity in the transverse dimensions and uniformity in the longitudinal direction. These types of fibers can show two-dimensional bandgap for the available longitudinal wavenumber, which prohibits the transverse propagation of certain range of frequencies in waveguide. When the defect is inserted in the photonic crystal fibers, frequencies in the bandgap can propagate only in the defect since they are restricted from propagating in the lattice and hence a waveguide is formed. Photonic crystal fiber is emerging field of research with vast application areas. The degree of freedom in designing offers ease to manipulate and obtain distinctive optical properties for a wide range of applications, like from nonlinearity for wavelength conversion in telecommunications to large mode area for materials processing [58].

With the growing interest of researchers to tailor the optical properties of PCFs, effective numerical modeling also gained attention and importance. To detect the propagating modes in the photonic crystal fiber researchers employed iterative eigensolver like MIT Photonic-Bands (MPB) package in frequency domain [59]. Well adapted to certain structures of photonic crystals, this method has few drawbacks for photonic crystal fiber waveguides. The defect introduced in the lattice should be large enough to eliminate the problem of boundary space influencing the guided mode. One possible approach to increase the dimension of the lattice results in increase in the problem space but it also increases the desired mode number among all modes in the waveguide. Under such situation to find guided modes, more number modes have to

be investigated making this technique as time consuming and inefficient. In the next section, we demonstrate the methods to overcome this problem.

### 2.2.1 FDTD Theory

We used the finite-difference-time-domain (FDTD) technique to model PCF in this research work. FDTD is the malleable algorithm suitable for various kinds of electromagnetic simulations. Although, in place of the sample length of PCF forced with a source from one end, as might be done for a metallic waveguide, here we assume that fields are initially present all along the length of PCF, and then proceed and carry out simulation in time with no additional sources. It is possible because the unguided modes exit from the fiber and are separated from the system by applying absorbing boundary conditions, unlike in a metallic waveguide.

Here model for a particular case system is modelled by storing the fields in a single two-dimensional transverse section by the fiber and presume that the all fields change periodically as $e^{-ik_z z}$, where the longitudinal wavenumber is $k_z$ and the fiber extends in the *z*-axis. The grid is so initialized so that with field pattern we can be easily obtain the mode pattern which is "close" to the required mode pattern This inferences that major portion of its energy is focused in the mid of centre defect and has no free charges so that $\boldsymbol{\nabla}.\mathbf{D} = 0$. This explains that we can identify initial fields methodically.

The frequency domain investigation help us to develop a deep understanding about the problem. Generally, the starting field will be having a agglomeration of eigenmodes of the fiber, and each mode having its own frequency. Any mode with frequencies which donot fall in the band gap can undergo diffraction through the lattice and be absorbed by any absorbing boundary like PML or other at the edge of the problem space.

The transverse magnetic field ($\mathbf{H}_\perp$) eigenvalue equation is

$$\boldsymbol{\nabla}_\perp \times \left(\frac{1}{\epsilon_r}\,\boldsymbol{\nabla}_\perp \times \boldsymbol{H}_\perp\right) - \frac{1}{\epsilon_r}\boldsymbol{\nabla}_\perp(\boldsymbol{\nabla}_\perp.\boldsymbol{H}_\perp) = \left(\mu\epsilon_0\omega^2 - \frac{k_z^2}{\epsilon_r}\right)\boldsymbol{H}_\perp \qquad (2.1)$$

here $\epsilon_r = \epsilon/\epsilon_0$ [60]. The relation $\boldsymbol{\nabla}.\mathbf{H} = 0$ is used to determine $H_z$ component , and the electric field can be estimated by expression below

$$\boldsymbol{E} = \frac{1}{i\omega\epsilon}\boldsymbol{\nabla} \times \boldsymbol{H} \tag{2.2}$$

With the constraint that the eigenvalue can relate frequency up to a sign, the initial field is expressed as below

$$\boldsymbol{H} = \sum_n \left(a_n e^{i\omega_n t} + b_n e^{-i\omega_n t}\right) \boldsymbol{H}_n \tag{2.3}$$

$$\boldsymbol{E} = \sum_n \left(a_n e^{i\omega_n t} - b_n e^{-i\omega_n t}\right) \boldsymbol{E}_n \tag{2.4}$$

here ($\mathbf{H}_n$,$\mathbf{E}_n$) is the eigenmode with frequency $\omega_n$ , the $a_n$ and $b_n$ are the complex numbers. Therefore, it is necessary to specify only one field; specifying the other just gives the complex relation between the $a_n$ and $b_n$. For example, setting $\mathbf{E} = 0$ gives $a_n = b_n$.

The eigen modes of the time-step operation on the FDTD grid will not necessarily represent the actual modes of the fiber. This is due to both discretization and the fact that the FDTD space only has a finite lattice surrounded by absorbing boundary conditions instead of an (ideally) infinite lattice. Thus only those modes, which are transversely confined in proximity to center of the PCF and have all their energy well inside the lattice, should be considered as guided modes. The extra modes will be affected by the presence of the boundary conditions will be lossy and eventually decay with the progress of simulation. The time- and *z*- averaged energy density can be expressed as below, with consideration of the loss coefficients of the $n^{th}$ mode is $\gamma_n$

$$u = \frac{\epsilon}{2}|E|^2 + \frac{\mu}{2}|H|^2 = \frac{1}{4}\sum_n (|a_n|^2 + |b_n|^2)\, e^{-2\gamma_n t}(\epsilon|E|^2 + \mu|H|^2) \tag{2.5}$$

### 2.2.2 FDTD method Implementation

Here only confined the fields in one direction, and apply periodic boundary condition to measure the *z* derivatives of the transverse fields. There are any *z* and $z_0$,$E_\perp(z) = e^{-ik_z(z-z_0)}E_1(z_0)$, so

$$\left.\frac{\partial E_\perp}{\partial z}\right|_{z=\Delta z/2} = -ik_z E_\perp|_{z=\Delta z/2}$$

$$= -ik_z e^{-ik_z \Delta z/2} E_\perp \big|_{z=0} \tag{2.6}$$

Accordingly,

$$\frac{\partial H_\perp}{\partial z} \big|_{z=0} = -ik_z e^{ik_z \Delta z/2} \big|_{z=\Delta z/2} \tag{2.7}$$

If both the **E** and **H** fields initially, we must compute $\mathbf{H}|^{1/2}$ from $\mathbf{E}|^0$ and $\mathbf{H}|^0$. For this, we use the first and second-order differential equations for **H**. Now, we have [61]

$$\frac{\partial H}{\partial t} = -\frac{1}{\mu} \nabla \times E \tag{2.8}$$

$$\frac{\partial^2 H}{\partial t^2} = -\frac{1}{\mu} \nabla \times \left( \frac{1}{\epsilon} \nabla \times H \right) \tag{2.9}$$

in finite difference form, this give

$$H|^{1/2} - H|^{1/2} = -\frac{\Delta t}{\mu} \nabla \times E|^0 \tag{2.10}$$

$$H|^{1/2} - 2H|^0 + H|^{-1/2} = -\frac{(\Delta t)^2}{4\mu} \nabla \times \left( \frac{1}{\epsilon} \nabla \times H \right) \big|^0 \tag{2.11}$$

after adding these equations, we find that

$$H|^{1/2} = H|^0 - \frac{\Delta t}{2\mu} \left[ \nabla \times E|^0 + \frac{\Delta t}{4} \nabla \times \left( \frac{1}{\epsilon} \nabla \times H \right) \big|^0 \right] \tag{2.12}$$

This is the method for initializing the FDTD grid given **E** and **H** at $t = 0$ [61].

The finite-difference-time-domain (FDTD) method along with periodic boundary conditions in the axial direction proves to be an efficient method to find modes in the PCFs. It is has an additional advantage of better speed over other frequency-domain methods.

## 2.3 Split-step Fourier method

In presence of nonlinear processes like higher-order dispersions, Raman delayed response, self-steepening and others the generalized nonlinear Schrödinger equation (GNLSE) Equation (1.29) normally does not contribute itself to analytic solutions. Thus often it is essential to use numerical method to understand the nonlinear

phenomena developed with the optical pulse propagation within the optical fibers [2]. The solutions of GNLSE can be obtained by number of different procedures developed [62] [63] [64], the Split-Step Fourier Method (SSFM) method is the widely used method. Another commonly used method is finite difference method [2], but the SSFM is a pseudo-spectral method which offers higher speed of order two magnitudes as compared to finite difference method. This method proves to be efficient and accurate for pulse widths of the order of ps [2] [62]. In the presented work here the solutions of GNLSE is calculated by SSFM to observe the supercontinuum generation in optical fibers (Chapter 4, 5 & 6). The next section presents the brief description of SSFM.

### 2.3.1 Split-step Fourier method for solving GNLSE

As the name suggests the Split-Step Fourier Method (SSFM) method separates the dispersive and nonlinear components in the equation from one another. Thus the components are assumed to be independent over a very small distance.

Accordingly, Equation (1.29) can be expressed as below

$$\frac{\partial A}{\partial z} = \left(\widehat{D} + \widehat{N}\right)A \tag{2.13}$$

here, the linear differential operator is $\widehat{D}$ that represents dispersion and absorption of the media and the effect of nonlinearities of fiber on pulse propagation is represented by nonlinear operator $\widehat{N}$ [2]. These operators can be defined as

$$\widehat{D} = -\frac{\alpha}{2} + \sum_{m\geq 2} \frac{j^{m+1}}{m!}\beta_m \frac{\partial^m A}{\partial T^m} \tag{2.14}$$

$$\widehat{N} = j\left(\gamma + j\frac{\alpha_2}{2A_{eff}}\right)\left(1 + \frac{j}{\omega_0}\frac{\partial}{\partial T}\right)\left(A(z,T)\int_{-\infty}^{\infty} R(T)\left|A(z,T-T')\right|^2 dT'\right) \tag{2.15}$$

After solving the Equation (2.13), find

$$A(z+h,T) = \exp\left[h\left(\widehat{D} + \widehat{N}\right)A(z,T)\right. \tag{2.16}$$

Generally, dispersion and nonlinearities work jointly along the complete length of the fiber. The split-step Fourier method calculates the result with an assumption that dispersive and nonlinear effects are independent for the optical field propagating

for a short distance $h$, the dispersive and nonlinear impacts can be supposed to act independently. The approximation of the results for the propagation of $z$ to $z+h$, is completed in two steps. In the first step, dispersion effect is zero i.e $\widehat{D}$ = 0 and non-linearity acts alone, and in the second step the non-linearity effect is zero i.e $\widehat{N}$ = 0 and dispersion acts alone in equation (2.13).

As per Baker-Hausdorff theory for two non-commuting operators we can state that [65]

$$\exp\left(h\widehat{D}\right)\exp\left(h\widehat{N}\right) = exp\left(h\left(\widehat{D}+\widehat{N}\right)+\frac{h^2}{2}\left[\widehat{D}\widehat{N}-\widehat{N}\widehat{D}\right]+\cdots\right) \quad (2.17)$$

On neglecting the higher terms in exponential and $h^2$ it can be approximate the following

$$\exp\left[h\left(\widehat{D}+\widehat{N}\right)\right] \approx \exp\left(h\widehat{D}\right)\exp\left(h\widehat{N}\right) \quad (2.18)$$

With this approximation the SSFM results in accuracy of closely second order because of $h^2$ and higher order terms in the Baker-Hausdorff expansion have been ignored. It is noteworthy that here the dispersive and non-linear terms do not commute with each other.

Accordingly, the expression below represents a solution of pulse envelope of equation (2.16)

$$A(z+h,T) \approx \exp\left(h\widehat{D}\right)\exp\left(n\widehat{N}\right)A(z,T) \quad (2.19)$$

The accuracy of the SSFM can be refined by modification of Equation (2.19) to well known form, symmetrised SSFM [66], which gives higher accuracy.

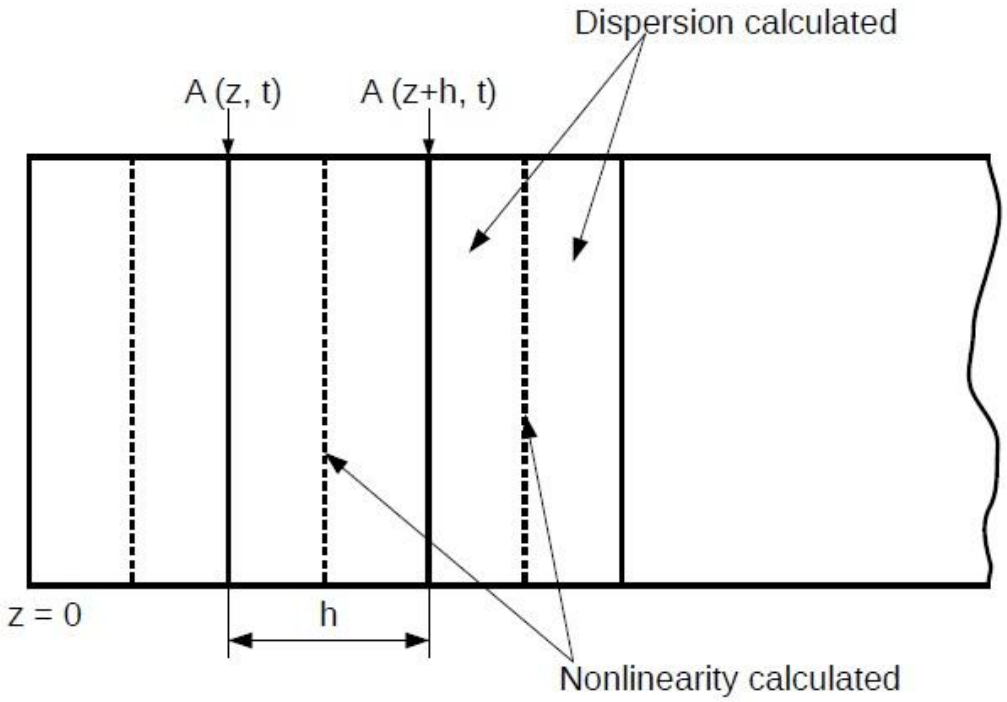


Figure 2.2 The pictorial representation of symmetrised SSFM for numerical simulations. The length of the fiber is divided into the various segments of width *h* and the impact of nonlinearity is fitted at the centre of the step depicted by a dashed line. (Reproduced from [2]).

The calculations of the nonlinear impacts in this method are obtained for centre of every step instead of the edges as depicted in Figure (2.2). The spatial dependence of the nonlinear term can be precisely expressed by an integral, and equation (2.19) can be approximately expressed as

$$A(z+h,T) = \exp\left(\frac{h}{2}\widehat{D}\right) exp\left(\int_z^{z+h} \widehat{N}(\hat{z})a\hat{z}\right) exp\left(\frac{h}{2}\widehat{D}\right) A(z,T) \qquad (2.20)$$

The use of the symmetrical form is more advantageous as with its use the accuracy is increased by the third order by using Baker-Hausdorff formula twice in the equation (2.20).

In order to improve the accuracy of split-step Fourier method the integral in equation (2.20) is evaluated more accurately, instead of approximating it by $h\widehat{N}(z)$. The use of trapezoid rule is simplest approach to estimate the integral from Equation (2.20) [2]

$$\int_z^{z+h} \widehat{N}(\hat{z})d\hat{z} \approx \frac{h}{2}\left(\widehat{N}(z) + \widehat{N}(z+h)\right) \quad (2.21)$$

As $\widehat{N}(z+h)$ is unknown at the midsegment located at $z + h/2$, it becomes essential to follow an iterative method which is initiated by replacing $\widehat{N}(z+h)$ by$\widehat{N}(z)$. The value of $A(z+h,T)$ can be directly calculated using the equation (2.20), and is further, utilized to determine the next new value of $\widehat{N}(z+h)$. No doubt the iteration procedures are time consuming, but the overall computation time can be reduced by increasing the step size h due to the enhanced accuracy of the numerical algorithm.

### 2.3.2 Split-step Fourier method implementation

In order to stimulate the generation of supercontinuum we have used MATLAB tool. To apply split-step Fourier method, the length of the waveguide is split to equally space large number of segments, as depicted in Fig. 2.7. The optical signal propagates from one section to another applying the procedure of Equation (2.20). Firstly the optical field $A(z,T)$ is made to propagate to $h/2$ distance along with the dispersion employing the Fast Fourier transform (FFT) algorithm [2]. After this the field is multiplied by a non-linear term, to include the effect of non-linearity over the entire length of segment $h$ in the centre plane. In remaining half distance $h/2$ the field propagates with dispersion to obtain $A(z+h,T)$. It is inferred that the non-linearity is agglomerated to the central plane of each of the segment with the dashed lines as marked in the Figure (2.2).

The Fourier transform of the dispersive terms and the aforementioned approximation collectively is used to implement the symmetrized split-step Fourier procedure as follows

$$A(z+h,T)$$
$$\approx \mathfrak{F}^{-1}\left\{exp\left(\frac{h}{2}\widehat{D}(j\omega)\right)\mathfrak{F}\left\{exp\left(\int_z^{z+h}\widehat{N}(\hat{z})d\hat{z}\right)\mathfrak{F}^{-1}\left\{exp\left(\frac{h}{2}\widehat{D}(j\omega)\right)\mathfrak{F}\{A(z,T)\}\right\}\right\}\right\} \quad (2.22)$$

## 2.4 Summary

This chapter presents review of the theoretical aspect of the numerical method which needs to be learned for an understanding the work presented. The mechanism of light guidance in various types of optical fibers, with the detailed explanation for the most widely used photonic crystal fibers have been presented here. The finite-difference-time-domain (FDTD) method based procedure has been used to obtain the modal solutions of photonic crystal fiber. The nonlinear pulse propagation equation (GNLSE) has been solved for obtaining evolution of the optical signal in the waveguide output by using split-step Fourier method including the results obtained through modal solutions by FDTD method.

# Chapter 3

## Timeline of SC generation

The creation of novel frequency components with the spectral expanding is one of the intrinsic characteristics of non-linear optics and has been interest of research since the early 1960s. The broadening of a narrowband incident pulse due to extreme nonlinear spectral broadening to generate a broadband spectrally continuous leads to supercontinuum generation [67]. In 1970 Alfano and Shapiro discovered the generation of supercontinuum generation in bulk BK7 glass [3] [68]. and since then has opened many new avenues of research for numerous explorations in a large range of nonlinear optical fibers and waveguides. The advent of microstructured photonic crystal fiber (PCF),a new class of optical fibers in late 1990 attracted the researchers all over the globe due to its application in the craetion of ultra-wideband spectra high luminance with supercontinuum generation [5] [6] [69]. The microstructure fibers offers more degree of freedom of the design, making it suitable choice to generate SC at a much wider range of parameters which was not feasible with the conventional planar waveguides or fibers. The results of various experiments report that SC generation is obtained for both unamplified input pulses with durations in range of tens of femtoseconds to a few nanoseconds, and continuous wave sources with high-power. Supercontinuum sources have innumerable applications in various fields like spectroscopy, bio-imaging, the optical coherent tomography (OCT), frequency metrology, pulse compression and the design of ultrafast tunable laser sources with response in range of femtosecond (fs).

A small FOM (Figure of merit) can result in significant saturation of the transmitted power before the desired nonlinear phase shift is reached, so large values of FOM are desired to obtain better performance for nonlinear devices. A large FOM can be obtained by adjusting the glass composition in order to shift the electronic band-gap and thus reducing the amount of multi-photon absorption.

| **Material** | **FOM** |
|---|---|
| Si | ≈0.37 |
| $As_2S_3$ | ≈12.9 |
| $As_2Se_3$ | ≈2 |
| $Ge_{11.5}As_{24}Se_{64.5}$ | ≈60 |
| $Ge_{33}As_{12}Se_{55}$ | ≈2.4 |

In reference to its application in telecommunications, the broad Spectra of SC is sliced to generate optical sources with multiple wavelengths for DWDM (dense wavelength division multiplexing). This chapter covers the outline of fundamental nonlinear optics literature in context to supercontinuum generation. The first Section 3.1 describes broadening of supercontinuum in bulk media. The next Section 3.2 was dedicated to study the generation of supercontinuum in conventional fibers. SC generation in silica microstructured fibers is covered in Section 3.3. Next Section 3.4 generation supercontinuum in nonsilica fibers and waveguides is discussed.

## 3.1 SCG in bulk media

In 1970 Alfano and Shapiro demonstrated SC generation in BK7 glass by introducing 5 mJ picosecond pulse at 530 nm to expand the spectrum of white light for the range of 400-700 nm which covered the entire visible range [3] [68].The SC range, achieved by the experiment of Alfano and Shapiro was more than ten times higher than all previously reported. The interesting point about this work was that they reported the discovery of nonresonant coupling of four-photon (four wave mixing) instead. It was Manassah *et al.* who formulated the process as "supercontinuum" [70]. Meanwhile, this process was referred as superbroadening [71] [72] [73].

In year 2000, Gaeta based on complete three-dimensional simulations of the propagation of light presented a consistent explanation [74]. The idea already presented by Werncke *et al.* latterly accepted that in bulk media, the generation of optical shock on the back of the pump pulses because of self-steepening and space-time focusing is responsible for continuum generation of white light [71]. Both multiphoton absorption and plasma generation prevents optical breakdown of the material by arresting the collapse of the beam. In bulk medium self-focusing was established to play a vital role in SCG, as it was generally observed that the threshold level of supercontinuum accorded with the crucial power for catastrophic collapse, normally related to generation of self-trapped filaments. In the bulk material due to beam collapse the SPM improves, which results in a rapid rise in peak intensity and generates many non-linear effects of higher order like multiphoton absorption, avalanche ionization, space-time focusing, self-steepening and free-electron plasma formation. The process may or may not form self-trapped filaments depending on the

time period of the pulse and on the relative strength of self-focusing, chromatic dispersion and plasma defocusing [75]. Along with agreement that SCG process is dependent on band gap of the material it is in agreement with other related observations [76]. In the material with small band gap, the process of self-focusing is stopped at lower intensities by free-electron defocusing which preventing the formation of a shock.

In bulk materials the generation of SC is a very complex process involving a complex coupling of temporal and spatial effects, requiring a high pumping power in order of MW. Whereas SC generation in planar optical waveguides, or in waveguides based on fiber geometries, includes only temporary dynamic processes with the transverse mode characteristics which are estimated by linear properties of the waveguide. Accordingly, this justifies the motivation to study the supercontinuum generation in planar waveguides and photonic crystal fibers with use of the dispersion engineering. As this helps to understand characteristics of temporal nonlinear propagation effects to further develop deepen understanding for much more complex waveguide design with bulk material.

## 3.2 SCG in conventional fibers

The generation of supercontinuum in optical fibers was firstly demonstrated by launching pulses of 10 ns duration from a dye laser source in 20-m long fiber in 1976 [77]. The peak power of 1 kW the spectrum of SC spread around 180 nm. Experimenting in 1987 the pulses with time period 25 ps supporting four modes at the 532 nm input wavelength were launched into a fiber with length of 15-m [78]. With the combined effects of Self phase modulation (SPM), Cross phase modulation (XPM), Stimulated raman scattering (SRS) and Four wave mixing (FWM), the output spectrum has increased by more than 50 nm. The results obtained were same as observed for the single-mode fiber [79]. A single-mode fiber in an experiment in 1987 produced a wide spectrum of 200 nm at the output end of the 1 km long fiber, with input pulse of 830 fs pulse width and peak power of 530 W [80]. Similar characteristics were subsequently obtained with longer pulses [81] [82].

SCG in single-mode fibers was applied as a functional tool for generating pulse trains at multiple wavelengths simultaneously by introducing a single picosecond pulse train at the wavelength near 1.55 μm [83] [84] [85] [86]. Such SC source finds

its important application as a laser source in system using wavelength division multiplexing. In an experiment, pulses with duration of 6 ps at the repetition rate of 6.3 GHz and with a peak power of 3.8 W, which was achieved by the amplification of the output of a semiconductor gain-switching laser operating at 1553 nm wavelength, were propagated along 4.9 km long fiber in the anomalous dispersion region [84]. The spectrum of supercontinuum was 40 nm broad and was sufficient to be filtered to produce 40 channels exhibiting periodic transmission peaks for WDM. The pulse width of resultant 6.3 GHz pulse sequence in several channels varied in range of 5-12 ps and pulse consisted of nearly transform limited pulses. With this technique in 1995 a 200 nm broad supercontinuum was achieved resulting in 200 channel WDM source [85]. The similar technique was employed to generate shorter pulses by enhancing the bandwidth of each transmission peak of the optical filter. It was in 1997, Morioka *et al.* made use of arrayed waveguide grating filter to tune pulse width in the range varying from 0.37-11.3 ps. The transmission of data with the bit rate of 1.4 Tb/s using SC source for seven WDM channels with 600-GHz spacing was demonstrated in 1997 [86].

The most of the supercontinuum generation studies in traditional optical fiber centered on the regime in which pumping used ultrafast pump pulses. The intricate physics underlying the SC generation with longer pump pulse or CW excitation continued to be a area of active research. In particular significant work was reported by [87] where the relationship between soliton dynamics, modulation instability and Raman scattering in continuous wave pumps conditions was explained with numerical simulations. This process underlined the aspect soliton dynamics is also involved in the generation of supercontinuum in the region of anomalous group velocity dispersion (GVD) using CW pumps as in case of pulsed excitation. The non availability of suitable high power CW sources restricted the follow-up experimental studies in this field.

## 3.3 SCG in silica microstructured fibers

The microstructured photonic crystal fibers (PCFs) consisting of a solid core in the central core surrounded by cladding structure consisting of series of air holes running along its length also demonstrated generation of supercontinuum. The systematic structure of air-hole surrounding the central core is referred as cladding has lower

effective index as compared to centre portion of the photonic crystal fiber, and light is guided due to slightly different, modified total internal reflection [88]. However, this concept is identical to the guidance principle in the conventional fibers, the abnormality in degrees of freedom provided by changing the size of air-hole dimension and length between air-hole to air-hole in such an index-guiding photonic crystal fibers pave the way to tailor the waveguide dispersive characteristics in such manner which are absent in ordinary fibers. In photonic crystal fiber, the total dispersion is due to the material dispersion and waveguide dispersion. The waveguide dispersion is different for the ordinary fiber and the photonic crystal fiber, but the material dispersion is identical in the two fibers. The high contrast of the index between the core-cladding interfaces in photonic crystal fiber has tight confinement of the light in the core enhancing the non-linearity of the PCF in comparison to the conventional fibers. PCF dispersive properties can be easily adjusted by changing the size of air hole and pitch that is not possible in ordinary fibers. Accordingly, these two properties have made photonic crystal fiber better choice for SCG than conventional silica fibers.

In was in the year 2000, when Ranka *et al.* by demonstrated SC spanning for the range 400 to 1600 nm pumped 100 fs pulses at wavelength 770 nm with peak power of 7 kW in 75 cm long silica based microstructured fiber showing anomalous dispersion around this wavelength [5]. That kind of short fiber supercontinuum was significantly wide and relatively flat for the complete bandwidth. Identical results were discovered in a different demonstration in the same year, in which silica based tapered photonic crystal fiber of length 9 cm and core diameter of 2 μm resulted spectra with pulses of duration 100 fs and power levels between 60 and 380 mW on an average [9]. In 2000 the generation of supercontinuum spectra with use of short PCF boosted the research activities during the years of 2002 and 2003 in this emerging area [89] [90] [91] [92] [93] [94]. The very important and critical factor for SCG in the fiber is found to be the wavelength of the pump with respect to the ZDW of the fiber [89]. Since the input pump wavelength falls in normal dispersion regime of fiber the higher-order solitons could not be formed, thereby reducing the spectral broadening significantly. It was in year 2002, Yb-doped fiber laser generating parabolic pulses the pump wavelength exceeding 1000 nm was experimented for the SCG [90]. In tapered fiber supercontinuum generation spreading from 1000 to 1700 nm was obtained in another experiment in year 2002 by pumping femtosecond pulses at 1260 nm with

energy of 750 pJ near second zero-dispersion wavelength (ZDW) [91]. During the same year an experiment demonstrated supercontinuum generation with pumped pulses of duration 18 fs in cobweb style 4.1 cm silica photonic crystal fiber with variable core diameters in range from 1 to 4 μm. The core of the PCF was not circular ideally so the fiber demonstrated birefringence. There was remarkable variation in spectral widths of generated supercontinuum spectra with the polarization angle of incident light in reference to the slow axis of the fiber. In a different experiment the supercontinuum spectra generated, demonstrated many discrete peaks on the long-wavelength side correlated to formation of Raman soliton after fission of high-order solitons, in a 6-m long photonic crystal fiber pumped at 850 nm with 200 fs duration pulses [92]. In 2003, an octave spanning supercontinuum was achieved for 1100 to 2200 nm in an experiment with 600-m long silica ($SiO_2$) fiber using pulses of 200 fs duration from a mode-locked erbium fiber laser [93]. In year 2005 an experiment demonstrated supercontinuum spreading from 1000 to 2500 nm in a 5-m long highly nonlinear polarization maintaining fiber [94].

## 3.4 SCG using nonsilica fibers

Supercontinuum generation attracted immense interest of researchers not only in theoretical aspect generating a broadband spectrum as a light pulse of high intensity transverse through a nonlinear medium, also due to its several applications in different fields like the optical frequency metrology, bio-imaging and spectroscopy [13]. The SCG in a silica based photonic crystal fiber and silica fiber tapers with use of a Ti:Sapphire laser influenced the pace of research in this field [5] [9]. Fused silica ($SiO_2$) fibers are widely experimented to generate a wide bandwidth supercontinuum with high brightness ranging from near-infrared (NIR) to mid-infrared (MIR). The intrinsic transmission window of quartz silica or fused silica limits and sets challenges to expand supercontinuum more than 2.2 μm [40] which diverted selection of different types of glasses having transparent transmission windows extending in the long wavelength side. Specifically silicon (Si), tellurite, ZBLAN and the chalcogenide were explored as non-linear media for the obtaining supercontinuum geneartion. As silicon depicts high value for Kerr nonlinearity making it suitable for supercontinuum generation in nanowires designed with silicon-on-insulator (SOI) [18] [95]. In region of near-infrared (NIR) Si offers minimum losses, but suffers with free-carrier

absorption (FCA) and two-photon absorption (TPA), both these effects clench spectral broadening and limit the required bandwidth when used for telecommunication band centered at 1550 nm. The nonlinear characteristics of ZBLAN are identical to silica while tellurite and chalcogenide may offer nonlinearities much higher tahn silica. As reported that is about 30 times more in case of tellurite and thousand times much higher than silica for chalcogenide. These glasses are most suitable for SC generation and application as ultrafast nonlinear switching when the nonlinearity is integrated with sensible low two-photon absorption (TPA). The linear and nonlinear refractive indices of fluoride glasses are identical to silicon dioxide, and ZBLAN offering lower loss in mid-infrared (MIR) region as compared to silica is more suitable for SCG experiments involving high powers [96]. The glasses made up of the heavy metal oxide, to name a few bismuth oxide, tellurite and lead silicate portrays linear indices from 1.8 μm to 2.0 μm, nonlinear indices ten times higher to silica and material zero dispersion wavelengths of 2-3 μm. The nonlinearities indices of chalcogenide glasses are higher in comparison to oxide glasses, and GLS, $As_2S_3$ have linear indices in range of 2.2 μm to 2.4 μm, whereas $As_2Se_3$, GeAsSe based fibers have linear indices 2.4 μm to 2.6 μm and ZDWs for these fibers is higher than 4 μm.

The experiment in 2003, supercontinuum expanded in the range 350-1750 nm with a 30-cm long fluoride-based fiber pumped with pulses of duration 60 fs at 1560 nm with energy 210 pJ. Due to the limit set by the optical spectrum analyzer employed the observed spectra was less than 1750 nm [97]. Later in year 2006 it was observed that the spectra expanded more than this limit with an infrared HgCdTe detector was observed that it extended to 3 $\mu$m for a fiber of length 5.7 mm [98]. The photonic crystal fiber of Schott SF6 lead silicate glass having nonlinearity 10 times larger than silica with core of 2.6 μm with two different fiber lengths like 0.57 cm and 70 cm was used for an experiment. Pulses of duration 110 fs and 80 MHz repetition rate, 1.55 $\mu$m pump wavelength and powers varying in the range from 1 to 70 mW was launched and SC up to 3000 nm was obtained with 70 mW highest peak power. It was inferred from the experiment in 2006 that the broadening of supercontinuum can be increased up to 4.5 $\mu$m by combining a silica fiber of 1-m in length with a fluoride fiber of some meters in length where the strong absorption exhibited by the wavelength beyond 4500 nm [99]. The greater width in the range of 565-5240 nm bandwidth was conducted in 2009, when a fluoride of 2-cm in length fiber was

pumped at wavelength of 1450 nm with pulses of 180 fs duration with 20 mW average power levels [100].

Supercontinuum generation is also reported in microstructured fibers designed with tellurite glass. In an experiment in 2008, the supercontinuum spectrum expanded in the range 0.79-4.87 $\mu$m in a 0.8-cm long photonic crystal fiber. The spectrum calculated at the -20 dB below the maximum spectral power with pulses of duration 100 fs and energy of 1.9 nJ at 1.55 $\mu$m wavelength [101]. In same time window in another experiment with 9-cm long tellurite PCF was pumped with 120 fs pulses to obtain supercontinuum broadening from 0.9 to 2.5 nm with a high effective mode area of 3000 $\mu m^2$ [102]. Further in year 2009, SC was pumped for range varying from the visible range to range beyond 2.4 microns using a hexagonal PCF of tellurite 6-cm long using 400 fs pulses with energies up to 1557 nm of 0.6 nJ impulse [103]. In the year 2011, M. Tiwari *et al.* by numerical analysis indicated SC spanning from 1000 to 3200 nm when pumped with pulses of 50 fs at1550 nm wavelength launched into a 100 mm length of a SF57 glass fiber demonstrated anomalous dispersion around this wavelength with 5 mW peak power [104]. In 2013, A. Agarwal *et al.* reported supercontinuum spreading from 970 nm to 4100 nm by spiral photonic crystal fiber with tellurite glass pumped at 1550 nm [105]. In 2016, M. Sharma *et al.* designed a lead silicate photonic crystal fiber for SC spanning from 1200 to 2600 nm using 50 fs pump pulses of 100 W peak power at 1550 nm pumping wavelength [106].

Recently chalcogenide (ChG) glasses have attracted the attentions and interests. These glasses offer transparency in region of MIR with high optical nonlinearities in order of hundred times more than silica and similar to silica can be easily shaped to fiber form [25]. It is inferred that the chalcogenide (ChG) based fibers can be employed to as a supercontinuum source, generating wavelength greater than 5 microns, in which the propagation loss of the materials like silica, ZBLAN and tellurite become significantly high and cannot be ignored. The chalcogenide glasses are stable glasses on a wide range of compositions having chalcogen elements of S, Se, Te bonded covalently to Ge, As, and Sb [107]. The careful selection of composition offers choice to engineer its optical properties like refractive index and nonlinearity. The refractive index of ChG glasses in general is high, resulting to high non-linear refractive index as per Miller rule. In reference to design of waveguide, a high value of refractive index is advantageous as it helpful in confining light tightly in reduced effective mode area and resulting an increase in nonlinear effects. The high

index contrast also reduces the radius of curvature of the waveguide, permitting integration of photonic devices in small area compactly. The mid-infrared transparency up to 14 microns can be obtained with selenide-based chalcogenide [108]. On the other hand GeAsSe glasses have emerged as an excellent choice for waveguide design for MIR broadband SC with relatively high third order nonlinearity and excellent film-forming properties [29]. The refractive index is in range from 2.4 to 2.8, helping tight confinement of optical fields, enabling suitable (small) form factors in designing the photonic chip, reduced radius of curvature for bend radii in waveguide, along with improved optical intensity to a greater efficiency of the nonlinear interaction. The chalcogenide glass can be designed into high-quality fiber (linear loss < 1 dB/m for step-indexed fiber at wavelength 1550 nm) [109] or designed as a planar waveguide of an oxidized silicon wafer (0.05 dB/cm propagation loss) [110]. With waveguide approach, a dispersion-engineered planar waveguide was pumped with ultra short pulses. The asymmetric structure resulted in cladding absorption and cut-off of the basic mode. Thus fiber designs surpass other choices with ease of fabrication, ruggedness and the excellent beam quality [111]. The distinctive inherent characteristics of photonic crystal fibers have attracted interest. The mode area and dispersion properties can be engineered with designing suitable structural parameters. The improved non-linear effects due to tight mode confinement and and dispersion management with resulting air holes cladding structure in PCF had made them more suitable and demanding [112].

Numerous theoretical studies and related experiments on the generation of the mid-infrared SC have been reported in planar ChG waveguides [53] [113] [114] and ChG fibers [28] [111] [115] [116] [117] [118] [119] [120] [121] [122] [123] [124] [125]. It was in the year 2008, Lamont *et al.* [53] experimented generation of SC with a bandwidth of 0.75 $\mu$m for the range 1.2-1.95 $\mu$m by launching pulses of duration 610 fs , 68 W peak power in a 6-cm-long dispersion tailored $As_2S_3$ rib waveguide. Supercontinuum generation from 2.9 microns to 4.2 microns in 6.6-cm long dispersion engineered $As_2S_3$ glass rib waveguide was reported by Gai *et al.* [113] with pumping pulses of duration 7.5 ps at 3.26 μm wavelength with 2 kW peak power. SC generation up to 4.7 microns was reported by Yu *et al.* [126] with a 4.7 cm length $As_2S_3$ glass rib waveguide using $MgF_2$ as a glass substrate and pulses of duration 7.5 ps pumped with 1 kW peak power at the wavelength of 3.26 microns. Flat supercontinuum spanning for the range 2.5 microns to 7.5 microns in 5 mm thick

$Ge_{11.5}As_{24}Se_{64.5}$ glass was observed when pumped with 150 fs duration pulses at 5.3 microns wavelength with peak power up to 20 MW. It was also reported by them that theoretically the supercontinuum can be obtained over 10 microns in a dispersion-tailored $Ge_{11.5}As_{24}Se_{64.5}$ all-chalcogenide glass rib waveguide by pumping pulses with 250 fs duration at 4 microns wavelength. It is reported recently by Yu *et al.* [114] broadband supercontinuum generation spreading from 1.8 microns to 7.5 microns can be achieved in dispersion-engineered $Ge_{11.5}As_{24}Se_{64.5}$ all-chalcogenide glass rib waveguide of 1 cm length pumped at 4 microns wavelength with pulses of duration 320 fs. A periodically-poled lithium niobate optical parametric amplifier with maximum power of 3260 W, pumped from commercially available mode-locked Yb laser was used as a pump source. SC generation in all-chalcogenide glass fibers is also reported by Salem *et al.* [127]. They theoretically showed mid-infrared (MIR) supercontinuum spreading in the range 3.14 to 6.33 microns by using 8 mm length tapered $As_2S_3$ photonic crystal fiber pumped at 4.7 microns wavelength with input pulse energy of 100 pJ. Kubat *et al.* [119] demonstrated a method for supercontinuum generation in MIR region varying from 0.9 to 9 microns by employing concatenating 10 m long fluoride and 10 cm long chalcogenide fibers, pumped with pulses of duration 3.5 ps at a wavelength of 2 microns from a Tm fiber laser . Hudson *et al.* [28] demonstrated generation of 1.9-octave supercontinuum in a $As_2S_3$ step index fiber spanning from 1.6 microns to 5.9 microns when pumped 3.1 microns wavelength, with 520 kW peak power. Al-Kadry *et al.* [125] demonstrated mid-infrared supercontinuum formation for range from 1.1 microns to 4.4 microns in 10 cm length $As_2Se_3$ micro wires pumped at wavelength of 1.94 microns with pulses of duration 800 fs and 500 pJ energy. Supercontinuum for range 1.4 to 13.3 microns was generated by Petersen *et al.* [120] with 100 fs duration pulses at wavelength 6.3 microns applied to 85 mm long $As_2S_3$ step-index fiber with a core size of 16 microns. Miller *et al.* [121] used 18-cm long low-loss, $As_{38}S_{62}$ fiber with suspended core and to generate supercontinuum spreading from 1.7 to 7.5 microns by pumping pulses of duration 320 fs at wavelength of 4.4 microns with a maximum power of 5.2 kW. Recently supercontinuum spanning from 1.8 to 10 microns in a GeAsSe-based fiber of length 11-cm was reported by Yu *et al.* [128] by pumping pulses of duration 320 fs at 4 microns wavelength and 3 kW peak power. It was in the year 2015, P. S. Maji *et al.* proposed a multi-material photonic crystal fiber with highly nonlinear $As_2S_3$ chalcogenide material and borosilicate glass, and achieved SC span from 2410 to 3150

nm at pumb wavelength 2.8 $\mu$m [129]. In the same year 2015, M. R. Karim *et al*. numerically demonstrated $Ge_{11.5}As_{24}Se_{64.5}$ chalcogenide glass based PCF and achieved the SC spanning from 1.3 $\mu$m to beyond 11 $\mu$m (approximately 12 $\mu$m) using 3 kW peak power at pump wavelength of 3.1 $\mu$m for 1 cm long fiber [130].

The $As_2S_3$ based fibers and waveguides exhibit increased losses in the higher wavelength region thus limiting the supercontinuum generation to 5 microns [111] [113] [122]. The $As_2Se_3$ chalcogenide glass has its edge in the long wavelength region of about 16 to 17 microns due to the loss, but the supercontinuum generation for MIR region with these materials is so far been limited due to requirement of pump sources with peak power. [21] [120] [125]. In all chalcogenide materials, $Ge_{11.5}As_{24}Se_{64.5}$ based chalcogenide glass offers excellent film-forming properties along with good optical stability and high thermal stability to intensified illuminations [29]. As chalcogenide glass with $Ge_{11.5}As_{24}Se_{64.5}$ has transparency up to 15 microns, they have attracted interest of researchers for designing and optimizing fibers for supercontinuum generation far into the MIR region. The group-velocity dispersion and zero-dispersion wavelength are suitably engineered near to the wavelength of the pump wavelength to generate broad SC in MIR region [53] [25].

## 3.5 Summary

The sources with SC generation was known since 1970, and the basic principles explaining their operation has been theoretically predicted and demonstrated experimentally in late 1980s. It is noted that there has been a tremendous development in fiber based supercontinuum sources in the last one decade. In this chapter, we first gave a brief outline of the supercontinuum generation using bulk media using the traditional fibers. Then supercontinuum generation using silica based microstructured fibers was briefly explained. In the end supercontinuum generation with nonlinear materials other than silica like tellurite and fluoride were explained in brief. Lastly chalcogenide glasses which are highly nonlinear materials were explained. The chalcogenide glasses offer new hopes to realize compact on-chip supercontinuum generation. The material presented in this chapter gives an overview of the generation of supercontinuum and its developement with the nonlinear optical process like dynamics of supercontinuum in optical fibers.

# Chapter 4

## Mid-IR SCG in GeAsSe Chalcogenide based Microstructured fibers

It has been keen interest of researchers to design supercontinuum(SC) sources which can be functional in range of wavelengths that fall in mid-infrared (MIR) range due to its innumerable applications in the MIR sciences [131]. Initial theoretical and experimental work and studies related to supercontinuum generation was centred on the fiber geometry, especially the photonic crystal fiber wherein the dispersion can be easily tailored due to the tight confinement due to the air-holes geometry. Silica-based PCF offers a strong confinement, but due to the low nonlinearity the peak power in kilowatts is required for supercontinuum generation. It was not possible to extend supercontinuum generation in MIR with silica-based designs due to serious absorption for wavelengths above 2.2 microns. The use of highly nonlinear glasses to enhance the nonlinearity of the optical fiber has opened new avenues for research. In reference to requirement of high nonlinearity the chalcogenide (ChG) glasses have gained more attraction, as the optical nonlinearities is thousands times of that of silica, moreover chalcogenide glasses are transparent for mid-infra-red and fibers can be drawn easily with present techniques. Accordingly, chalcogenide fiber is the most suitable candidate for SC laser source above 5 microns, whereas all the other choices like silica, ZBLAN, and tellurite fibers offer a very high propgation loss in this range.

The transparency window in MIR can be reach up to 14 microns with use of selenide-based fibers [108].The GeAsSe glasses has attracted attention of researchers to design and optimize fibers of GeAsSe glasses to generate broadband supercontinuum in MIR region as they not only offer high valued offer third-order nonlinearity but also exhibit excellent film-forming property [29]. A number of experimental and theoretical studies on the generation of the MIR SC has been reported. In the results reported both planar waveguides ChG [113] [126] [114] [35] and ChG PCFs [28] [117] [118] [119] [120] [121] [128] have been reported by different groups. In one of the experimental set up the ultrashort pump pulses were launched in a planar waveguide designed with tailored dispersion. The asymmetric structure has a major drawback of cut-off of the fundamental mode and it also suffers

from cladding absorption. Due to inherited properties like ruggedness, excellent beam quality and ease of manufacturing fiber-based designs still remain the first choice [111]. The microstructured fibers (MOFs) are considered as significant optical waveguides due to its inherent modal characteristics like controllable mode area and tailored dispersion by careful designing of geometry and design parameters. The photonic crystal fibers are of special interest as they offer improved non-linear effects due to tight mode confinement and an easy management of the dispersion with careful design of air-hole geometry in cladding [112]. The chalcogenide glasses are made from series of glass compounds as $As_2S_3$, $As_2Se_3$, $Ge_{11.5}As_{24}S_{64.5}$ $Ge_{11.5}As_{24}Se_{64.5}$ and have been used for manufacturing the optical waveguide [120] [121] [128].The compound $Ge_{11.5}As_{24}Se_{64.5}$ falling in category of chalcogenide glass is reported to exhibit high third-order nonlinearity making it interesting for manufacturing photonic crystal fibers (PCFs) as laser sources for the generation of broadband supercontinuum. They offer refractive index in order of 2.6 and transparency more than 14 microns making them suitable for designing compact optical circuit waveguides for NIR and MIR range. The chalcogenide glass are attractive for all-optical signal processing, as high refractive index indicates a higher nonlinear refractive index ($n_2$) that induces ultrafast third-order (Kerr) nonlinearity in order of thousands time more than silica [25] [26] [27]. Aforesaid useful properties motivated us to design and optimize dispersion engineered chalcogenide $Ge_{11.5}As_{24}Se_{64.5}$ based PCF for broadband SC generation. Here, few more chalcogenide materials were investigated for mid-infrared supercontinuum generation. The most promising among them were Li-containing ternary compounds, $LiGaSe_2$, LiGISe ($LiGa_{0.5}In_{0.5}Se_2$), $LiGaS_2$.

This chapter gives detailed interpretations of the chalcogenide photonic crystal fibers design for generation of supercontinuum. In Section 4.1 we present a brief overview of the material properties of GeAsSe based chalcogenide glasses. Section 4.2 discusses the MIR SC generation from 1.4 to 10 $\mu$m for input pump pluse width of 85 fs of 5 kW at 3.1 $\mu$m wavelength. The PCF design and tailored dispersion curve accordingly for required SCG are also presented. In section 4.3 we discuss numerically simulated and achieved SC in MIR region (1 to 10 $\mu$m) with the $Ge_{11.5}As_{24}Se_{64.5}$ based chalcogenide PCF for input pump pluse of 3 kW at 3.1 $\mu$m wavelength. In Section 4.4 the PCF design with improved and more flat dispersion curve was achieved for the SC generation from 1 to 15 $\mu$m. In the last Section 4.5, we present the summary of the study carried out.

## 4.1 Material properties of GeAsSe ChG glasses

Chalcogenide based glasses portray few distinctive properties which makes them suitable and applicable for nonlinear waveguide optics in infrared range and due to heavy elements composition. As the name suggests the glass is made up of one or many more chalcogen element from group number 16 of the periodic table of elements (Te, Se, and S except for oxygen) making covalent bonds with Li, Gb ,As, Si ,Sb, Ge or P etc. The weak bonded heavy element is responsible for unique and important optical and physical properties. The weak energy bond is responsible for optical gaps in the visible and the near infrared along with less energy to *Tg*, moderate glass transition temperatures which varies from 100°C to 400°C. The range of optical transparency for sulphides expands to 8 microns and it extends to 14 microns in case of selenides and is reported to be greater than 20 microns for telluride is due to the weak vibrational energies of the bonds. The long wavelength transmission is limited due to presence of impurities in bulk glasses or films. As glasses are fabricated from "high purity" chemical contents which generally contain significant amounts of C, O, and H which are responsible for absorption bands in the entire range of 1.4 microns up to 15 microns. Numerous different techniques have been developed to purify the starting materials. The impurity level is reduced below $10^{-5}$% by weight, which is helpful to increase the transparency in infrared region [21] [25] [132].

The properties of chalcogenide glasses are related to their composition is reported in the literature [25] [133] [134, 135, 136], whereby researchers have shown a substantial improvement in understanding the network topology of ternary system ChG namely $LiGaSe_2$, LiGISe ($LiGa_{0.5}In_{0.5}Se_2$), $LiGaS_2$ and GeAsSe. In a recent comparative study of characteristics of GeAsSe films with bulk glass, it is proposed that composition films when formed by thermal evaporation technique are also self-organized making the chemical bonds identical as those of bulk glass [25] [137]. The ChGs films formed by highly non equilibrium process of physical vapour deposition on cooled surface, suffers with large number of molecular clusters or defect bonds. Therefore, it is customary that thin film formed by evaporation process of ChG will have different physical properties to name a few band gap, refractive index and density etc. from the bulk glass. The films created by self-organising have shown better thermal stability, thus self-organizing tendency of the networks is essential for the formation of film.

The properties of ChG have inspired the researchers to explore composition like $Ge_{11.5}As_{24}Se_{64.5}$ for fabricating optical waveguides which are thermally stable and highly nonlinear. To describe the formation of GeAsSe chalcogenide glass at the atomic level it is defined as continuous and random arranged network. The mean coordination number is an important parameter related to atomic scale structures. As per crystallography the parameter mean coordination number (MCN) is related as the sum of the products of the individual abundance and the valency of the constituent atoms. In chalcogenide glass with binary compositions like $As_2Se_3$, the As-Se network is located in two-dimensions. The layers are weakly bonded with van der Waals. The insertion of germanium doped atoms leads to a three dimensional network due to creation of bonds between the layers. This increases network rigidness, *Tg*, hardness and strength. It was reported by Gai *et al*. that the glass compositions whose MCN is in range 2.45 to 2.5 and are from intermediate phase of the GeAsSe system are most suitable glass composition for fabrication of the optical waveguides [25] [132] [137]. It was reported by them that films deposited by thermal evaporation technique in the suitable range have physical properties identical to those of bulk glass. The refractive index, band gap, density are indistinguishable from those of the bulk glass [25] [137]. It is to be noted that significantly different characteristics from bulk are obtained for films with higher (or lower) MCN. It can be concluded that properties of the films do not change on the thermal annealing in the intermediate phase and a large change can occur outside this region. It is inferred that material stability of $Ge_{11.5}As_{24}Se_{64.5}$ based chalcogenide glass is most appropriate for fabricating optical waveguides.

The waveguides designed with ChG offer almost negligible linear propagation loss due to material absorption. On reducing the waveguides size to submicron range, the losses are noteworthy. The losses due to scattering of the optical signal at the core-cladding interface can be more distinguishable in the transition regime of the tapered fiber waist. Hitherto, the loss of about 1.5 dB/cm for wavelength 1550 nm is reported for GeAsSe chalcogenide based smallest planar waveguide/nanowires fabricated with improved processes [25].For larger planar waveguides the optical losses of about 0.05 dB/cm at wavelength 1550 nm is reported [110]. This akin to the minimum loss achieved in silica based planar waveguides and signifies that it is possible to design complex circuits which require long path lengths. The absorption due to impurity in the glass films has to be tactfully regulated to preserve the optical transparency, in order to fabricate low-loss waveguides operating over wide ranges in mid-infrared

region. This necessitates the use of starting materials with highest purity to make films and processes followed during the device manufacturing [25].

To further develop more understanding about the nonlinear behaviour of the Chalcogen glasses we studied the basics of the temporal variation of the Raman response function $h_R(t)$. A comparative study was done for silica [44], $As_2Se_3$ glass [138] and $Ge_{11.5}As_{24}Se_{64.5}$ glass [139] as shown in Figure 4.1. It can be stated from the responses in Figure 4.1 that the temporal response of $Ge_{11.5}As_{24}Se_{64.5}$ glass was the longer than $As_2Se_3$ and silica. Thus the Raman response extends to 300 fs for silica material, 1000 fs for $As_2Se_3$ glass and for $Ge_{11.5}As_{24}Se_{64.5}$ glass it extended to 1400 fs.

The Raman gain spectra of the three materials in consideration are given in Figure 4.2. It is clearly observed from plots in Figure 4.2 that Raman gain of $Ge_{11.5}As_{24}Se_{64.5}$ glass is four times greater than fused silica and $As_2Se_3$ glass. Further the Raman frequency shift for the silica material (≈ 13.2 THz) [2] is greater than $As_2Se_3$ glass (≈ 6.9 THz) [33] and $Ge_{11.5}As_{24}Se_{64.5}$ glass (≈ 7.1 THz) [140].

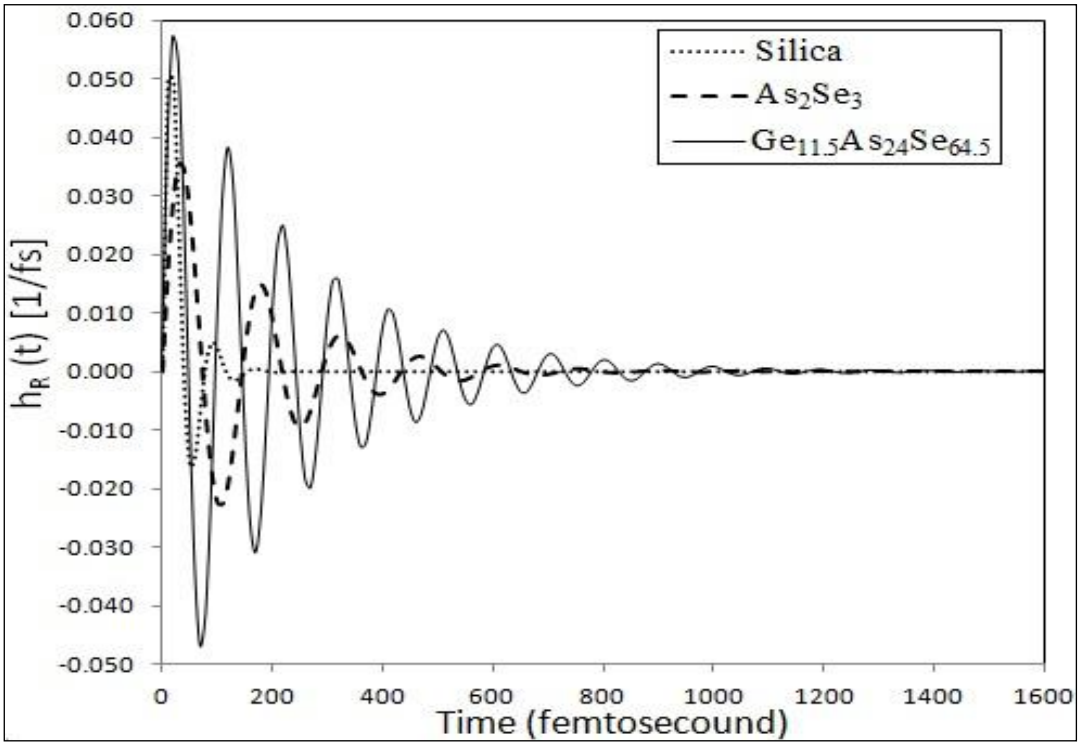


Figure 4.1. Temporal Raman response functions calculated for $Ge_{11.5}As_{24}Se_{64.5}$ glass (solid line), $As_2Se_3$ glass (dash line) and silica materials (dotted line) (Reproduced from [141]).

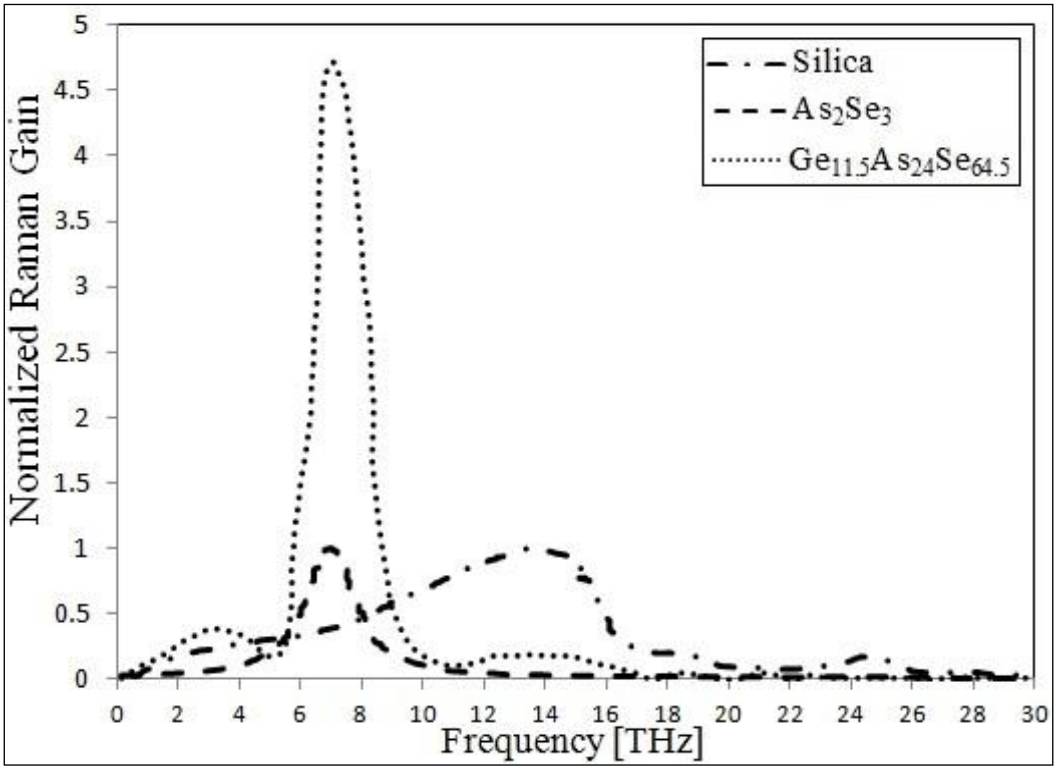


Figure 4.2. Normalized Raman gains for $Ge_{11.5}As_{24}Se_{64.5}$ glass (dotted line), $As_2Se_3$ glass (dash line) and silica materials (dash-dot line) (Reproduced from [141]).

## 4.2 SCG (1-10 $\mu$m) using GeAsSe glass for 5 kW pump pulse

In this neoteric age, photonic crystal fiber finds its application in diverse fields like communication, medical sciences, sensors and many more. PCFs are also named as microstructured fibers and holey fibers. They have microscopically arranged air holes around the core that run along the entire length of fiber that provides design pliancy for tailoring dispersion and the nonlinearity.

In comparison to silica as a base material for designing PCF, nonsilica materials can be used to obtain interesting optical properties due to the different material properties. One such important property is nonlinearity, $\gamma = 2\pi n_2/\lambda A_{eff}$, which governs spectral broadening of the optical pulses. The nonlinearity is related to effective mode area and nonlinear refractive index. The high values of nonlinearity can be achieved by tailoring effective mode area ($A_{eff}$) [2] and choosing any material having high nonlinear refractive index ($n_2$) to name a few lead silicate glass [142] [104], bismuth oxide glass [143], tellurite glass [144] [105] and chalcogenide glass [145]. With PCF designs, it is possible to obtain anomalous dispersion regime for materials offering high dispersion.

In last few years chalcogenide glasses have emerged as the most suitable nonlinear material in designing devices to be in the mid-infrared (MIR) range. The Chalcogenide materials have numerous distinctive properties and advantages over other materials, which make them most desirable for the fabricating waveguides and fibers for generation of supercontinuum (SC) in mid-infrared (MIR) region [25]. Chalcogenide glasses are useful to achieve mid-infrared (MIR) transparency with suitable materials. With the sulphides transparency can be extended beyond 8.5 μm, and with the selenides the transparency can be extended beyond 14 μm and with the tellurites it can be extended up to 20 μm [21]. The high nonlinear effective index and ease of fabricating planar waveguides and fibers with Chalcogenide glasses for supercontinuum generation (SC) in mid-infrared (MIR) region have gained interest by researchers all over. Some of the chalcogenide material like $As_2S_3$, $As_2Se_3$, $Ge_{11.5}As_{24}S_{64.5}$ and $Ge_{11.5}As_{24}Se_{64.5}$ are highly compatible for designing both active and passive devices in mid-infrared (MIR) range region. Under intense illumination, $Ge_{11.5}As_{24}Se_{64.5}$ chalcogenide material exhibits high optical and thermal stability along with excellent film-forming properties [35].

In 2010, Xin Gai, *et al* [27] fabricated a 18 mm long nanowire of size 600 × 500 nm with $Ge_{11.5}As_{24}Se_{64.5}$ material for SC generation extending from 1000 nm to 2200 nm and determined nonlinear coefficient ($\gamma$) ≈ 136 ± 7 $W^{-1}m^{-1}$ at 1550 nm (1.55 μm). In 2011, M. Spurny, *et al* [139] demonstrated designing and fabrication of photonic crystal fiber with $Ge_{11.5}As_{24}Se_{64.5}$ chalcogenide glass. In 2014, M. R. Karim, *et al* [108] reported supercontinuum broadening up to 4600 nm (4.6 μm) with numerically simulated results of five different nanowire structures with varying widths in range from 0.7 μm to 0.8 μm. In 2015, Panarit Sakunasinha, *et al* [146] reported simulation results for supercontinuum generation extending from 1300 nm to 3300 nm in a 1 cm long $Ge_{11.5}As_{24}Se_{64.5}$ waveguide with $MgF_2$ lower cladding. Further with similar design in 2015, M. R. Karim, *et al* [35] demonstrated the supercontinuum spectrum extending in the range of 1800-7700 nm.

In this section, we focus on the SCG for mid-infrared (MIR) range spreading from 1 μm to 10 μm with the highly nonlinear $Ge_{11.5}As_{24}Se_{64.5}$ based chalcogenide photonic crystal fiber. The effectuation of the entire work was carried out in two parts. In the first part, with careful selection of design parameters a $Ge_{11.5}As_{24}Se_{64.5}$ chalcogenide glass based photonic crystal fiber (PCF) suitable for MIR SCG

expanding from 1 µm to 10 µm was designed. In the next phase the designed photonic crystal fibre was simulated and to obtain SCG in desired range.

### 4.2.1 Fiber Design for pump wavelength 3.1 $\mu$m

In this section, we discuss a $Ge_{11.5}As_{24}Se_{64.5}$ based photonic crystal fiber design suitable for SCG at 3.1 µm pumping. The conventional geometry of the GeAsSe chalcogenide based hexagonal photonic crystal fiber as illustrated in Fig. 2.1 (c) in Chapter 2 was numerically investigated. In the design numerically simulated consisted of five rings of air-hole with the missing central air-hole. The wavelength dependent refractive index of $Ge_{11.5}As_{24}Se_{64.5}$ based chalcogenide material was calculated by using Sellimeier equation [29] as mentioned below.

$$n^2(\lambda) = 1 + \frac{5.78525\lambda^2}{\lambda^2 - 0.28795^2} + \frac{0.39705\lambda^2}{\lambda^2 - 30.39338^2} \quad (4.1)$$

As mentioned in previous chapters (1.2.2), a broadband supercontinuum source can be obtained by pumping pulses with sufficient power in proximity to zero dispersion wavelengths (ZDW) in the length of the fiber. Various methods have been employed to tailor and design the ZDW of $Ge_{11.5}As_{24}Se_{64.5}$ ChG glass which is located near 7.1 µm, in the direction of the shorter wavelengths [40] [117] [118]. The designs were optimized for dispersion in anomalous region. The $Ge_{11.5}As_{24}Se_{64.5}$ based chalcogenide PCF design was tailored to shift ZDW close to 3.1 µm with the pump wavelength in the anomalous dispersion region. The chromatic dispersion curve for the designed fiber is illustrated in Fig. 4.4. The cross section view of the design is presented in Figure 4.3. Here we have considered five rings hexagonal PCF structure with pitch (Λ), d/Λ, air-hole diameter (d) as 2.6 µm, 0.7, 1.82 µm, respectively.

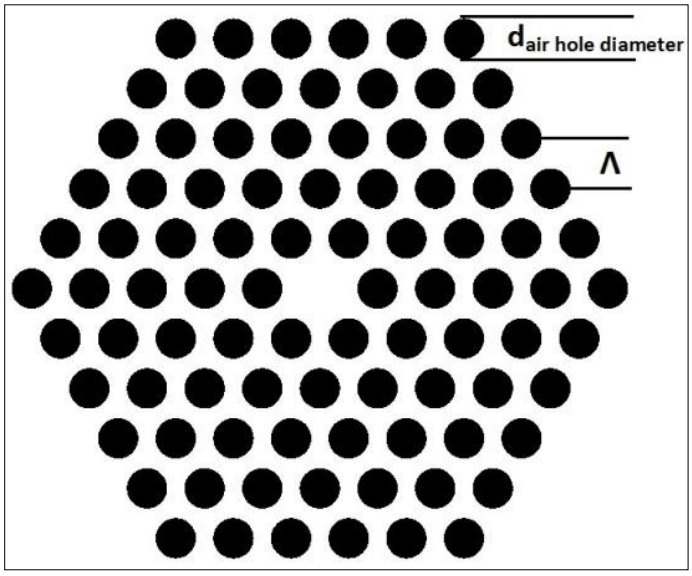


Figure 4.3 The basic layout of the $Ge_{11.5}As_{24}Se_{64.5}$ based PCF for 3.1 $\mu$m pumping wavelength and 5 kW pump pulse.

The chromatic dispersion, waveguide dispersion and material dispersion of the designed photonic crystal fiber (PCF) are shown here in Figure 4.4. By carefully choosing the pitch (Λ) and air hole diameter (d), we found a flat dispersion profile from about 2 µm to 10 µm with two zero dispersion wavelength 3 µm and 10 µm. The pumping wavelength of 3.1µm is the in anomalous dispersion regime. In Figure 4.4 the dash-dot line shows waveguide dispersion, dash line shows the material dispersion and the dotted line shows chromatic dispersion.

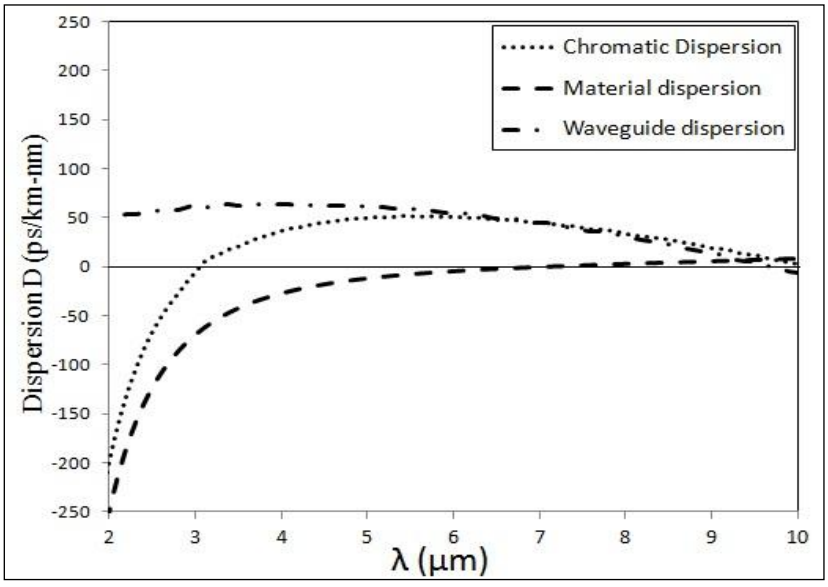


Figure.4.4 Dispersion curve of $Ge_{11.5}As_{24}Se_{64.5}$ PCF for 3.1 $\mu$m pumping wavelength and 5 kW pump pulse.

### 4.2.2 Supercontinuum Generation in proposed PCF

The split-step Fourier technique was used to estimate Generalized Nonlinear Schrödinger Equation as described in Chapter 2. We numerically simulated SC in a 150 mm long fiber with 3.98 $\mu m^2$ effective mode area ($A_{eff}$) and nonlinear coefficient ($\gamma$) as 2191 $W^{-1}km^{-1}$, by pumping sech optical pulses at 3.1 µm wavelength. The pumping in anomalous regime results in spectral broadening towards longer wavelength side due to solitons fission and the Raman soliton self-frequency shift. In the beginning, the modulation instability is responsible to initiate the spectral broadening. Later, spectral broadening is caused by Self-Phase Modulation (SPM), intrapulse Raman scattering and four-wave mixing (FWM) along with higher order dispersion. The pulse duration is 85 fs (FWHM), propagation loss ($\alpha$) is 0.5 dB/cm [35] and peak power is 5 kW were the set parameters used in the numerical simulation. The spectral escalation for different lengths has been displayed in Figure 4.7.The SC spectral broadening in the range from 1.4 µm to 10 µm was observed for the 150 mm long fiber. Figure 4.5 & 4.6, depict the density plot of spectral and temporal broadening.

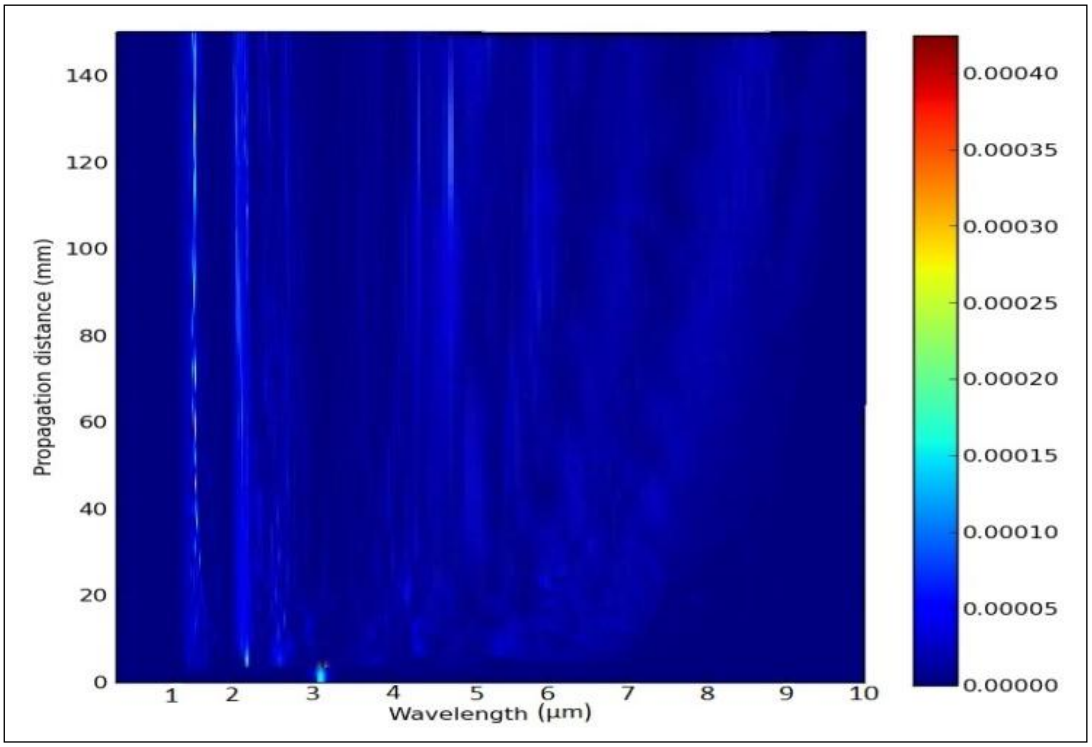


Figure 4.5 Spectral escalation of SC in PCF by pumping 85 femtosecond pulse of 5 kW peak power.

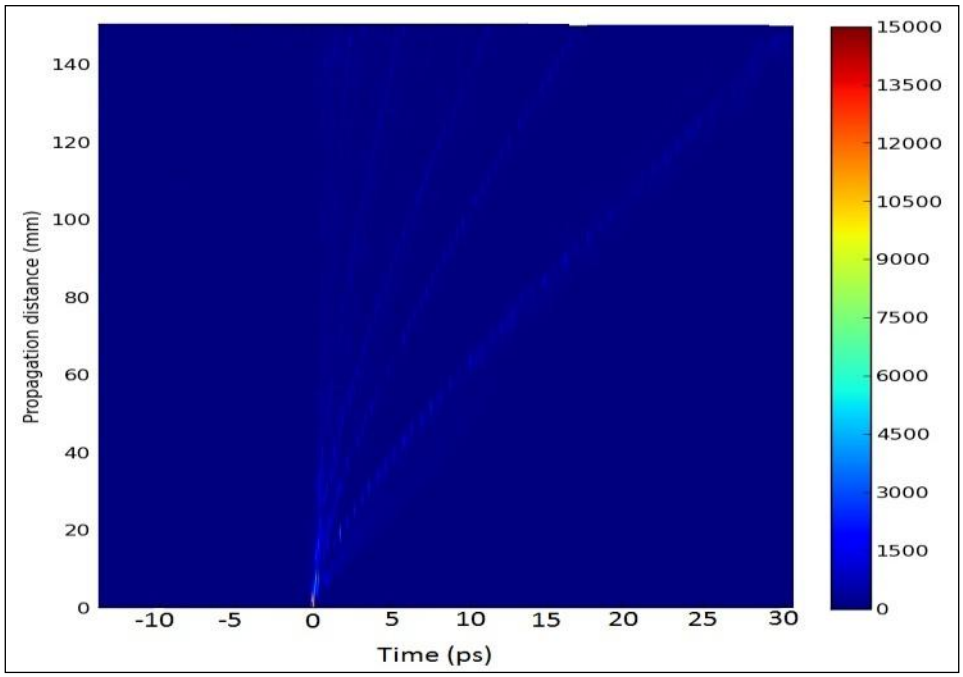


Figure 4.6 Temporal escalation of SC in PCF by pumping 85 femtosecond pulse of 5 kW peak power.

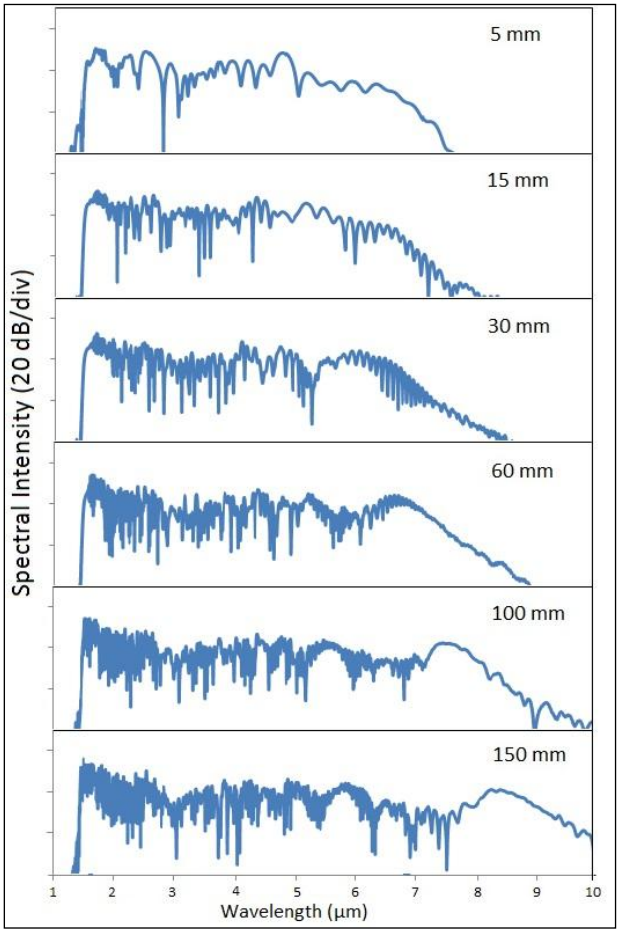


Figure 4.7 Spectra of SC for different lengths, 5 kW peak power.

### 4.2.3 Results and discussions

In this section, we demonstrated supercontinuum generation in 150 mm long $Ge_{11.5}As_{24}Se_{64.5}$ glass based solid core photonic crystal fiber with hexagonal cladding of air holes. A photonic crystal fiber was designed for achieving flat dispersion from 2 µm to 10 µm. The estimated values for effective area ($A_{eff}$), nonlinear coefficient ($\gamma$), and chromatic dispersion ($D_c(\lambda)$) at the 3.1 µm wavelength were 3.98 $\mu m^2$, 2191 $W^{-1}$ $km^{-1}$, and 5 ps/km/nm, respectively. Supercontinuum spectra extending from 1.4 µm to 10 µm was obtained by using 85 femtosecond pump pulses of 5 kW peak power at the wavelength 3.1 µm in the numerical simulation.

## 4.3 SCG (1-10 $\mu$m) using GeAsSe glass for 3 kW pump pulse

As reported that high nonlinear coefficients and flat dispersion are desirable to obtain SCG in MIR region. In the work carried out, the effect of geometry on nonlinear coefficient and dispersion was studied. It was observed that the air-hole diameter

variation play a significant role effecting the nonlinear coefficient and dispersion. The designs were investigated and further optimized by varying air-hole diameter to obtain flat dispersion and low values of effective mode area which resulted in high valued nonlinear coefficient. The observations of this section were incorporated in the work carried out in previous section and resulted in a optimized design to generate SC in 1-10 $\mu$m with reduced pump energy of 3 kW.

### 4.3.1 Fiber Design for 3kW input pump pulse

The $Ge_{11.5}As_{24}Se_{64.5}$ based chalcogenide photonic crystal fiber is the best choice for supercontinuum generation due to its high nonlinearity refractive index ($n_2$). We have designed a $Ge_{11.5}As_{24}Se_{64.5}$ based PCF which is suitable for SCG at 3.1 μm pumping. The proposed designs were carefully tailored to achieve the desired dispersion characteristics. The cross section view of the designs has been displayed in Figure 4.8 (a, b & c). All the PCF designs discussed in this section consist of five rings. The three different design of the photonic crystal fibers are denoted as PCF-1, PCF-2, PCF-3 in this section. The different design parameters with the values are tabulated in Table 4.1.

Table 4.1: Designing parameters of PCF for 3kW input pump pulse.

| **Chalcogenide glass ($Ge_{11.5}As_{24}Se_{64.5}$)** | **Number of Rings** | **Pitch (Λ)** | **$d_1$/ Λ** | **$d_2$/ Λ** | **$d_3$/ Λ** | **$d_4$/ Λ** | **$d_5$/ Λ** |
|---|---|---|---|---|---|---|---|
| PCF-1 | 5 | 2.5 μm | 0.7 | | | | |
| PCF-2 | | | 0.7 | 0.8 | | | |
| PCF-3 | | | 0.7 | 0.8 | | 0.9 | |

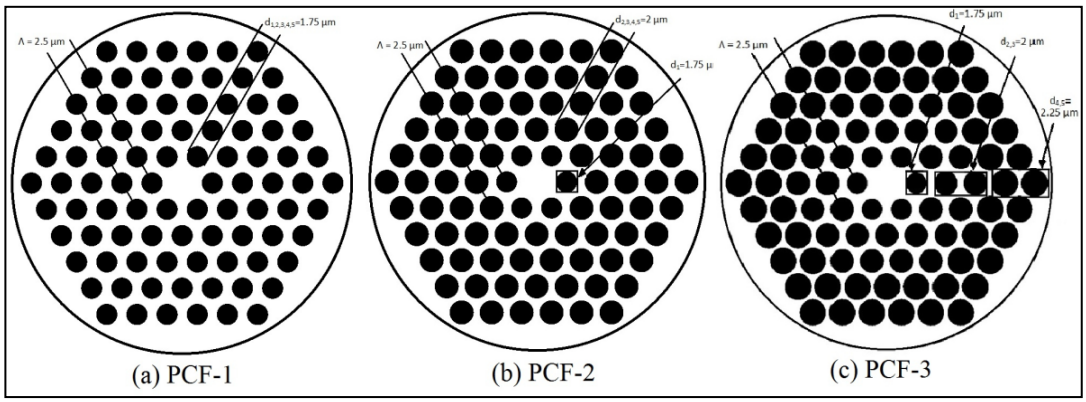


Figure 4.8 The structure of the hexagonal PCFs for 3 kW input pump pulse

In view to obtain dispersion curve for the range of wavelengths, firstly we calculated the effective refractive index ($n_{eff}$) of the fundamental mode of the PCF for the same range of wavelengths as drawn in Figure 4.9. The Figure 4.9 is helpful to understand the effect of variation pitch and air hole on the effective refractive index ($n_{eff}$). In all the three designs under discussion consists of same number of five rings and a constant pitch ($\Lambda$ = 2.5). The diameter of air-holes is denoted as $d_i$ where, i denotes the ring number. In PCF-1 $d/\Lambda$=0.7, PCF-2 $d_1/\Lambda$=0.7 and $d_{2,3,4,5}/\Lambda$=0.8, PCF-3 $d_1/\Lambda$=0.7, $d_{2,3}/\Lambda$ =0.8 and $d_{4,5}/\Lambda$=0.9. With Figure 4.9 we can draw the inference that the effective refractive index ($n_{eff}$) decreases on increasing the diameter of air holes. It can be inferred that increased air hole diameter reduces the index contrast between core and cladding and thus results in reduced effective refractive index [147].

The variation in chromatic dispersion of the fiber with wavelength of the three proposed designs has been plotted in Figure 4.10. By careful selection of design parameters like pitch ($\Lambda$) and air hole diameter (d), a flat dispersion curve from about 2.7 µm to 10 µm with two zero dispersion wavelengths (ZDW) was obtained. It is reported that SCG can be maximized with a low and flat dispersion profile. It can reduce the temporal walk-off effect at the time of spectral boarding process [141]. The pump wavelength of 3.1 µm lies in the anomalous dispersion region for all three PCFs. In Figure 4.10, the black solid line represents the material dispersion of $Ge_{11.5}As_{24}Se_{64.5}$ glass. It is to be noted, in Figure 4.9 the value of $n_{eff}$ is consistently decreased from PCF-3 to PCF-1. In Figure 4.10, the chromatic dispersion curve for PCF-3 was more flat in comparison to other two. It could develop the understanding that on decreasing $n_{eff}$ the dispersion curve can be made more flat. The dispersion parameters ZDWs of three PCFs are tabulated in Table 4.2.

Table 4.2: The dispersion parameters of three PCFs

| **Chalcogenide Crystals ($Ge_{11.5}As_{24}Se_{64.5}$)** | **ZDW-1** | **ZDW-2** |
|---|---|---|
| PCF-1 | 2.85 µm | 8.9 µm |
| PCF-2 | 2.87 µm | 9.5 µm |
| PCF-3 | 2.7 µm | 10 µm |
| Material Dispersion | 7.1 µm | ----- |

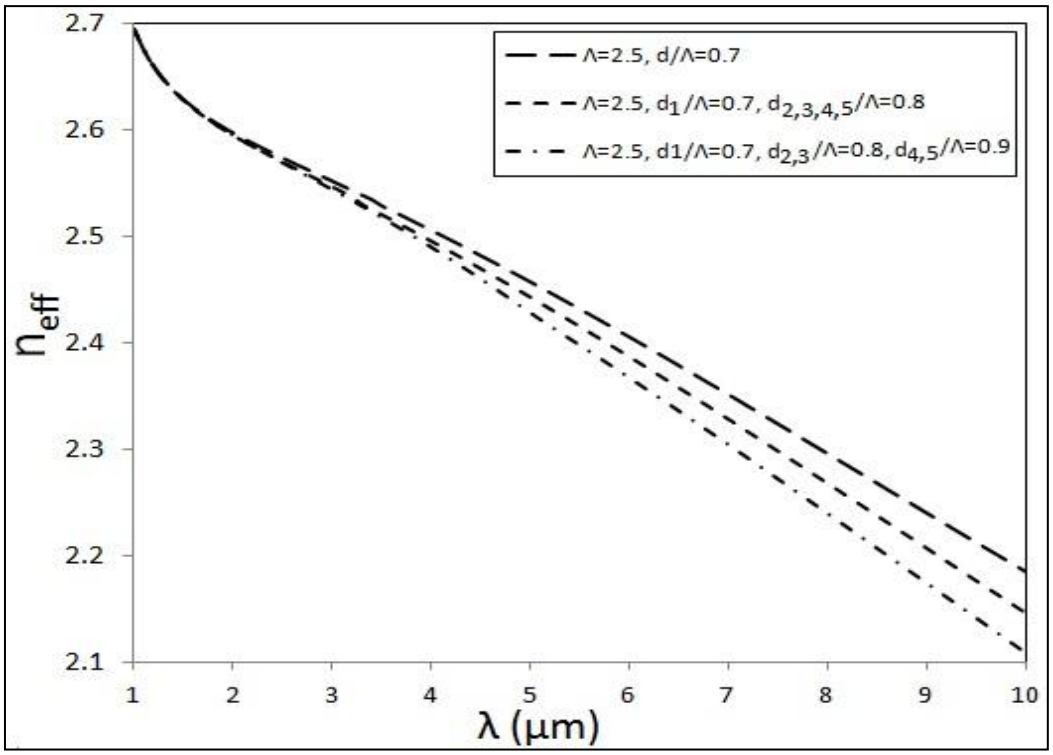


Figure 4.9 Effective refractive index of PCFs

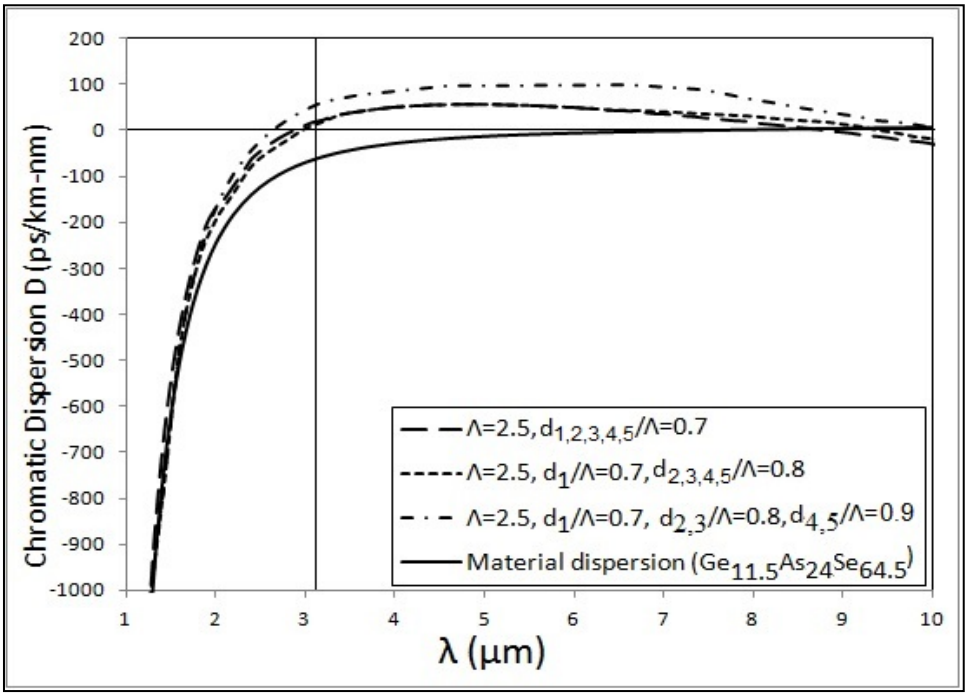


Figure 4.10 The chromatic dispersion curve PCFs

### 4.3.2 Supercontinuum Generation in proposed PCF

The GNLSE is solved by the split-step Fourier method. We have taken 100 mm long PCF. As the dispersion curve of PCF-3 matched closely to the desired dispersion

curve it was simulated for SCG. In the numerical simulation, sech optical pulses at pump wavelength 3.1 μm were pumped in the fiber. The calculated effective area ($A_{eff}$) was 3.7634 $\mu m^2$, the nonlinear coefficient ($\gamma$) was 2317 $W^{-1}$ $km^{-1}$ and confinement loss was $-1.5209\times10^{-7}$ dB/km at pump wavelength 3.1 μm. The pumping wavelength 3.1 μm exists in anomalous dispersion region with flat dispersion extending from 2.7 μm to 10 μm. In the anomalous regime, the primary broadening originates from four-wave mixing. Further propagation increases the spectral broadening in the long-wavelength region. This is mainly caused by Raman soliton self-frequency shift and soliton fission, as well as by generation of dispersive waves on the short-wavelength side of the zero dispersion wavelength points, which eventually merge to a broad supercontinuum spectrum [141]. The pulse duration is 85 fs (FWHM) and peak power is 3 kW. The spectral spans of SCG in the $Ge_{11.5}As_{24}Se_{64.5}$ PCF-3 are shown in Figure 4.11 and spectral escalation for different lengths has been displayed in Figure 4.12.

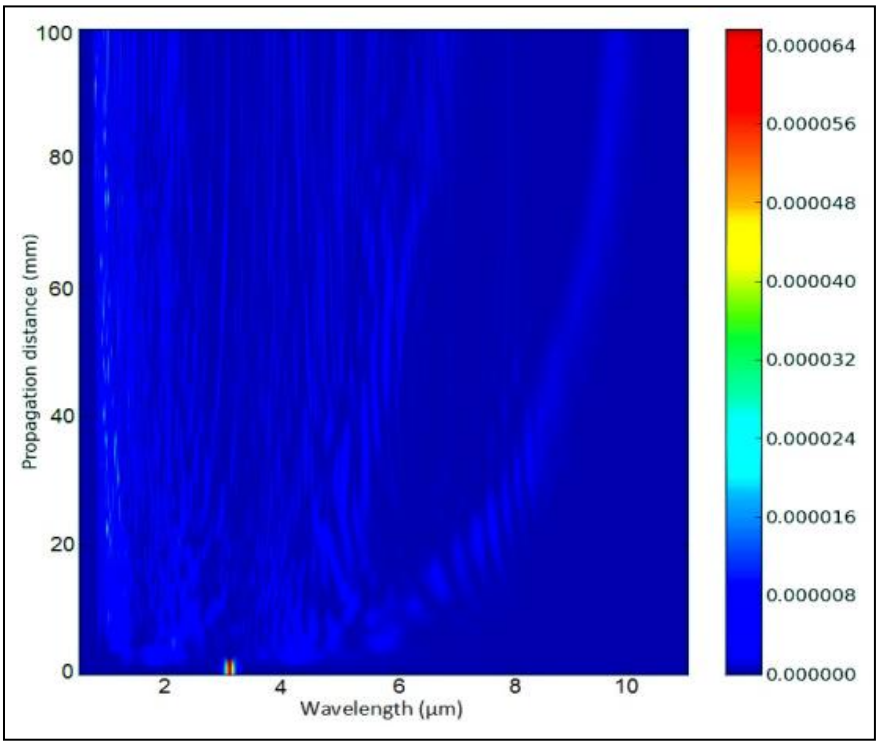


Figure 4.11 Spectral escalation of SC in PCF-3 with 3 kW input pump pulse.

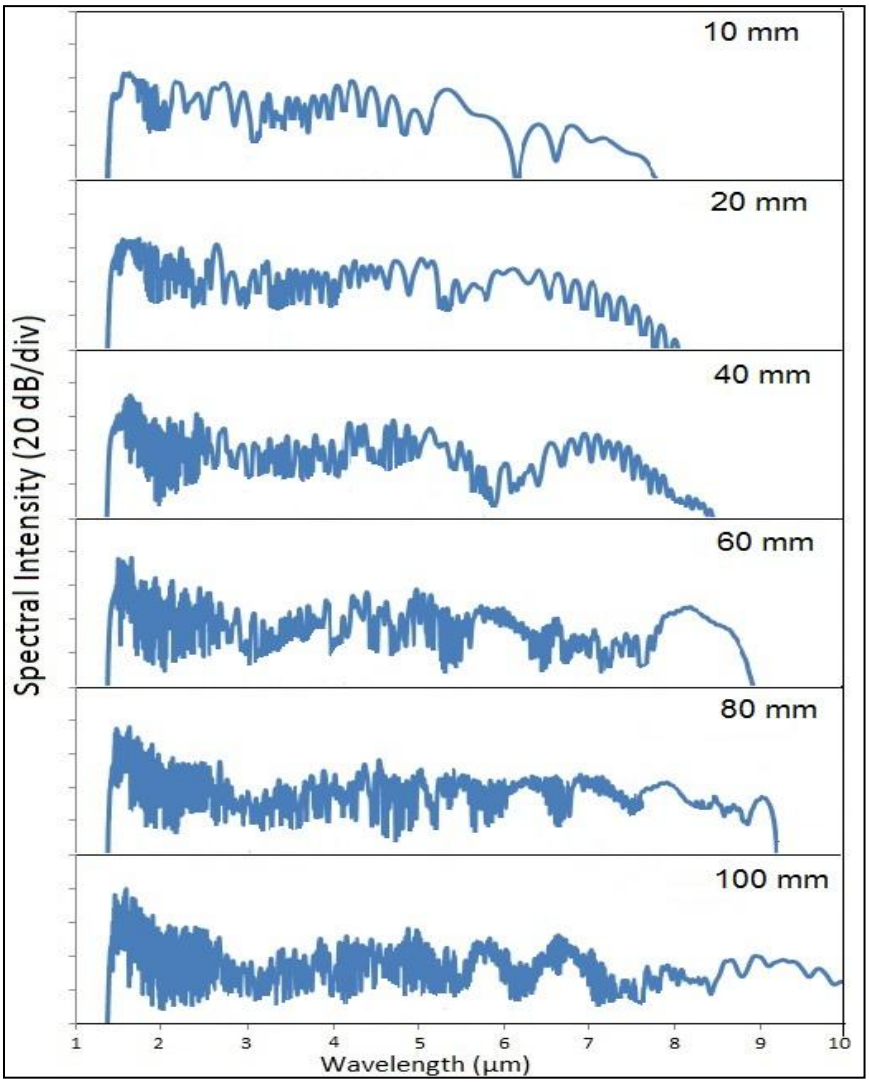


Figure 4.12 Spectra of SC for different lengths, 3 kW pump pulse

### 4.3.3 Results and discussions

In this section, we demonstrated supercontinuum generation in 100 mm long $Ge_{11.5}As_{24}Se_{64.5}$ glass based solid core PCF with hexagonal cladding of air holes. We have designed three PCFs to achieve a flat dispersion from 2 μm to 10 μm. With the design PCF-3 matched perfectly our requirements. The parameters effective area ($A_{eff}$), nonlinear coefficient (γ), and dispersion at the 3.1 μm wavelength (λ) for the design were calculated as 3.7634 $\mu m^2$, 2317 $W^{-1}$ $km^{-1}$and 52 ps/km-nm, respectively. The photonic crystal fiber design was also numerically simulated for supercontinuum generation spreading from 1 μm to 10 μm using 85 fs pump pulses of 3 kW peak power at a wavelength 3.1 μm.

## 4.4 SCG (1-15 $\mu$m) using GeAsSe glass

In the previous section, we proposed a PCF with $Ge_{11.5}As_{24}Se_{64.5}$ based chalcogenide glass that enables us to extend the SC up to 10 μm. In this section, we investigated photonic crystal fiber design to achieve underlined improvements

(1) A flat dispersion below 100 ps/km-nm.
(2) Two ZDW at 2.9 μm and 13.1 μm.
(3) Ultraflat supercontinuum generation ranging from 1 μm to 15 μm.

### 4.4.1 Fiber Design for SCG (1-15 $\mu$m)

We have designed a $Ge_{11.5}As_{24}Se_{64.5}$ based PCF which is suitable for SCG at 3.1 μm pumping. In this section, we have improved our previous design to achieve a better flat dispersion profile. In our proposed design, the pitch and air-hole diameter were carefully tailored to obtain the dispersion characteristics. The cross section view of the designed fiber has been displayed in Figure 4.13. It is to be noted from the electric field distribution of propagating mode as shown in Figure 4.14 that proposed fiber is a single mode fiber.

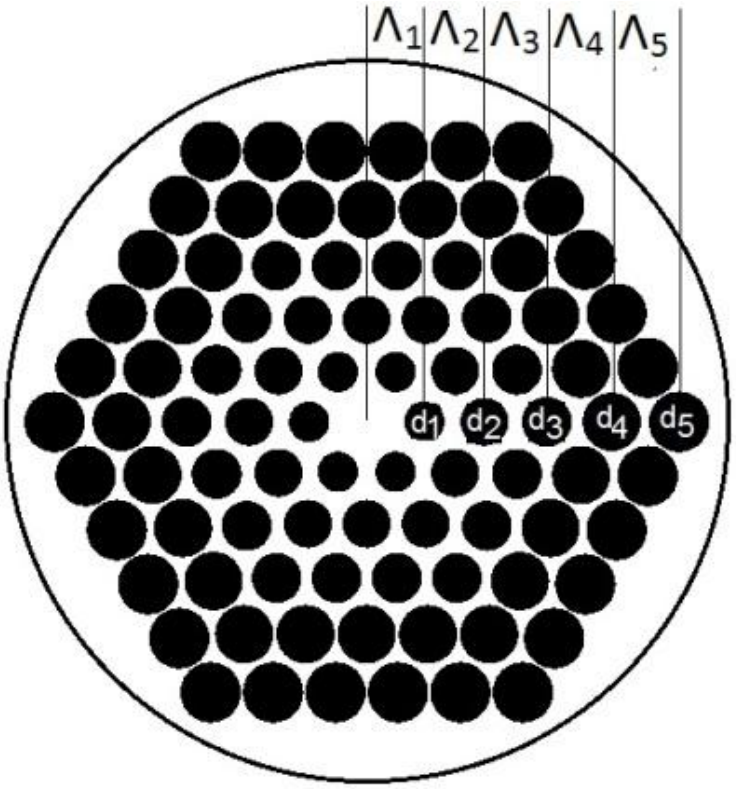


Figure 4.13 The structure of the hexagonal PCF for 1 to 15 $\mu$m SCG

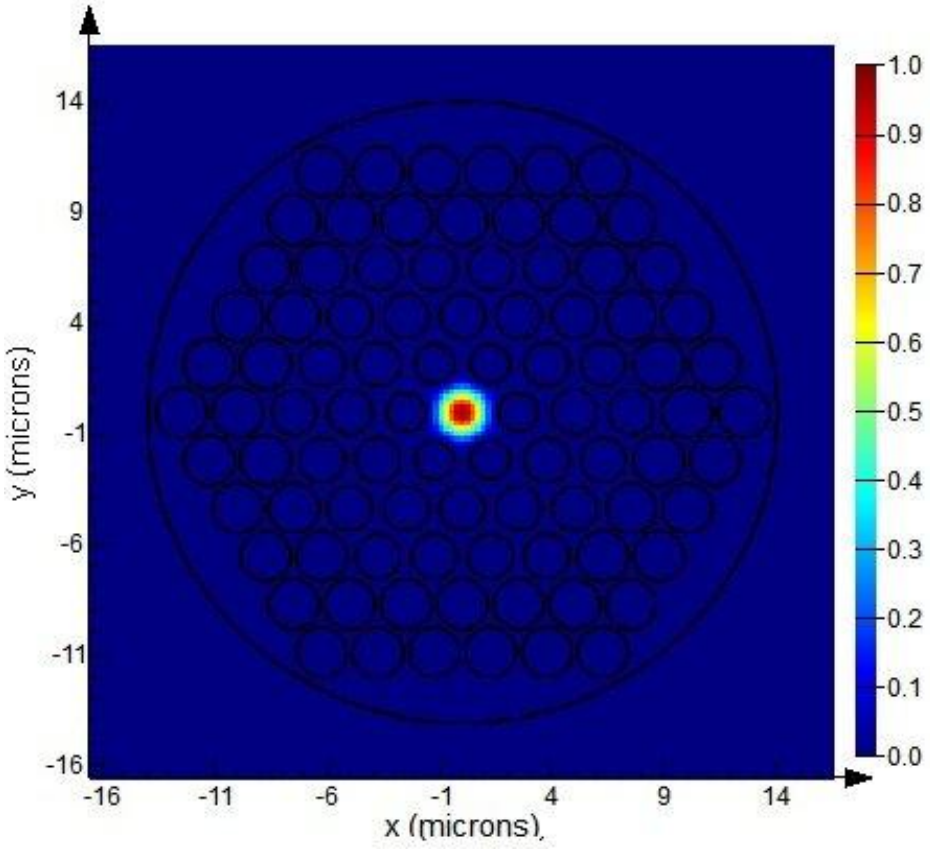


Figure 4.14 The electric field distribution of propagating mode at 3.1 μm.

The designed PCF consists of five ring air-hole structure. The pitch was linearly increased moving towards the outer ring from $\Lambda_1$ to $\Lambda_5$, and the diameter of air-holes in a particular ring is represented by $d_i$ where, i represent the ring number. The value of $\Lambda_1$ to $\Lambda_5$ and $d_1/\Lambda_1$ to $d_5/\Lambda_5$ are tabulated in Table 4.3.

The variation in chromatic dispersion in accordance to the wavelength of the proposed design fiber has been plotted in Figure 4.15. A flat dispersion profile from about 2 μm to 15 μm with two ZDW, at 2.9 μm and 13.1 μm were obtained by adjusting the pitch ($\Lambda$) and air hole diameter (d). The pitch was linearly increased in outward direction keeping the smallest pitch in inner most ring to maintain minimized effective area ($A_{eff}$) and flat dispersion profile from longer wavelength side. SCG can be maximized by achieving a low and flat dispersion profile. The pump wavelength of 3.1 μm is in the anomalous dispersion region. It can reduce the temporal walk-off effect at the time of spectral broadening process [141]. In Figure 4.15 the black solid line shows the material dispersion, dash line shows the chromatic dispersion and the dash-dot line shows the $\beta_2$ of proposed PCF.

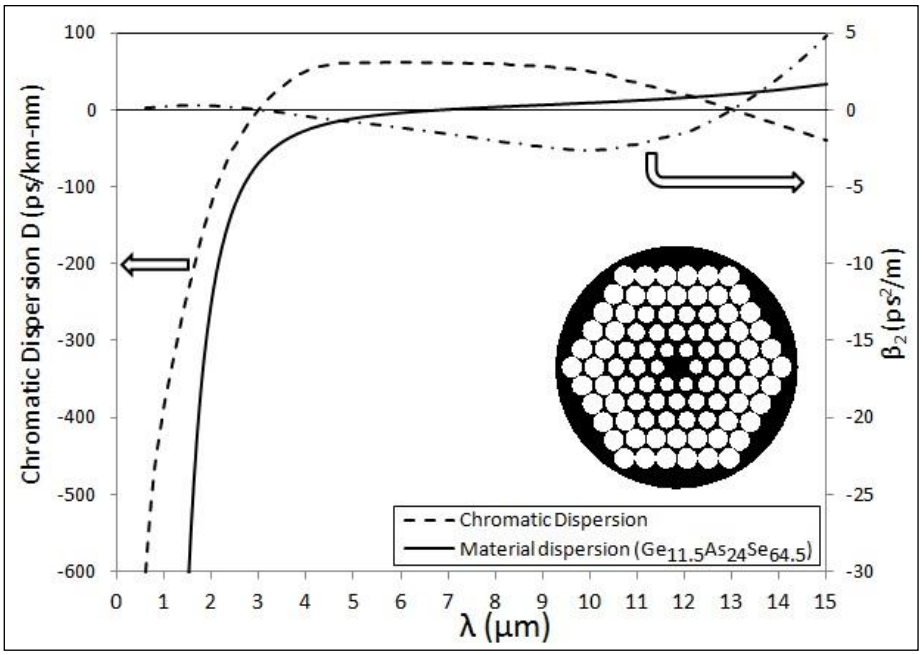


Figure 4.15 The dispersion curves of purposed $Ge_{11.5}As_{24}Se_{64.5}$ glasses PCF to SCG (1-15 $\mu$m).

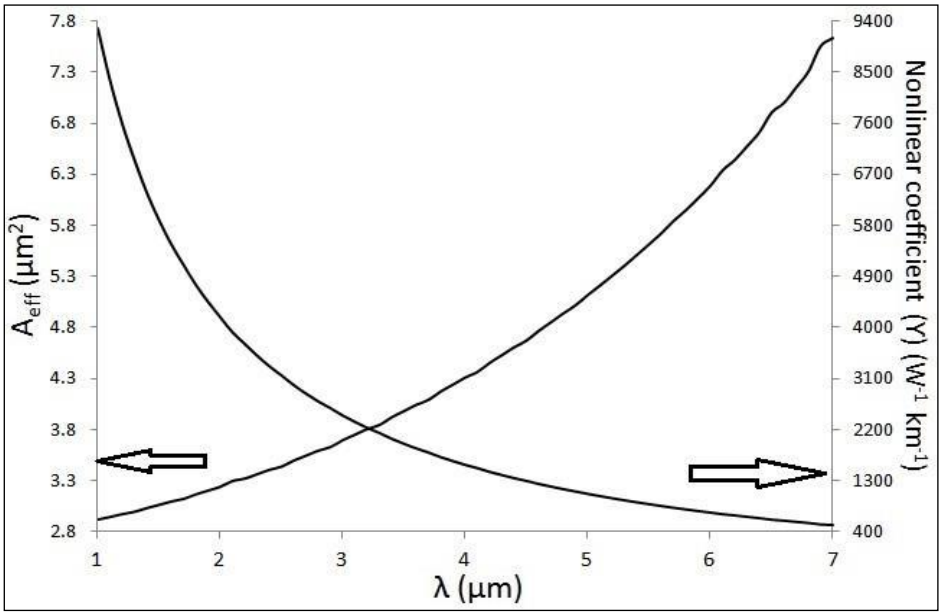


Figure 4.16 The effective area and the corresponding nonlinear coefficient for SCG (1-15 $\mu$m).

The wavelength dependent effective area ($A_{eff}$) of propagating mode and suitable nonlinear coefficient ($\gamma$) has been illustrated in Figure 5.16. Numerically calculated

values of the effective area ($A_{eff}$) and nonlinear coefficient ($\gamma$) are 3.5241 $\mu m^2$ and 2474 $W^{-1}$ $km^{-1}$.

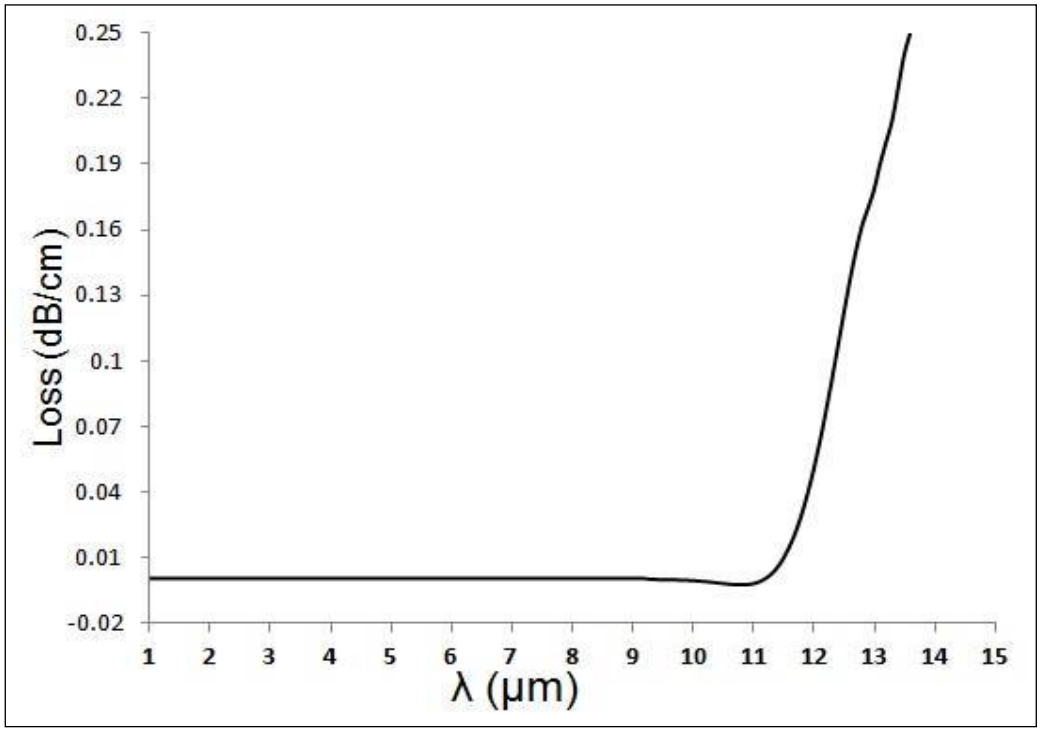


Figure 4.17 The confinement loss of propagating mode of proposed fiber for SCG (1-15 $\mu$m).

Table 4.3: Designing parameters of PCFs

| Chalcogenide glasses ($Ge_{11.5}As_{24}Se_{64.5}$) | Rings | $\Lambda_1$ | $\Lambda_2$ | $\Lambda_3$ | $\Lambda_4$ | $\Lambda_5$ | $d_1/\Lambda_1$ | $d_2/\Lambda_2$ | $d_3/\Lambda_3$ | $d_4/\Lambda_4$ | $d_5/\Lambda_5$ |
|---|---|---|---|---|---|---|---|---|---|---|---|
| PCF | 5 | 2.4 | 2.5 | 2.6 | 2.7 | 2.8 | 0.7 | 0.8 | 0.8 | 0.9 | 0.9 |

In Figure 4.17, confinement loss of photonic crystal fiber is plotted corresponding to range of wavelength. As $Ge_{11.5}As_{24}Se_{64.5}$ is the low−loss material [148], the confinement loss and propagation loss at 3.1 pump wavelength was $3.65\times10^{-10}$ dB/m and 0.68 dB/m respectively. For the proposed photonic crystal fiber, the confinement loss is meaningful at long wavelengths above ~11 μm.

### 4.4.2 Supercontinuum Generation in proposed PCF

The GNLSE is solved by the split-step Fourier method. The designed PCF was numerically investigated to generate supercontinuum in designed PCF by pumping sech optical pulses at 3.1 μm wavelength. The typical value of the calculated effective area ($A_{eff}$) was 3.5241 $\mu m^2$ and nonlinear coefficient ($\gamma$) was 2474 $W^{-1}$ $km^{-1}$ at pump wavelength 3.1 μm. The pumping wavelength 3.1 μm lies in anomalous dispersion regime. The PCF results in flat dispersion curve from 2 μm to 15 μm as shown in Figure 5.15. The anomalous regime pumping increases spectral broadening in long wavelength side which is mainly caused by solitons fission and Raman soliton self-frequency shift. The initial broadening happens because of four-wave mixing. After that, further propagation increases the spectral broadening in long wavelength side mainly caused by Raman solution self-frequency shift and soliton fission, along the generation of the analogous dispersive waves on the short-wavelength side of the ZDW, which finally merges to generate a broader SC spectrum [141]. The extraordinary broadening is possible in the anomalous dispersion regime mainly due to soliton dynamics. In the soliton fission, the input pulse splits up into a series of sequential soliton pulses, each pulse exhibiting its unique temporal and spectral properties that are highly susceptible to pump pulse shot noise [149].

The pulse duration is 85 fs (FWHM) with 160 kHz repetition rate [150] [151], input peak power is 3 kW. The spectral spans of SCG in the PCF with peak powers 3 kW are shown in Figure 5.18. The spectral escalation of the 3 kW input pulse for different lengths has been displayed in Figure 5.19. It is noticeable in Figure 5.18 that SC spectral broadening is from 1 μm to 15 μm. The spectral power density at the end of the fiber is 74.67 mW/nm (average).

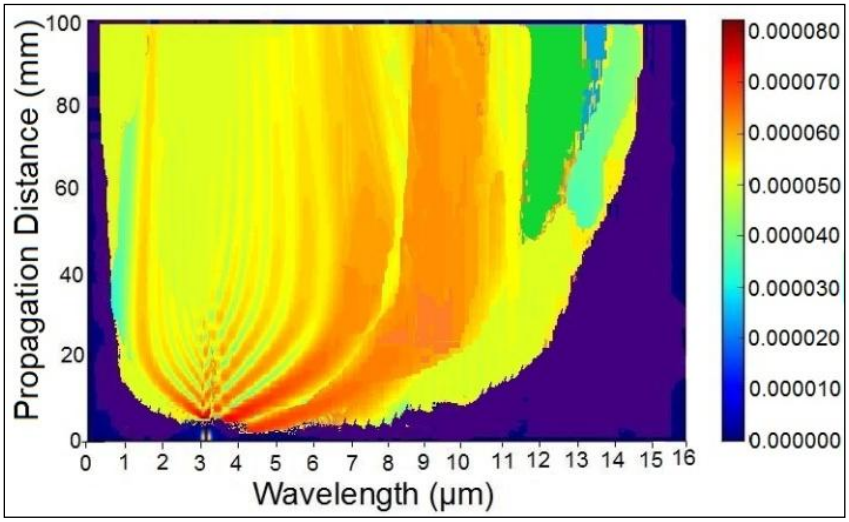


Figure 4.18 Spectral escalation of SC in PCF (spectral intensity in dB, scale bar on the right).

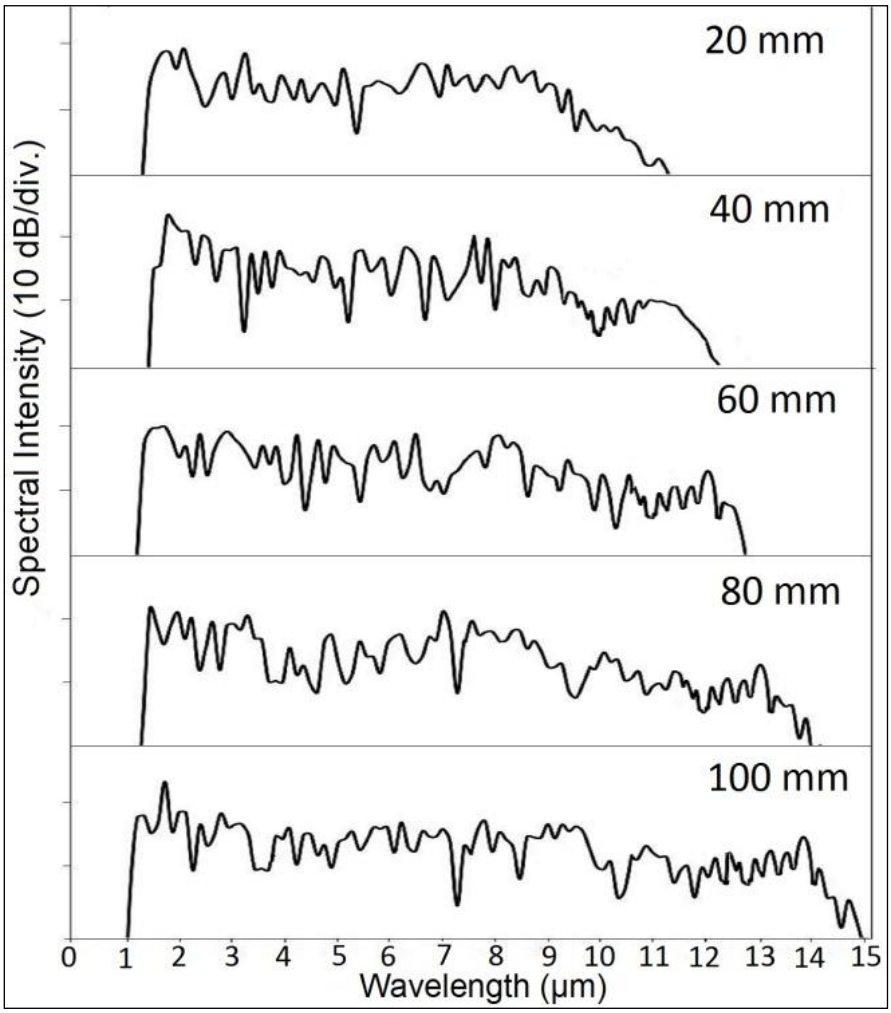


Figure 4.19 Spectra of SC for different lengths for SCG (1-15 $\mu$m).

### 4.4.3 Results and discussions

In this section, we numerically simulated supercontinuum generation in 100 mm long $Ge_{11.5}As_{24}Se_{64.5}$ glass based solid core PCF with hexagonal cladding of air holes. We have designed a PCF to achieve a flat dispersion from 2 μm to 15 μm. The typical values of accomplishable effective area ($A_{eff}$) ,nonlinear coefficient (γ) and dispersion at the 3.1 μm wavelength (λ) are 3.5241 $\mu m^2$, 2474 $W^{-1}$ $km^{-1}$ and 8.014 ps/km/nm, respectively. The PCF was numerical simulated for supercontinuum generation using pump pulses of power 3 kW at wavelength 3.1 μm and 85 fs pulse duration.The supercontinuum bandwidth extending in range from 1 μm to 15 μm for 3 kW peak power was achieved.

## 4.5 Summary

In this chapter, with numerical simulations we demonstrated generation of ultrabroadband supercontinuum spectra with dispersion tailored $Ge_{11.5}As_{24}Se_{64.5}$ chalogenide based microstructured optical fibers for mid-infrared region. Firstly a conventional PCF designed with $Ge_{11.5}As_{24}Se_{64.5}$ glass was simulated and optimized to obtain required dispersive characteristics with careful selection of design parameters. Supercontinuum spectrum spreading in range from 1.4 μm to 10 μm was achieved by pumping pulses with peak power of 5 kW at the 3.1 μm wavelength. In this case, effective area ($A_{eff}$) ,nonlinear coefficient (γ), and chromatic dispersion ($D_c(\lambda)$) at the 3.1 μm wavelength were 3.98 $\mu m^2$ , 2191 $W^{-1}$ $km^{-1}$and 5 ps/km/nm, respectively. In the second case, we improved our PCF design by varying the diameter of air holes with a constant value of pitch in aim to reduce the input power. In our research work in this chapter we proposed three different designs to observe effects on effective refractive index ($n_{eff}$) and chromatic dispersion. In this segment, we successfully reduced the value of the effective mode area ($A_{eff}$) and increased value of the nonlinear coefficient (γ) which is an essential requisite of SCG. The effective area ($A_{eff}$) calculated was 3.7634 $\mu m^2$ and the nonlinear coefficient (γ) was determined as 2317 $W^{-1}$ $km^{-1}$ at pump wavelength 3.1 μm. The design resulted SC spectrum for range 1 to 10 μm with the pump pulse 3 kW. As reported by M. Karim [130] the SC spectrum expanded in range from 1.3 to 11 μm with pump power of 3 kW. Our proposed design demonstrates significant improvement with the SC spectra expanding in range from 1 to 15 μm for same pump power. We obtained a flat dispersion profile

from about 2 μm to 15 μm with two ZDW, 2.9 μm and 13.1 μm and effective mode area ($A_{eff}$) and nonlinear coefficient ($\gamma$) are 3.5241 $\mu m^2$ and 2474 $W^{-1}$ $km^{-1}$. The design proposed demonstrates significant improvement in SC generation resulting in broad spectra with reduced pump power.

# Chapter 5

## MID-SCG by Multi-material PCF

In this section, we report that all anomalous, ultra-flat, two-zero dispersion profile can be obtained by the photonic crystal fiber structure with background $As_2S_3$ and replacing the first internal ring and center air holes by borosilicate glass. With the introduction of borosilicate internal air holes in the ring resulted in change in the effective index helping us to obtain desired dispersion profile keeping diameter of both air –hole and borosilicate rods identical.

The production of that kind of chalcogenide PCF with multi-material composition will be of extreme interest because there are several factors for this design. It is difficult to keep PCF parameters along the length of the fiber. Moreover, problems may occur such as the preparation of stable stoichiometric compounds glass, low loss, stable, for proper control of the viscosity between the different glasses involved in the stretching temperature of the fibers, and much more. It can be highlighted that however there is a big difference in glass transition temperature (Tg) of the two glass systems identified in our design modeling, a complimentary (however less difference in values of Tg) argument occurs for borosilicate glass and silica glass frequently used in polarization maintaining fibers manufacture, that can be solved by right choice of fiber drawing temperature and concentration of the impurities like boron [152]. For the manufacture of this type of multi-material optical fiber, it is not only Tg but also the viscosity and the thermal expansion coefficients of the constituent glasses that also play a role. We have to use a variety of techniques for such multi-material [153] [154] [155]. A nowadays developed approach based on pressure-assisted melt-filling technique is also useful to produce the similar fibers [156] [157]. This combination of certain material has also been proposed by different research groups [158]. Furthermore, to manufacture several chalcogenide PCFs, we already have well-matured manufacturing technologies [21] [159] [160] [161].

In 2015, Maji *et al*. [129] purposed a similar design of PCF for SCG in mid-IR range. With the design, Maji observed all-normal flattened dispersion of −0.087 ps/nm/km around the wavelength of 2.8 μm and SCG for the bandwidth of 740 nm in

the mid-IR region. Here, in this section improved the PCF design and achieved dispersion curve in the anomalous dispersion region. Our optimized designed is suitable for 1.6 μm to 4.2 μm SCG bandwidth with pump wavelength at 2.5 μm.

This chapter, the sequence is under mentioned. Section 5.1.1 concisely investigates the modal properties of $As_2S_3$ and borosilicate based multi-material chalcogenide photonic crystal fiber. We have solved the second-order sellmeier equation for material and a full modal analysis of the optical parameters of photonic crystal fiber to calculate refractive index, the chromatic dispersion ($D_c$), effective area ($A_{eff}$) and nonlinear coefficient ($\gamma$). In Section 5.1.2, we present results on supercontinuum generation in few millimeters (mm) of multi-material photonic crystal fiber with different input pulses. The generalized nonlinear Schrödinger equation is used to examine supercontinuum generation.

## 5.1 Multi-material PCF Design

Here, a new idea is proposed to obtain high refractive index by the replacement of the air holes with material from a series of high refractive index. To obtain this tailored application, particular fiber designs for mid-IR applications, we have considered an arsenic sulfide ($As_2S_3$)-based photonic crystal fiber structure which consists of four rings with hexagonal geometry. In all the four cladding rings, the inner air-hole ring and center air-hole are replaced with borosilicate rods as depicted in red color in the schematic of the PCF design in Figure 5.1 with the background of $As_2S_3$. The diameter of each air-hole is kept constant in purposed design.

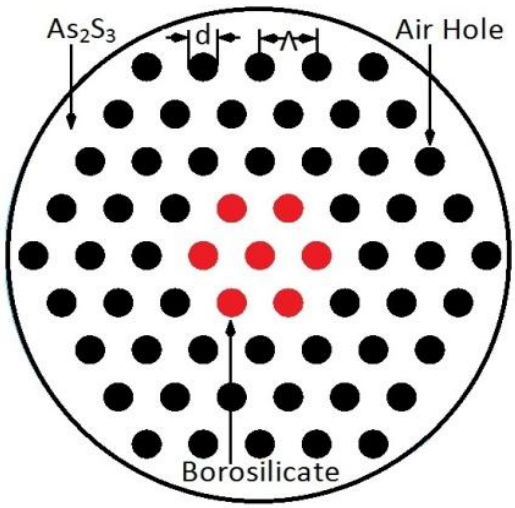


Figure 5.1 The schematic design of proposed Multi-material PCF.

The chalcogenide $As_2S_3$ based photonic crystal fiber offers high nonlinearity coefficient (γ) making it most popular and suitable for SCG. In order to investigate the dispersion of the fiber we estimated the effective refractive index ($n_{eff}$) of the fundamental mode of the designed photonic crystal fiber (PCF). The proposed photonic crystal fiber design consists of four rings with uniform fixed d/Λ = 0.5310734 ratio. Here, air-holes and borosilicate rod diameter is 0.94 $\mu$m. We can calculate the wavelength related refractive index of $As_2S_3$ glass and borosilicate material by following Sellmeier equation (5.1) and (5.2), respectively, as [129].

$$n^2(\lambda) = 1 + \frac{1.898367\lambda^2}{\lambda^2 - 0.15^2} + \frac{1.922297\lambda^2}{\lambda^2 - 0.25^2} + \frac{0.87651\lambda^2}{\lambda^2 - 0.35^2} + \frac{0.11887\lambda^2}{\lambda^2 - 0.45^2} + \frac{0.95699\lambda^2}{\lambda^2 - 27.3861^2} \quad (5.1)$$

and

$$n^2(\lambda) = 1 + \frac{0.967\lambda^2}{\lambda^2 - 0.020452} + \frac{0.00511\lambda^2}{\lambda^2 - 107.9261} + \frac{0.000233\lambda^2}{\lambda^2 - 0.34938} \quad (5.2)$$

Figure 5.2 displays the variation in chromatic dispersion and material dispersion change with wavelength of the proposed fiber for photonic crystal fiber. The careful selection of the pitch (Λ) and air hole diameters (d), the flat dispersion profile extending from 1.5 μm to 4.3 μm we obtained two zero dispersion wavelength (ZDW) at 2.27 μm and 3.3 μm. A flat and low dispersion profile helps to enhance the SCG. It can reduce the temporal walk-off effect at the time of spectral boarding process here the pump wavelength of 2.5 μm was used in the anomalous dispersion for photonic crystal fiber. In Figure 5.2 the black solid line shows the chromatic dispersion ($D_c$) of purposed fiber, dash line shows the material dispersion of borosilicate and the dash-dot line shows the material dispersion of $As_2S_3$ glass.

Here, the nonlinear refractive indices of $As_2S_3$ based chalcogenide glass is $n_2$ = 4 x $10^{-18}$ $m^2/W$ at 2.5 μm [129]. The variation in effective mode area ($A_{eff}$) and corresponding nonlinear coefficient of the purposed fiber have been displayed in Figure 5.3.

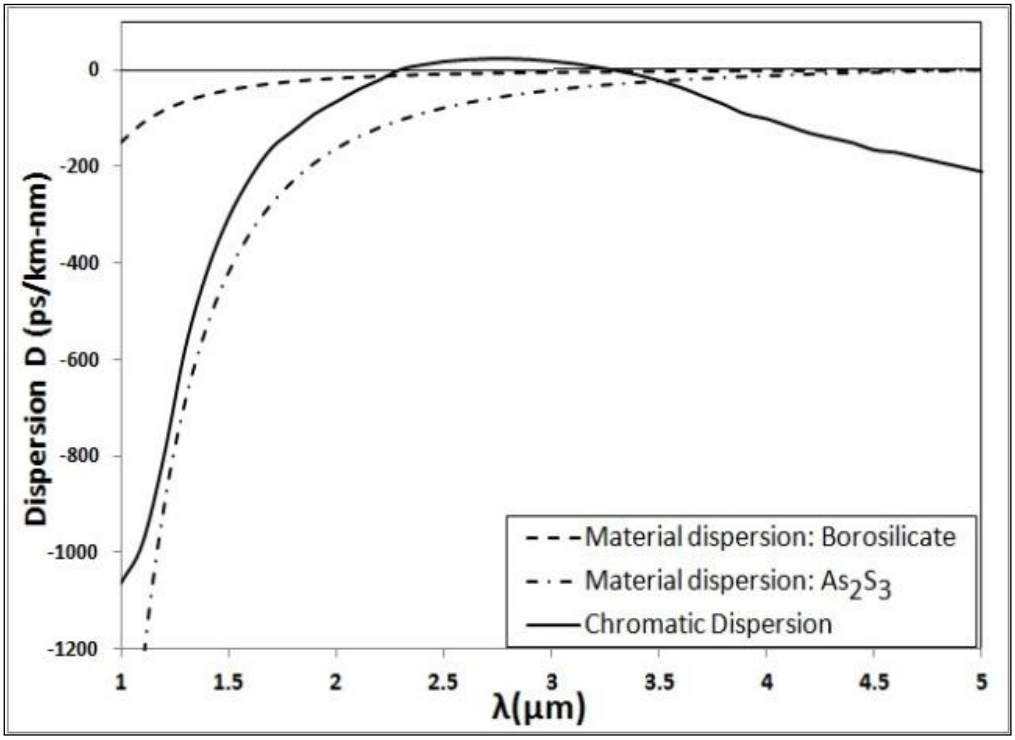


Figure 5.2 The dispersion plot of proposed Multi-material PCF.

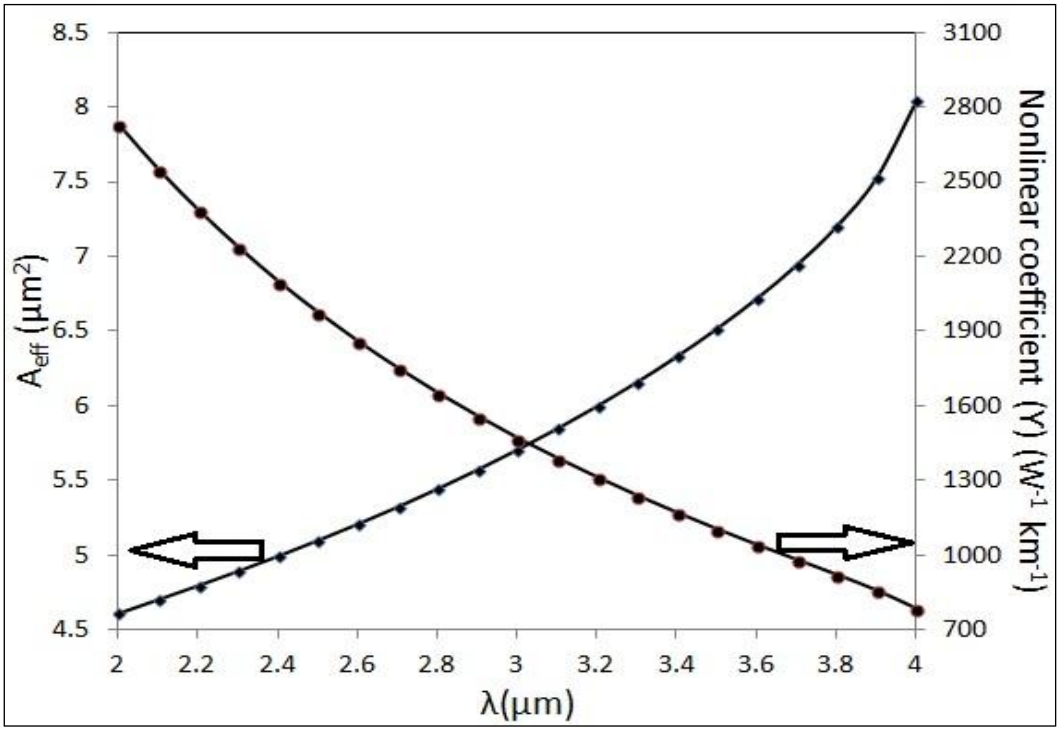


Figure 5.3 The effective mode area and nonlinear coefficient of Multi-material PCF.

## 5.2 Supercontinuum Generation in proposed PCF

The proposed fiber design was simulated for SCG. The spilt-step Fourier method was used to solve GNLSE. A PCF of 100 mm length was selected and was pumped with optical pulses of 2.5 μm for the numerical simulation. At this pump wavelength, the value of $A_{eff}$ obtained was 5.10019 $\mu m^2$ and $\gamma$ was 1972 $W^{-1}km^{-1}$. The pumped wavelength 2.5 μm is in anomalous dispersion regime and flat dispersion obtained for the range from 1.5 μm to 4.3 μm. The increase in anomalous regime pumping results in spectral broadening in long wavelength side. The solitons fission and Raman soliton self-frequency shift are the main reason for this. In the initial stage, the broadening of the pulse is mainly due to SPM and as the pulse propagates a few millimeters the spectrum breaks into two major peaks, after moving outward from the original pump wavelength the number of sub-peaks in between two major peaks keeps on increasing continuously. The pulse duration is 85 fs (FWHM) with the peak power as 350 W. The Figure (5.4 & 5.5) portrays spectral and temporal spans of SCG in the $As_2S_3$ based PCF with different input pump pulse. The spectral escalation of input pulse for different input power has been displayed in Figure 5.6.

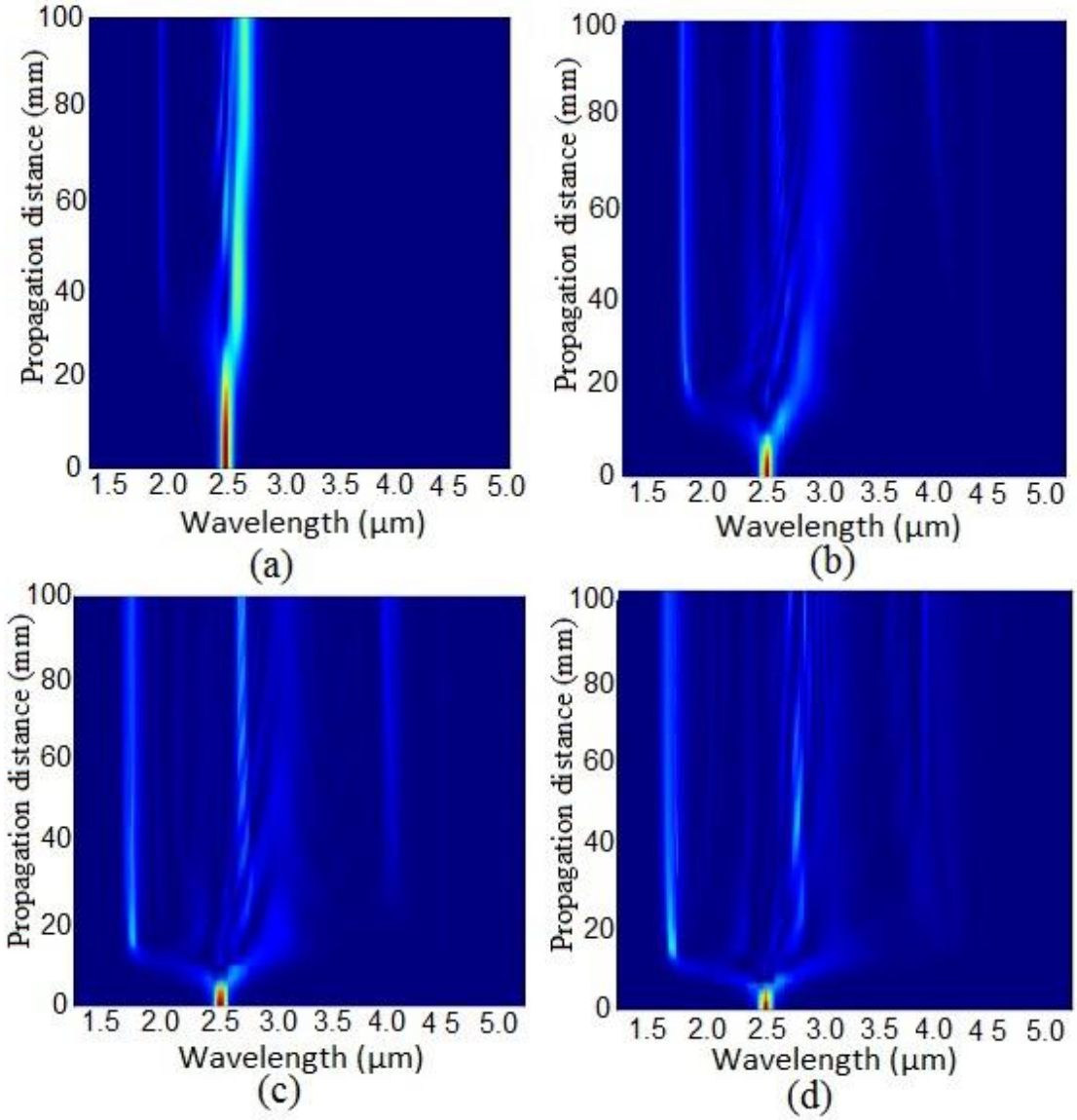


Figure 5.4 Spectral escalation of SC in Multi-material PCF designed with various input pump pulse (a) 50 W (b) 150 W (c) 250 W and (d) 350 W.

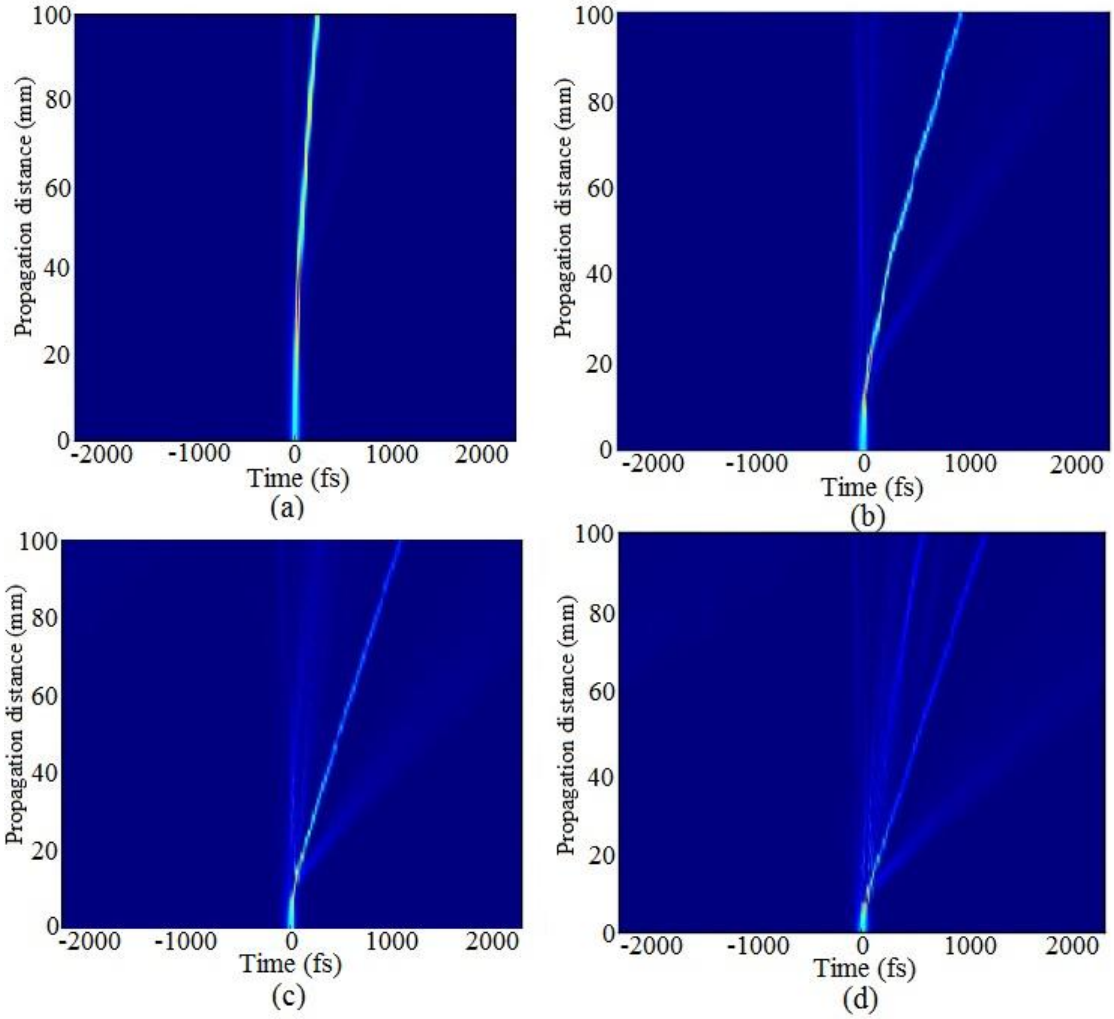


Figure 5.5 Temporal escalation of SC in Multi-material PCF designed with various input pump pulse (a) 50 W (b) 150 W (c) 250 W and (d) 350 W.

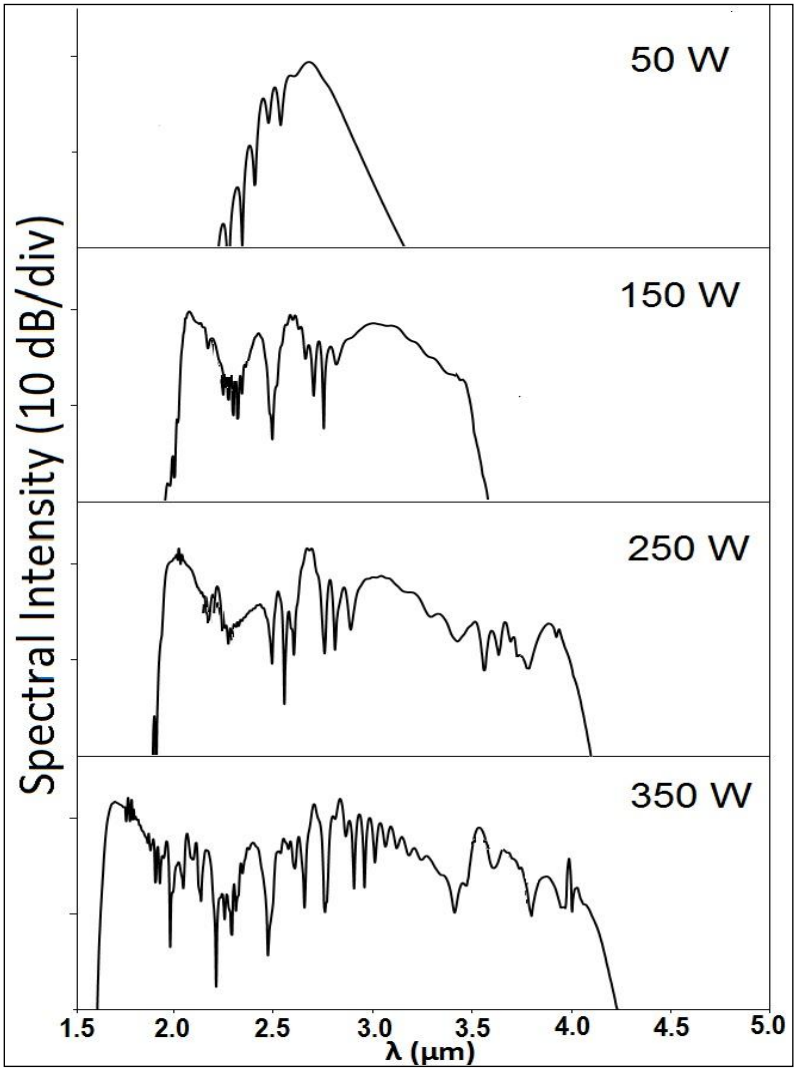


Figure 5.6 Spectra of SC for different input power in Multi-material PCF.

## 5.3 Results and discussions

In this paper, we have demonstrated SCG for 100 mm long multi-material photonic crystal fiber with air holes arranged in a hexagonal lattice. The range for flat dispersion of the proposed photonic crystal fiber design is from 1.5 μm to 4.3 μm. The effective area ($A_{eff}$), nonlinear coefficient (γ), and dispersion of the fiber launched with a pulse wavelength (λ) 2.5 μm are 5.10019 $\mu m^2$, 1972 $W^{-1}km^{-1}$, and 18.5545 ps/km-nm, respectively for the designed optical fiber. The photonic crystal fiber was numerically simulated for generation of supercontinuum using pump pulses of duration 85 fs at wavelength 2.5 μm with 350 W peak powers. The results of simulation generate supercontinuum for the bandwidth values from 1.6 μm to 4.2 μm with 350 W input power.

## 5.4 Summary

Its new tailoring technique of dispersion in index guiding photonics crystal fibers has been used to design a highly nonlinear anomalous dispersion-flattened photonics crystal fiber for mid-IR utilisation. This new design composed of four rings in the cladding with the inner air-hole ring and center air-hole replaced through borosilicate glass with $As_2S_3$ background. Therefore the design shows a unique RI profile which not only offers a large nonlinear coefficient but also a flat dispersion curve along with the low leakage loss. The PCF was numerically analysed for supercontinuum generation by applying pump pulses of 85 fs duration at wavelength 2.5 μm with 350 W peak powers. The values of effective area ($A_{eff}$), nonlinear coefficient ($\gamma$) and dispersion for the design of the fiber at the wavelength ($\lambda$) 2.5 μm are 5.10019 $\mu m^2$, 1972 $W^{-1}$ $km^{-1}$ and 18.5545 ps/km-nm respectively. The outcomes of simulation that supercontinuum with the bandwidth values of 1.6 μm to 4.2 μm generated. Our design analysis will be very useful for mid-IR applications particularly with the mature technologies available.

# Chapter 6

## Dispersion tailoring of Li-containing ternary compounds

In this section studied the suitable dispersion curve for a mid-infrared supercontinuum generation with Li-containing ternary compounds. As discussed earlier that for efficient SCG requires a flat dispersion curve and pump pulse exists in the anomalous dispersion reason. Here investigated the lithium ternary compounds chalcogenide PCFs such as $LiGaSe_2$, $LiGaS_2$ and LiGISe ($LiGa_{0.5}In_{0.5}Se_2$). $LiGaSe_2$ and $LiGaS_2$ are very potential nonlinear materials for conversion of laser radiation to the mid-IR spectral range that are transparent down to the visible and ultraviolet (UV). $LiGa_{0.5}In_{0.5}Se_2$ (LGISe) is a new mixed chalcogenide material, its solid solution of the $LiGaSe_2$ and $LiInSe_2$. It has the same orthorhombic structure as the parent compounds ($LiGaSe_2$ and $LiInSe_2$). The nonlinear refractive index of all the materials is approximate 3 x $10^{-15}$ $m^2/W$ which is $10^5$ times higher in comparison to silica. The transparency window and band gap energy of all material show in table 6.1 [162] [163].

Table 6.1: Transparency window and band gap energy of $LiGaSe_2$, $LiGaS_2$ and LiGISe chalcogenide material

| **Chalcogenide crystals** | **Transparency Window** | **Band Gap Energy** |
|---|---|---|
| $LiGaSe_2$ | 0.37 − 13.2 μm | 3.34 eV |
| $LiGaS_2$ | 0.32 − 11.6 μm | 4.15 eV |
| LiGISe ($LiGa_{0.5}In_{0.5}Se_2$) | 0.47 − 13 μm | 2.94 eV |

## 6.1 Fiber Design for pump wavelength 2.2 $\mu$m

In this section, we have designed $LiGaSe_2$, $LiGaS_2$, LiGISe ($LiGa_{0.5}In_{0.5}Se_2$) based photonic crystal fiber which is suitable for SCG at 2.2 $\mu$m pumping. The dispersion tailoring has been done very carefully to achieve the desired dispersion characteristics, as dispersion and also the zero dispersion wavelength(s) play a crucial role in achieving

the desired characteristics of supercontinuum like spectral shape, width and flatness. In the process to obtain flat and wide spectrum, we have designed hexagonal PCF whose basic layout in XY plane is depicted in Figure 6.1 and the designing parameters are shown in table 6.2.

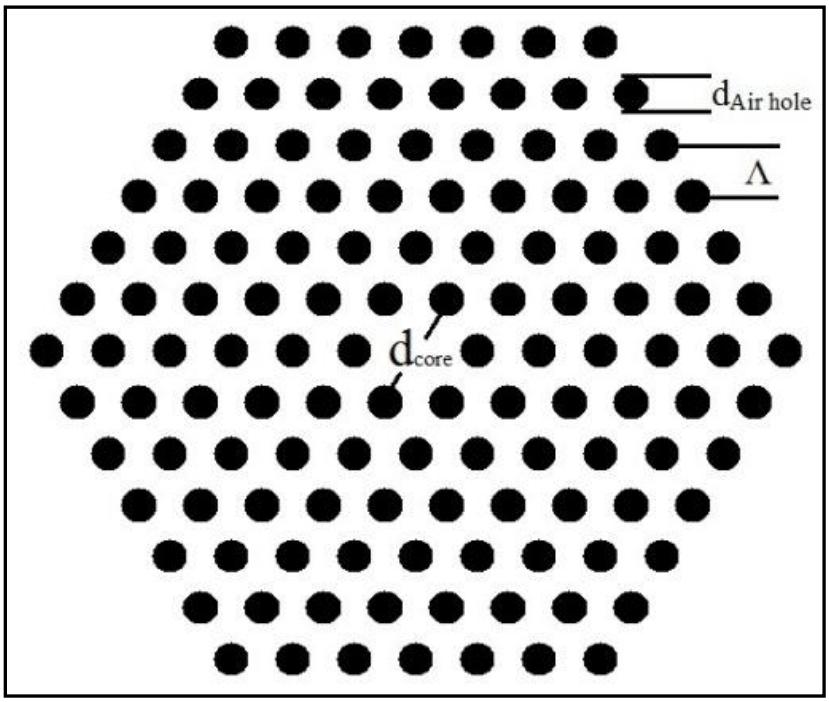


Figure 6.1 The purposed structure of the hexagonal PCF ($LiGaSe_2$, $LiGaS_2$ and LiGISe) for 2.2 $\mu$m pumping wavelength.

Table 6.2: Designing parameters of purposed PCF ($LiGaSe_2$, $LiGaS_2$ and LiGISe) for 2.2 $\mu$m pumping wavelength.

| **Chalcogenide crystals** | **Number of Rings** | **Fiber core diameter ($d_{core}$)** | **Pitch (Λ)** | **d/Λ** |
|---|---|---|---|---|
| $LiGaSe_2$ | 6 | 0.96 µm | 3.2 µm | 0.7 |
| $LiGaS_2$ | 6 | 1.6 µm | 4.0 µm | 0.6 |
| LiGISe ($LiGa_{0.5}In_{0.5}Se_2$) | 6 | 0.64 µm | 3.2 µm | 0.8 |

The refractive index and material dispersion of chalcogenide glass are calculated by the Sellmeier's equation (6.1) [162] [163]. The Sellmeier coefficients for each crystal are in table 6.3.

$$n^2 = A + \frac{B}{\lambda^2 - C} - D\lambda^2 \quad (6.1)$$

Table 6.3: Sellmeier coefficients of ($LiGaSe_2$, $LiGaS_2$ and LiGISe) chalcogenide material

| **Chalcogenide crystals** | **A** | **B** | **C** | **D** |
|---|---|---|---|---|
| $LiGaSe_2$ | 5.22442 | 0.18365 | 0.07493 | 0.00232 |
| $LiGaS_2$ | 4.493881 | 0.1177452 | 0.0337004 | 0.0037767 |
| LiGISe ($LiGa_{0.5}In_{0.5}Se_2$) | 5.26219 | 0.21331 | 0.0755 | 0.00209 |

### 6.1.1 Results and discussions

The chromatic dispersion of the PCF has been computed using FDTD method which is a very efficient and fast method of computing dispersion for symmetric and nonsymmetric fiber structure. The chromatic dispersion of the designed PCF is shown in Figure 6.2. The Zero Dispersion Wavelength (ZDW) of chromatic dispersion is ~ 2.2 μm.

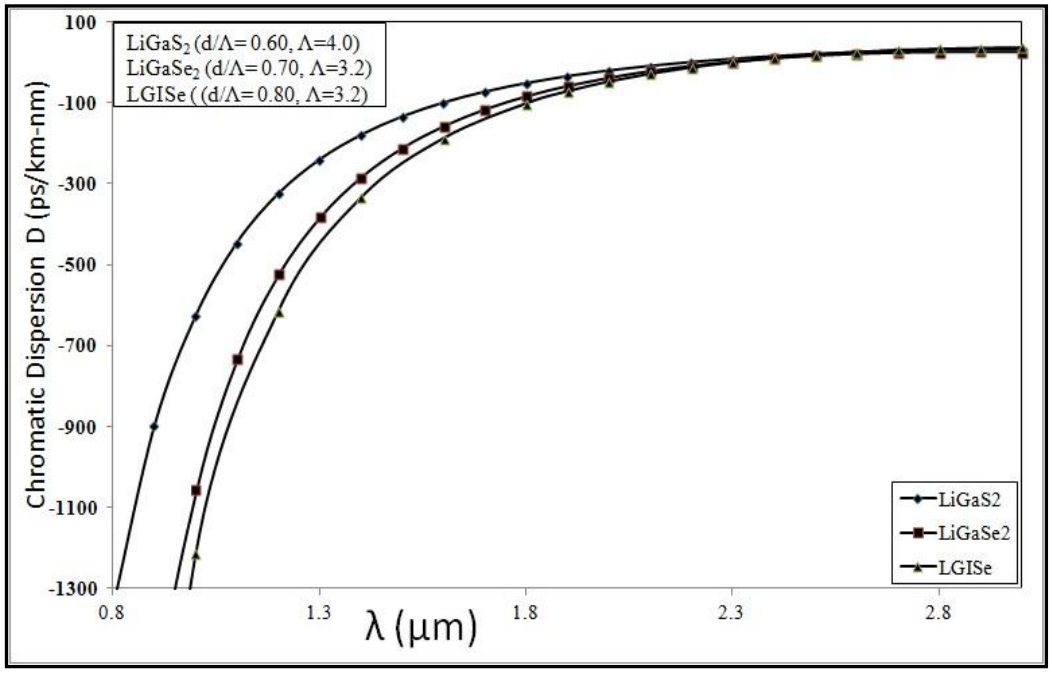


Figure 6.2 Dispersion properties of the purposed ($LiGaSe_2$, $LiGaS_2$ and LiGISe) based chalcogenide material PCFs, ZDW at 2.2 μm.

We have designed a highly nonlinear chalcogenide photonic crystal fiber suitable for supercontinuum generation at pump wavelength at 2.2 μm. The fiber has very flat dispersion in the anomalous region which is desirable characteristics for a flat supercontinuum spectrum. Due to the high intrinsic nonlinearity of $LiGaSe_2$, $LiGaS_2$, LiGISe ($LiGa_{0.5}In_{0.5}Se_2$) and small effective area the nonlinearity of the γ of very high.

## 6.2 Fiber Design for pump wavelength 1.55 $\mu$m

In this work, designed and characterized a highly nonlinear photonic crystal fiber that has Zero Dispersion Wavelength (ZDW) around 1.55 μm and a very flat dispersion profile in anomalous dispersion region. The chalcogenide material used in this work is $LiGaS_2$. The nonlinear refractive index of $LiGaS_2$ is $3 \times 10^{-15}$ $m^2/W$ which is $10^5$ times higher in comparison to silica. In the process to obtain flat and wide spectrum, we have designed four variants of the hexagonal PCF whose basic layout in XY plane is depicted in Figure 6.3.

where,

Fiber core: 4.25 μm

Pitch (Λ) = 2.25 μm

$d_1$ = 0.25 μm

$d_2$ = 2.0 μm

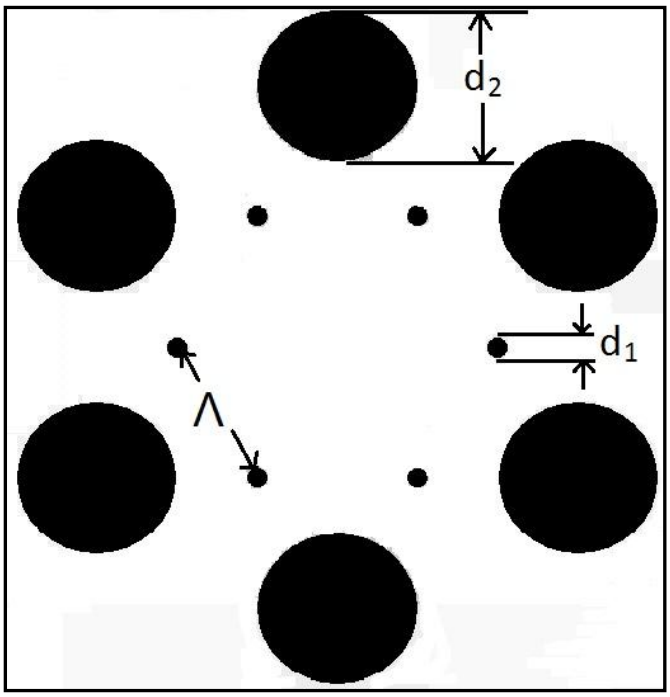


Figure 6.3 The purposed structure of the PCF ($LiGaS_2$) for 1550 nm pumping wavelength.

### 6.2.1 Results and discussions

The chromatic dispersion of the designed PCF is shown in Figure 6.4. The Zero Dispersion Wavelength (ZDW) is ~ 1.55 µm.

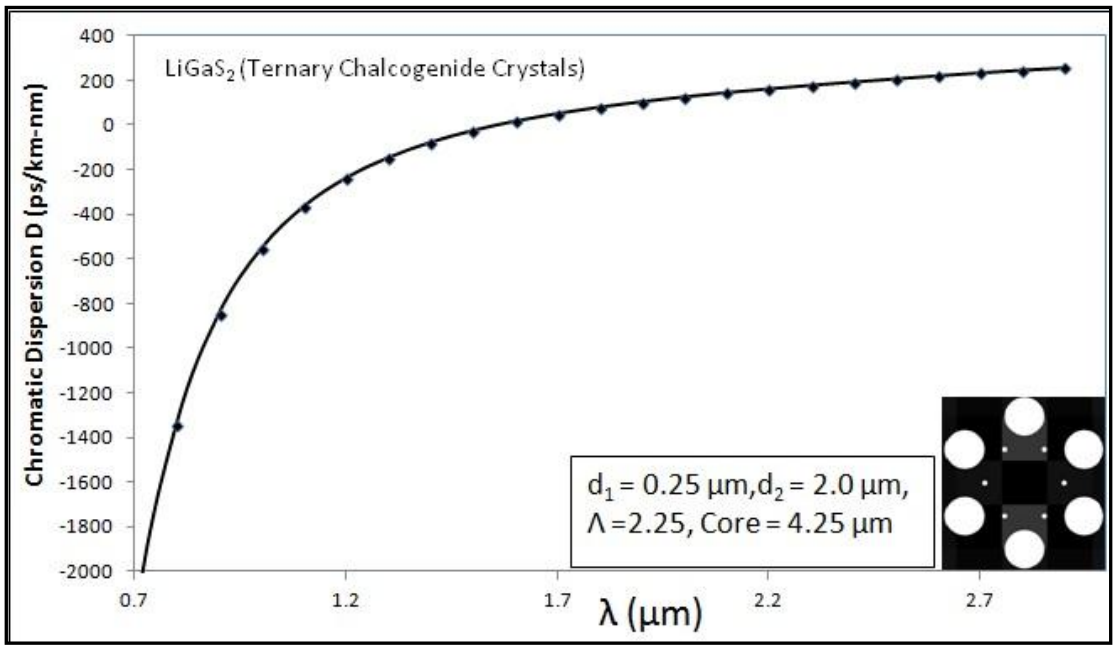


Figure 6.4 Dispersion properties of the purposed $LiGaS_2$ based chalcogenide material PCFs, ZDW at 1.55 µm

We designed a highly nonlinear chalcogenide photonic crystal fiber suitable for supercontinuum generation at pump wavelength at 1.5 $\mu$m. The fiber has very flat dispersion in the anomalous region which is desirable characteristics for a flat supercontinuum spectrum. Because of the high intrinsic nonlinearity of $LiGaS_2$ and small effective area, the nonlinearity of the $\gamma$ of very high.

## 6.3 Summary

In this chapter, we are exploring new potential chalcogenide material for a mid-IR supercontinuum generation. These are the lithium-containing nonlinear optical glasses such as $LiGaSe_2$, $LiGaS_2$ and LiGISe ($LiGa_{0.5}In_{0.5}Se_2$). As mentioned at the start of this chapter, these are the new class of material with wide band-gap nonlinear glasses transparent in the mid-IR spectrum range. Here we designed PCFs for tailored the dispersion curve suitable for pump wavelength 2.2 $\mu$m and 1.55 $\mu$m that open a new area of research with these materials.

# Chapter 7

## Conclusion and Future work

The objective of the entire study and research was to investigate and optimize the application of photonic crystal fiber to generate broadband supercontinuum in near-infrared region to mid-infrared region (MIR) using highly nonlinear chalcogenide material. The complete work was carried out in two stages. Chalcogenide microstructured optical fibers have been considered to design such supercontinuum sources that could be used for NIR and MIR applications. The fiber designs proposed for supercontinuum generation were improved with tailoring to obtain optimized results. Numerous rigorous numerical calculations were carried out with finite-difference-time-domain (FDTD) method to obtain results for dispersion analysis. In our research work spilt-step Fourier method (SSFM) was opted to numerically investigate generalized nonlinear Schrödinger equation (GNLSE) for obtaining SC generation for the proposed designs. In this thesis firstly, we tailored $Ge_{11.5}As_{24}Se_{64.5}$ chalcogenide based microstructured fibers to generate SC generation for NIR and MIR region. Next, we presented the possibility of mid-infrared supercontinuum generation with multi-material PCF, by using $As_2S_3$ and borosilicate glass. The results obtained with numerical simulations show significant improvement in SC generation in MIR range. At last, we examined the future scope of SCG in Li-containing ternary compounds chalcogenide material.

In the initial phase the researchers designed PCFs with silica as base material and optimized the design to generate supercontinuum with pump energy of 25W at 1.55 μm wavelength. In order to have supercontinuum generation in region extending in MIR, the pump wavelength should lie in the range of 3-4 microns. Since silica PCFs suffer from serious absorption in the region beyond 3 microns, making it difficult to shift the pump wavelength in long wavelength region to extend supercontinuum spectra in long wavelength. Therefore, for producing a broadband MID-IR supercontinuum $Ge_{11.5}As_{24}Se_{64.5}$ based chalcogenide PCF were selected. The previous reported work demonstrated theoretical investigation on $Ge_{11.5}As_{24}Se_{64.5}$ based ChG planar waveguides for spreading supercontinuum into the MIR region, but

the asymmetric nature of planar waveguide are responsible for the cladding absorption at the longer wavelengths. The Photonic crystal fiber based designs are more promising and have attracted the attention of researcher to applicate them for generation of SC in mid-infrared region. Further it is noteworthy that in the long wavelength region the losses due to absorption are negligible. Another important advantage is that they can easily be drawn into fibers with existing technologies. In our theoretical study, we could infer that limitations in planar waveguides and conventional fibers can be eliminated by using photonic crystal fibers and the supercontinuum generation expanding in the mid-infrared region can be achieved. In the work presented, we have numerically simulated and validated that by tailoring dispersion in chalcogenide photonic crystal fibers we can generate ultra-broadband supercontinuum extending up to 15 μm in MIR region.

In the chapter 4 supercontinuum generation in $Ge_{11.5}As_{24}Se_{64.5}$ chalcogenide photonic crystal fiber design was investigated with suitable pumping power at the 3.1 $\mu$m as pump wavelength. The rigorous numerical simulation based on FDTD was carried out to obtain required anomalous dispersion for chalcogenide based photonic crystal fiber near 3.1 $\mu$m pump wavelength. To achieve so the design parameters, air-hole diameter and pitch were carefully engineered. The observations from the design were quite satisfactory, which further motivated and directed our research work. Our research work focused on three designs, and anomalous dispersion of all designs was tailored to exhibit two zero-dispersion wavelengths at suitable pump wavelength. Supercontinuum simulations have been performed for all the three photonic crystal fibers designs. An optimized design to achieve a generation of SC broadband in MIR region was obtained. To start with, the supercontinuum generation with $Ge_{11.5}As_{24}Se_{64.5}$ glasses was firstly investigated in a basic hexagonal design and the dispersion curve was tailored for pump wavelength 3.1 $\mu$m in the anomalous dispersion region. The design parameters like number of rings, pitch and air- hole diameter were carefully selected to achieve two ZDW dispersion curve and the first ZDW in proximity of pump wavelength. On simulating the design with suitable pump energy at 3.1 μm wavelength the effective area ($A_{eff}$), nonlinear coefficient ($\gamma$), and chromatic dispersion ($D_c$ ($\lambda$)) obtained were 3.98 $\mu m^2$, 2191 $W^{-1}km^{-1}$, and 5 ps/km-nm, respectively. The design resulted in a broad SC spreading from 1 to 10 $\mu$m up to the fiber length for 150 mm with input power requirement 5 kW. Taking our research work ahead, later we improved our design by the changing air-hole diameter of

various ring and observed their effect on parameters effective mode index ($n_{eff}$) and dispersion. Herewith, we simulated the SC generation for the improved design and estimated values of nonlinear coefficient (γ), effective area ($A_{eff}$) and dispersion at the wavelength (λ) 3.1 μm as 2317 $W^{-1}$ $km^{-1}$, 3.7634 $\mu m^2$ and, 52 ps/km-nm, respectively. A broad spectra for SC spreading in range from 1 to 10 $\mu$m was observed with 100 mm long fiber when pumped with pulses of 3 kW power. This work significantly helped us to reduce the length and pump energy. The results observed from optimized $Ge_{11.5}As_{24}Se_{64.5}$ based chalcogenide PCF design were remarkable. The design proposed offer increased freedom to control the dispersion curve. We achieved a flat dispersion curve with two ZDW and the pump pulse existing in the anomalous dispersion region. In another design, we reduced the effective mode area as compared to previous designs, resulting in increased nonlinearity which is essential parameter for SCG. In reference to this design we obtained nonlinear coefficient (γ), effective area ($A_{eff}$) and dispersion at the wavelength (λ) 3.1 μm as 2474 $W^{-1}km^{-1}$, 3.5241 $\mu m^2$ and 8.014 ps/km-nm, respectively. The proposed design of PCF was investigated with numerical simulation for supercontinuum generation using 85 fs pump pulses at a 3.1 μm pump wavelength and 3 kW peak power. Supercontinuum bandwidth for range 1 μm to 15 μm for 3 kW peak power was demonstrated. Our design has significantly improved the expansion of SC spectra from 1 to 15 μm with pump energy of 3 kW over 1.3 to 11 μm with same pump energy as reported by M. Karim [130].

In chapter 4 theoretical investigation on $Ge_{11.5}As_{24}Se_{64.5}$ chalcogenide glass based microstructured fiber for extending spectra of SC in the mid-infrared regime was presented. Motivated with satisfactory observations and results in our research work we proposed an idea to obtain a higher effective index by replacing the air holes with a high refractive index valued material as discussed in Chapter 5. To design fibers which may find their applications in mid-infrared region, we considered an arsenic sulfide ($As_2S_3$)-based photonic crystal fiber structure consists of four rings with hexagonal geometry. In all four cladding rings, the inner air-hole ring and center air-hole was replaced by borosilicate glass rods. With this cutting edge technique of dispersion in index guiding photonics crystal fibers we designed a highly nonlinear anomalous dispersion-flattened photonics crystal fiber for mid-IR utilization. The designed photonic crystal fiber was numerically investigated for supercontinuum generation applying pump pulses of duration 85 fs at 2.5 μm wavelength and 350 W peak powers. After simulations and calculation the values for the effective area ($A_{eff}$),

nonlinear coefficient (γ), and dispersion for the design obtained were 5.10019 μm$^2$, 1972 W$^{-1}$km$^{-1}$ and 18.5545 ps/kmnm, respectively at the wavelength (λ) 2.5 μm. The spectra of SC generated expanded from 1.6 μm to 4.2 μm. The results obtained were significantly improved with the design as reported by P. S. Maji [129], where the bandwidth for SC generated expanded from 2.41 to 3.15 μm for same pumping conditions. Analyses of our design are very useful for applications in the mid-infrared, especially for the mature technology available.

In chapter 6, we discussed about the new potential chalcogenide material for a mid-IR supercontinuum generation. These new materials are the lithium ternary compounds chalcogenide glasses like $LiGaSe_2$, $LiGaS_2$ and LiGISe ($LiGa_{0.5}In_{0.5}Se_2$) which have very high non linear refractive index. The nonlinear refractive index of all the materials is approximately 3 x 10$^{-15}$ m$^2$/W as reported which is 10$^5$ times higher as compared to silica. And also have wide band-gap nonlinear glasses transparent in the mid-IR spectrum range up to 13 $\mu$m. Designs were engineered for dispersion curve suitable for pump wavelength 2.2 $\mu$m and 1.55 $\mu$m which will be numerically simulated to observe efficient SC generation in near future.

The results obtained from numerical simulations are satisfactory very promising. This inspirits us to experimentally validate the results in this research work, in order to take our designs for fabrication for real life applications in future.

# Author Publications

## SCI indexed journals

- S. Vyas, T. Tanabe, M. Tiwari, and G. Singh, "*Ultraflat broadband supercontinuum in highly nonlinear $Ge_{11.5}As_{24}Se_{64.5}$ photonic crystal fibers*", Ukrainian Journal of Physical Optics, Volume 17, Issue 3, p. 132-139, 2016. DOI: 10.3116/16091833/17/3/132/2016.

  Impact Factor: 0.783
  Publisher: Ukrainian Journal of Physical Optics

- S. Vyas, T. Tanabe, M. Tiwari, and G. Singh, "*A Chalcogenide Photonic Crystal Fiber for Ultraflat Mid-infrared Supercontinuum Generation*", Chinese Optics Letter, Volume 14, Issue 12, p. 123201-1 - 123201-5, 2016. DOI: 10.3788/COL201614.123201.

  Impact Factor: 1.899
  Publisher: Optical Society of America (*OSA*)

## International Conference

- **S. Vyas**, G. Singh, and M. Tiwari, "A Highly Nonlinear Photonic Crystal Fiber for Supercontinuum Generation" in international conference on 'Thailand-Japan MicroWave 2014', Bangkok (Nov. 26-28), **Thailand.**

- **S. Vyas**, G. Singh, and M. Tiwari, "Ultrabroad supercontinuum generation with different nonlinear material by novel structure of photonic crystal fibers" in international conference on 'IKSS-2014',Krutan (June 8-14), **Poland**.

- **S. Vyas**, G. Singh, M. Tiwari, and T. Tanabe, "Chalcogenide ($LiGSe_2$, LiGISe, $LiGaS_2$): A perfect material to design highly nonlinear PCFs for supercontinuum generation" Proc. of the *ICRCWIP*, DOI 10.1007/978-81-322-2638-2638-3_47, pp. 409–413, **@Springer Publication** 2016.

- **S. Vyas**, G. Singh, and M. Tiwari, "A Highly Nonlinear Chalcogenide Based PCF for Mid–IR Supercontinuum Generation" in international conference on "International Conference on Optics & Photonics 2015 (ICOP 2015)", Calcutta (Feb. 19, 2015), India.
- **S. Vyas**, T. Tanabe, G. Singh, and M. Tiwari, "Broadband Supercontinuum Generation and Raman Response in $Ge_{11.5}As_{24}Se_{64.5}$ based chalcogenide Photonic Crystal Fiber," ***IEEE International Conference*** *(ICCTICT-2016)*, pp. 562-566, March 2016. DOI:10.1109/ICCTICT.2016.7514651 .

- **S. Vyas**, T. Tanabe, M. Tiwari, and G. Singh, "Mid-infrared supercontinuum generation in $Ge_{11.5}As_{24}Se_{64.5}$ based chalcogenide photonic crystal fiber," ***IEEE International Conference*** *Advances in Computing, Communications and Informatics (ICACCI*), pp. 2547-2552, September ($21^{st}$-$24^{th}$) 2016. DOI: 10.1109/ICACCI.2016.7732436

## Reference

[1] J. M. Dudley and J. R. Taylor, Supercontinuum Generation in Optical Fibers, Cambridge University Press, 2010.

[2] G. P. Agrawal, Nonlinear Fiber Optics 5th ed., vol. 5, San Diego, California: Academic Press, 2013.

[3] R. R. Alfano and S. L. Shapiro, "Emission in the region 4000 to 7000 Á via four-photon coupling in glass," *Phys. Rev. Lett.*, vol. 24, no. 11, p. 584–587, 1970.

[4] J. K. Ranka, R. S. Windeler and A. J. Stentz, "Visible continuum generation in air-silica microstructure optical fibres with anomalous dispersion at 800 nm," *Opt. Lett.*, vol. 25, pp. 25-27, 2000.

[5] J. C. Knight, T. A. Birks, P. S. Russell and J. P. De-Sandro, "Properties of photonic crystal fibre and effective index model," *J. Opt. Soc. Am. B*, vol. 15, pp. 748-752, 1998.

[6] P. S. J. Russell, "Photonic-crystal fibres," *Science*, vol. 299, no. 5605, pp. 358-362, 2003.

[7] G. Chang, T. B. Norris and H. G. Winful, "Optimization of supercontinuum generation in photonic crystal fibres for pulse compression," *Opt. Lett.*, vol. 28, pp. 546-548, 2003.

[8] K. M. Hilligsoe, T. V. Andersen, H. N. Paulsen, C. K. Nielsen, K.Molmer, S. Keiding, R. Kristiansen, K. P. Hansen and J. J. Larsen, "Supercontinuum generation in a photonic crystal fibre with two zero dispersion wavelengths," *Opt. Exp.*, vol. 12, pp. 1045-1054, 2004.

[9] T. A. Birks, W. J. Wadsworth and P. S. J. Russell, "Supercontinuum generation in tapered fibres," *Opt. Lett.*, vol. 25, no. 19, pp. 1415-1417, 2000.

[10] P. Falk, M. H. Frosz and O. Bang, "Supercontinuum generation in a photonic crystal fibre with two zero-dispersion wavelengths tapered to normal dispersion

at all wavelengths," *Opt. Exp.*, vol. 13, no. 19, pp. 7535-7540, 2005.

[11] F. Poletti, K. Furusawa, Z. Yussoff, N. G. R. B. P. Petropoulos, T. M. Monro and D. J. Richardson, "Nonlinear tapered holey fibres with high SBS threshold and controlled dispersion," *J. Opt. Soc. Am. B,* vol. 24, no. 9, pp. 2185-2194, 2007.

[12] F. Luan, M. D. Pelusi, M. R. E. Lamont, D. Y. Choi, S. Madden, B. Luther-Davies and B. J. Eggleton, "Dispersion engineered $As_2S_3$ planar waveguides for broadband four-wave mixing based wavelength conversion of 49 Gb/s signals," *Opt. Exp.*, vol. 17, no. 5, pp. 3514-3520, 2009.

[13] J. M. Dudley, G. Genty and S. Coen, "Supercontinuum generation in photonic crystal fibre," *Rev. Mod. Phys.*, vol. 78, p. 1135–1184, 2006.

[14] S. Coen, A. H. L. Chau, R. Leonhardt, J. D. Harvey, J. C. Knight, W. J. Wadsworth and P. S. J. Russell, "Supercontinuum generation by stimulated Raman scattering and parametric four-wave mixing in photonic crystal fibres," *J. Opt. Soc. Am. B,* vol. 19, no. 4, p. 753–764, 2002.

[15] J. M. Dudley, L. Provino, N. Grossard, H. Maillotte, R. S. Windeler, B. J. Eggleton and S. Coen, "Supercontinuum generation in air-silica microstructured fibres with nano second and femtosecond pulse pumping," *J. Opt. Soc. Am. B,* vol. 19, no. 4, p. 765–771, 2002.

[16] J. Herrmann, U. Griebner, N. Zhavoronkov, A. Husakou, D. Nickel, J. C. Knight, W. J. Wadsworth, P. S. J. Russell and G. Korn, "Experimental evidence for supercontinuum generation by fission of higher-order solitons in photonic crystal fibres," *Phy. Rev. Lett.*, vol. 88, no. 17, p. 173901, 2002.

[17] T. Cheng, K. Nanasaka, T. H. Tuan, X. Xue, M. Matsumoto, H. Tezuka, T. Suzuki and Y. Ohishi, "Mid-infrared supercontinuum generation spanning 2.0 to 15.1 μm in a chalcogenide step-index fiber," *Opt. Letters,* vol. 41, no. 9, pp. 2117-2120, 2016.

[18] L. Yin, Q. Lin and G. P. Agrawal, "Soliton fission and supercontinuum generation in silicon waveguides," *Opt. Lett.*, vol. 32, no. 4, pp. 391-393, 2007.

[19] L. Yin and G. P. Agrawal, "Impact of two-photon absorption on self-phase modulation in silicon waveguides," *Opt. Lett.,* vol. 32, no. 14, pp. 2031-2033, 2007.

[20] J. Lousteau, N. G. Boetti, D. Negro, E. Mura, G. C. Scarpignato, G. Perrone, D. Milanese and S. Abrate, "Photonic glasses for IR and mid-IR spectral range," in *International Conference on Space Optics (ICSO),* Ajaccio (France), 2012.

[21] B. J. Eggleton, B. Luther-Davies and K. Richardson, "Chalcogenide photonics," *Nat. Photonics,* vol. 5, pp. 141-148, 2011.

[22] D. Yeom, E. C. Mägi, M. R. E. Lamont, M. A. F. Roelens, L. Fu and B. J. Eggleton, "Low-threshold supercontinuum generation in highly nonlinear chalcogenide nanowires," *Opt. Lett.,* vol. 33, no. 7, pp. 660-662, 2008.

[23] D. D. Hudson, S. A. Dekker, E. C. Mägi, A. C. Judge, S. D. Jackson, E. Li, J. S. Sanghera, L. B. Shaw, I. D. Aggarwal and B. J. Eggleton, "Octave spanning supercontinuum in an $As_2S_3$ taper using ultralow pump pulse energy," *Opt. Lett.,* vol. 36, no. 7, pp. 1122-1124, 2011.

[24] D. D. Hudson, E. C. Mägi, A. C. Judge, S. A. Dekker and B. J. Eggleton, "Highly nonlinear chalcogenide glass micro/nanofibre devices: Design, theory, and octave-spanning spectral generation," *Opti. Commun.,* vol. 285, pp. 4660-4669, 2012.

[25] X. Gai, T. Han, A. Prasad, S. Madden, D. Y. Choi, R. Wang, D. Bulla and B. Luther-Davies, "Progress in optical waveguides fabricated from chalcogenide glasses," *Opt. Exp.,* vol. 18, no. 25, pp. 26635-26646, 2010.

[26] I. D. Aggarwa and J. S. Sanghera, "Development and applications of chalcogenide glass optical fibres at NRL," *J. Optoelectron. Adv. Mater.,* vol. 4, no. 3, pp. 665-678, 2002.

[27] X. Gai, S. Madden, D. Y. Choi, D. Bulla and B. Luther-Davies, "Dispersion engineered $Ge_{11.5}As_{24}Se_{64.5}$ nanowires with a nonlinear parameter of 136 $W^{-1}m^{-1}$ at 1550 nm," *Opt. Exp.,* vol. 18, no. 18, pp. 18866-188874, 2010.

[28] D. D. Hudson, M. Baudisch, D. Werdehausen, B. J. Eggleton and J. Biegert,

"1.9 octave supercontinuum generation in a $As_2S_3$ step-index fibre driven by mid-IR OPCPA," *Opt. Lett.*, vol. 39, no. 19, p. 5752–5755, 2014.

[29] P. Ma, D. Y. Choi, Y. Yu, X. Gai, Z. Yang, S. Debbarma, S. Madden and B. Luther-Davies, "Low-loss chalcogenide waveguides for chemical sensing in the mid-infrared," *Opt. Exp.*, vol. 21, no. 24, p. 29927–29937, 2013.

[30] R. R. Alfano and S. L. Shapiro, "Emission in the region 4000 to 7000 Á via four-photon coupling in glass," *Phys. Rev. Lett.*, vol. 24, no. 11, p. 584–587, 1970.

[31] B. M. A. Rahman and A. Agrawal, Finite Element Modelling Methods for Photonics, London: Artech house, 2013.

[32] J. B. Davies, Numerical Techniques for Microwave and Milimetre-wave Passive Structures, New York: Wiley, 1989.

[33] A. B. Salem, R. Cherif and M. Zghal, "Raman Response of a Highly Nonlinear $As_2Se_3$-based Chalcogenide Photonic Crystal Fiber," in *Progress In Electromagnetics Research Symposium Proceedings*, Marrakesh (Morocco), Mar. 20-23 (2011).

[34] F. X. Kärtner, D. J. Dougherty, H. A. Haus and E. P. Ippen, "Raman noise and soliton squeezing," *J. Opt. Soc. Am. B*, vol. 11, pp. 1267-1276, 1994.

[35] M. R. Karim, B. M. A. Rahman and G. P. Agrawal, "Mid-infrared supercontinuum generation using dispersion-engineered $Ge_{11.5}As_{24}Se_{64.5}$ chalcogenide channel waveguide," *Opt. Exp.*, vol. 23, no. 5, pp. 6903-6914, 2015.

[36] H. Ebendorff-Heidepriem, K. Furusawa, D. R. Richardson and T. M. Monro, "Fundamentals and applications of silica and non-silica holey fibres," in *Proc. SPIE, Photonics West*, San Jose, 2004.

[37] V. Finazzi, T. M. Monro and D. J. Richardson, "Small core silica holey fibres: nonlinearity and confinement loss trade-off," *J. Opt. Soc. Am. B*, vol. 20, no. 7, pp. 1427-1436, 2003.

[38] F. Poli, A. Cucinotta and S. Seller, Photonic crystal fibres: properties and

applications, Dordecht: Springer, 2007.

[39] J. C. Baggett, T. M. Monro, J. R. Hayes, V. Finazzi and D. J. Richardson, "Improving bending losses in holey fibres," in *Proceedings of OFC*, Anaheim, 2005.

[40] J. Hu, C. R. Menyuk, L. B. Shaw, J. S. Sanghera and I. D. Aggarwal, "Maximizing the bandwidth of supercontinuum generation in $As_2Se_3$ chalcogenide fibres," *Opt. Exp.*, vol. 18, no. 3, p. 6722–6739, 2010.

[41] W. H. Reeves, J. C. Knight, P. S. J. Russell and P. J. Roberts, "Demonstration of ultra-flattened dispersion in photonic crystal fibers," *Opt. Express*, vol. 10, pp. 609-613, 2002.

[42] A. V. Husakou and J. Herrmann, "Supercontinuum generation, four wave mixing, and fission of higher-order solitons in photonic crystal fibres," *J. Opt. Soc. Am. B*, vol. 19, p. 2171–2182, 2002.

[43] R. H. Stolen, J. P. Gordon, W. J. Tomlinson and H. A. Haus, "Raman response function of silica-core fibres," *J. Opt. Soc. Am. B*, vol. 6, no. 6, pp. 1159-1166, 1989.

[44] K. J. Blow and D. Wood, "Theoretical description of transient stimulated Raman scattering in optical fibres," *IEEE J. Quan. Elect.*, vol. 25, p. 2665–2673, 1989.

[45] N. Akhmediev and M. Karlsson, "Cherenkov radiation emitted by solitons in optical fibres," *Phy. Rev. A*, vol. 51, pp. 2602-2607, 1995.

[46] P. K. A. Wai, C. R. Menyuk, H. H. Chen and Y. C. Lee, "Soliton at the zero group dispersion wavelength of a single-model fibre," *Opt. Lett.*, pp. 628-630, 1987.

[47] P. K. A. Wai, H. H. Chen and Y. C. Lee, "Radiations by solitons at the zero group dispersion wavelength of single-mode optical fibres," *Phy. Rev. A*, vol. 41, pp. 426-439, 1990.

[48] K. Okamoto, Fundamentals of Optical Waveguides 2nd ed., Academic press, Elsevier, 2006.

[49] T. A. Birks, J. C. Knight and P. S. J. Russell, "Endlessly single mode photonic crystal fibre," *Opt. Lett.*, vol. 22, p. 961–963, 1997.

[50] W. Wadsworth, A. Witkowska, S. Leon-Saval and T. Birks, "Hole inflation and tapering of stock photonic crystal fibres," *Opt. Exp.*, vol. 13, p. 6541–6549, 2005.

[51] M. El-Amraoui, G. Gadret, J. C. Jules, J. Fatome, C. Fortier, I. Skripatchev, Y. Messaddeq, J. Troles, L. Brilland, W. Gao, T. Suzuki, Y. Ohishi and F. Smektala, "Microstructured chalcogenide optical fibres from $As_2S_3$ glass: towards new IR broadband sources," *Opt. Exp.*, vol. 18, p. 26655–26665, 2010.

[52] J. H. V. Price, T. M. Monro, H. Ebendorff-Heidepriem, F. Poletti, P. Horak, V. Finazzi, J. Y. Y. Leong, P. Petropoulos, J. C. Flanagan, G. Brambilla, X. Feng and D. J. Richardson, "Mid-IR supercontinuum generation from nonsilica microstructured optical fibres," *IEEE J. Sel. Top. in Quan. Elect.*, vol. 13, p. 738–749, 2007.

[53] M. R. E. Lamont, B. Luther-Davies, D. Y. Choi, S. Madden and B. J. Eggleton, "Supercontinuum generation in dispersion engineered highly nonlinear ($\gamma$ = 10 /W/m) $As_2S_3$ chalcogenide planar waveguide," *Opt. Exp.*, vol. 16, no. 19, p. 14938–14944, 2008.

[54] J. Lagsgaard, "Mode profile dispersion in the generalised nonlinear Schrödinger equation," *Opt. Exp.*, vol. 15, p. 16110–16123, 2007.

[55] K. Okamoto, Fundamentals of Optical Waveguides 2nd ed., Academic press, Elsevier, 2006.

[56] F. Benabid, J. C. Knight, G. Antonopoulos and P. S. J. Russell, "Stimulated Raman scattering in hydrogen-filled hollow-core photonic crystal fibre," *Science*, vol. 298, no. 5592, p. 399–402, 2002.

[57] J. D. Joannopoulos, R. D. Meade and J. N. Winn, Photonic Crystals: Molding the Flow of Light, New Jersey: Princeton University Press, Princeton, 1995.

[58] R. E. Kristiansen, "Guiding Light with Holey Fibers," Spie's OE Magazine, 2002.

[59] S. G. Johnson and J. D. Joannopoulos, "Block-iterative frequency-domain methods for Maxwell's equations in a planewave basis," *Optics Express*, vol. 8, no. 3, pp. 173-190, 2001.

[60] B. Cowan, "FDTD modeling of photonic crystal fibers," ARDB Technical Notes Volume 4, California, 2003.

[61] A. Taflove and S. C. Hagness, "Computational Electrodynamics: The Finite-Difference Time-Domain Method, 2nd ed.," Artech House, London, 2000.

[62] T. E. Murphy, Simulation software split-step Fourier propagation software (SSPROP), Washington D.C: University of Maryland, 2006.

[63] P. L. Francois, "Nonlinear propagation of ultrashort pulses in optica lfibres: total field formulation in the frequency domain," *J. Opt. Soc. Am. B,* vol. 8, no. 2, pp. 276-293, 1996.

[64] I. Cristiani, R. Tediosi, L. Tartara and V. Degiorgio, "Dispersive wave generation by solitons in microstructured optical fibres," *Opt. Exp.*, vol. 78, pp. 124-135, 2003.

[65] G. H. Weiss and A. A. Maradudin, "The Baker-Hausdorff formula anda problem in crystal physics," *J. Math. Phys.*, vol. 3, pp. 771-777, 1962.

[66] J. A. Fleck, J. R. Morris and M. D. Feit, "Time-dependent propagation of high energy laser beams through the atmosphere," *Appl. Phys. A,* vol. 10, pp. 129-160, 1976.

[67] N. Bloembergen, "Nonlinear optics: Past, present, and future," *IEEE J. Sel. Top. Quantum Electron.*, vol. 6, pp. 876-880, 2000.

[68] R. R. Alfano and S. L. Shapiro, "Observation of self-phase modulation and small-scale filaments in crystals and glasses," *Phys. Rev. Lett.*, vol. 24, no. 11, pp. 592-594, 1970.

[69] J. C. Knight, "Photonic crystal fibres," *Nature*, vol. 424, pp. 847-851, 2003.

[70] J. T. Manassah, P. P. Ho, A. Katz and R. R. Alfano, "Ultrafast supercontinuum laser source," *Photonics Spectra*, vol. 18, pp. 53-59, 1984.

[71] W. Werncke, A. Lau, M. Pfeiffer, K. Lenz, H. J. Weigmann and C. D. Thuy, "An anomalous frequency broadening in water," *Opt. Commun.,* vol. 4, pp. 413-415, 1972.

[72] N. Bloembergen, "The influence of electron plasma formation on superbroadening in light filaments," *Opt. Commun.,* vol. 8, pp. 285-288, 1973.

[73] R. L. Fork, C. V. Shank, C. Hirlimann, R. Yen and W. J. Tomlinson, "Femtosecond white-light continuum pulses," *Opt. Lett.,* vol. 8, pp. 1-3, 1983.

[74] A. L. Gaeta, "Catastrophic collapse of ultrashort pulses," *Phys. Rev. Lett.,* vol. 84, pp. 3582-3585, 2000.

[75] N. Akozbek, M. Scalora, C. M. Bowden and S. L. Chin, "White light continuum generation and filamentation during the propagation of ultra-short laser pulses in air," *Opt. Commun.,* vol. 191, pp. 353-362, 2001.

[76] A. Brodeur and S. L. Chin, "Band-gap dependence of the ultrafast white-light continuum," *Phys. Rev. Lett.,* vol. 80, pp. 4406-4409, 1998.

[77] C. Lin and R. H. Stolen, "New nanosecond continuum for excited-state spectroscopy," *Appl. Phys. Lett.,* vol. 28, pp. 216-218, 1976.

[78] P. L. Baldeck and R. R. Alfano, "Intensity effects on the stimulated four photon spectra generated by picosecond pulses in optical fibers," *J. Lightwave Technol.,* vol. 5, pp. 1712-1715, 1987.

[79] B. Gross and J. T. Manassah, "Supercontinuum in the anomalous group velocity dispersion region," *J. Opt. Soc. Am. B,* vol. 9, pp. 1813-1818, 1992.

[80] P. Beaud, W. Hodel, B. Zysset and H. P. Weber, "Ultrashort pulse propagation, pulse breakup, and fundamental soliton formation in a single-mode optical fiber," *IEEE J. Quantum Electron.,* vol. 23, pp. 1938-1946, 1987.

[81] M. N. Islam, G. Sucha, I. Bar-Joseph, M. Wegener, J. P. Gordon and D. S. Chemla, "Femtosecond distributed soliton spectrum in fibers," *J. Opt. Soc. Am. B,* vol. 6, pp. 1149-1158, 1989.

[82] I. Ilev, H. Kumagai, K. Toyoda and I. Koprinkov, "Highly efficient wideband

continuum generation in a single-mode optical fiber by powerful broadband laser pumping," *Appl. Opt.*, vol. 35, pp. 2548-2553, 1996.

[83] T. Morioka, K. Mori and M. Saruwatari, "More than 100-wavelength channel picosecond optical pulse generation from single laser source using supercontinuum in optical fibres," *Electron. Lett.*, vol. 29, pp. 862-864, 1993.

[84] T. Morioka, K. Mori, S. Kawanishi and M. Saruwatari, "Multi-WDM channel, Gbit/s pulse generation from a single laser source utilizing LD-pumped supercontinuum in optical fibers," *IEEE Photon. Technol. Lett.*, vol. 6, pp. 365-368, 1994.

[85] T. Morioka, K. Uchiyama, S. Kawanishi, S. Suzuki and M. Saruwatari, "Multiwavelength picosecond pulse source with low jitter and high optical frequency stability based on 200 nm supercontinuum filtering," *Electron. Lett.*, vol. 31, pp. 1064-1066, 1995.

[86] S. Kawanishi, H. Takara, K. Uchiyama, I. Shake, O. Kamatani and H. Takahashi, "1.4 Tbit/s (200 Gbit/s × 7 ch) 50 km optical transmission experiment," *Electron. Lett.*, vol. 33, pp. 1716-1717, 1997.

[87] E. A. Golovchenko, P. V. Mamyshev, A. N. Pilipetskii and E. M. Dianov, "Mutual influence of the parametric effects and stimulated Raman scattering in optical fibers," *IEEE J. Quantum Electron.*, vol. 26, pp. 1815-1820, 1990.

[88] T. A. Birks, J. C. Knight and P. S. J. Russell, "Endlessly single-mode photonic crystal fiber," *Opt. Lett.*, vol. 22, pp. 961-963, 1997.

[89] G. Genty, M. Lehtonen, H. Ludvigsen, J. Broeng and M. Kaivola, "Spectral broadening of femtosecond pulses into continuum radiation in microstructured fibers," *Opt. Exp.*, vol. 10, pp. 1083-1098, 2002.

[90] J. H. V. Price, W. Belardi, T. M. Monro, A. Malinowski, A. Piper and D. J. Richardson, "Soliton transmission and supercontinuum generation in holey fiber, using a diode pumped Ytterbium fiber source," *Opt. Exp.*, vol. 10, pp. 382-387, 2002.

[91] J. M. Harbold, F. O. Ilday, F. W. Wise, T. A. Birks, W. J. Wadsworth and Z.

Chen, "Long-wavelength continuum generation about the second dispersion zero of a tapered fiber," *Opt. Lett.,* vol. 27, pp. 1558-1560, 2002.

[92] A. Ortigosa-Blanch, J. C. Knight and P. S. J. Russell, "Pulse breaking and supercontinuum generation with 200-fs pump pulses in photonic crystal fibers," *J. Opt. Soc. Am. B,* vol. 19, pp. 2567-2572, 2002.

[93] J. W. Nicholson, M. F. Yan, P. Wisk, J. Fleming, F. DiMarcello, E. Monberg, A. Yablon, C. Jorgensen and T. Veng, "All-fiber, octave spanning supercontinuum," *Opt. Lett.,* vol. 28, pp. 643-645, 2003.

[94] J. Takayanagi, N. Nishizawa, H. Nagai, M. Yoshida and T. Goto, "Generation of high-power femtosecond pulse and octave-spanning ultrabroad supercontinuum using all-fiber system," *IEEE Photon. Technol. Lett.,* vol. 17, no. 1, pp. 37-39, 2005.

[95] I. W. Hsieh, X. G. Chen, X. P. Liu, J. I. Dadap, N. C. Panoiu, C. Y. Chou, F. N. Xia, W. M. Green, Y. A. Vlasov and R. M. Osgood, "Supercontinuum generation in silicon photonic wires," *Opt. Exp.,* vol. 15, no. 23, pp. 15242-15249, 2007.

[96] C. Xia, M. Kumar, M. Y. Cheng, R. S. Hegde, M. N. Islam, A. Galvanauskas, H. G. Winful, F. L. Terry, M. J. Freeman, M. Poulain and G. Maze, "Power scalable mid-infrared supercontinuum generation in ZBLAN fluoride fibers with up to 1.3 watts time-averaged power," *Opt. Exp.,* vol. 15, pp. 865-871, 2007.

[97] H. Hundertmark, D. Kracht, D. Wandt, C. Fallnich, V. V. R. K. Kumar, A. K. George, J. C. Knight and P. S. J. Russel, "Supercontinuum generation with 200 pJ laser pulses in an extruded SF6 fiber at 1560 nm," *Opt. Exp.,* vol. 11, pp. 3196-3201, 2003.

[98] F. G. Omenetto, N. A. Wolchover, M. R. Wehner, M. Ross, A. Efimov, A. J. Taylor, V. V. Kumar, A. K. George, J. C. Knight, N. Y. Joly and P. S. Russell, "Spectrally smooth supercontinuum from 350 nm to 3 μm in subcentimeter lengths of soft-glass photonic crystal fibers," *Opt. Exp.,* vol. 14, no. 2006, pp. 4928-4934, 2006.

[99] C. Xia, M. Kumar, O. P. Kulkarni, M. N. Islam, F. L. Terry, M. J. Freeman, M.

Poulain and G. Mazé, "Mid-infrared supercontinuum generation to 4.5 μm in ZBLAN fluoride fibers by nanosecond diode pumping," *Opt. Lett.,* vol. 31, no. 17, p. 2553–2555, 2006.

[100] G. Qin, X. Yan, C. Kito, M. Liao, C. Chaudhari, T. Suzuki and Y. Ohishi, "Ultrabroadband supercontinuum generation from ultraviolet to 6.28 μm in a fluoride fiber," *Appl. Phys. Lett.,* vol. 95, no. 16, p. 161103, 2009.

[101] P. Domachuk, N. A. Wolchover, M. Cronin-Golomb, A. Wang, A. K. George, C. M. B. Cordeiro, J. C. Knight and F. G. Omenetto, "Over 4000 nm bandwidth of Mid-IR supercontinuum generation in subcentimeter segments of highly nonlinear tellurite PCFs," *Opt. Exp.,* vol. 16, pp. 7161-7168, 2008.

[102] X. Feng, W. H. Loh, J. C. Flanagan, A. Camerlingo, S. Dasgupta, P. Petropoulos, P. Horak, K. E. Frampt, N. M. White, J. H. V. Price, H. N. Rutt and D. J. Richardson, "Single mode tellurite glass holey fiber with extremely large mode area for infrared nonlinear applications," *Opt. Exp.,* vol. 16, p. 13651, 2008.

[103] M. Liao, C. Chaudhari, G. Qin, X. Yan, T. Suzuki and Y. Ohishi, "Tellurite microstructure fibers with small hexagonal core for supercontinuum generation," *Opt. Exp.,* vol. 17, no. 14, p. 12174–12182, 2009.

[104] M. Tiwari and V. Janyani, "Two-Octave Spanning Supercontinuum in a Soft Glass Photonic Crystal Fiber Suitable for 1.55 μm Pumping," *J. of Lightwave Tech.,* vol. 29, no. 23, pp. 3560-3565, 2011.

[105] A. Agrawal, M. Tiwari, Y. O. Azabi, V. Janyani, B. M. A. Rahman and K. T. V. Grattan, "Ultrabroad Supercontinuum Generation in Tellurite Equiangular Spiral Photonic Crystal Fiber," *J. of Mod. Opti.,* vol. 60, no. 12, pp. 956-962, 2013.

[106] M. Sharma and S. Konar, "Broadband supercontinuum generation in lead silicate photonic crystal fibers employing optical pulses of 50 W peak power," *Opt. Comm.,* vol. 380, pp. 310-319, 2016.

[107] J. S. Sanghera, L. B. Shaw, L. E. Busse, V. Q. Nguyen, P. C. Pureza, B. C. Cole, B. B. Harbison, I. D. Aggarwal, R. Mossadegh, F. Kung, D. Talley, D. Roselle and R. Miklos, "Development and infrared applications of chalcogenide glass

optical fibers," *Fiber and Integrated Optics*, vol. 19, pp. 251-274, 2000.

[108] M. R. Karim, B. M. A. Rahman and G. P. Agrawal, "Dispersion engineered $Ge_{11.5}As_{24}Se_{64.5}$ nanowire for supercontinuum generation: A parametric study," *Opt. Exp.*, vol. 22, no. 25, p. 31029–31040, 2014.

[109] R. E. Slusher, G. Lenz, J. Hodelin, J. Sanghera, L. B. Shaw and I. D. Aggarwal, "Large Raman gain and nonlinear phase shifts in high purity $As_2Se_3$ chalcogenide fibers," *J. of Opt. Soc. of Am. B*, vol. 21, pp. 1146-1155, 2004.

[110] S. J. Madden, D. Y. Choi, D. A. Bulla, A. V. Rode, B. Luther-Davies, V. G. Ta'eed, M. D. Pelusi and B. J. Eggleton, "Long, low loss etched As2S3 chalcogenide for all-optical signal regeneration," *Opt. Exp.*, vol. 15, no. 22, pp. 14414-14421, 2007.

[111] L. B. Shaw, R. R. Gattass, J. S. Sanghera and I. D. Aggarwal, "All fiber mid-IR supercontinuum source from 1.5 to 5 μm," *Proc. SPIE,* vol. 7914, no. 79140P, pp. 1-5, 2011.

[112] J. Fatome, C. Fortier, T. N. Nguyen, T. Chartier, F. Smektala, K. Messaad, B. Kibler, S. Pitois, G. Gadret, C. Finot, J. Troles, F. Desevedavy, P. Houizot, G. Renversez, L. Brilland and N. Traynor, "Linear and nonlinear characterizations of chalcogenide photonic crystal fibres," *J. Lightwave Technol.*, vol. 27, no. 11, pp. 1707-1715, 2009.

[113] X. Gai, D. Choi, S. Madden, Z. Yang, R. Wang and B. Luther-Devies, "Supercontinuum generation in the mid-infrared from a dispersion engineered $As_2S_3$ glass rib waveguide," *Opt. Lett.*, vol. 37, no. 18, pp. 3870-3872, 2012.

[114] Y. Yu, B. Zhang, X. Gai, P. Ma, D. Choi, Z. Yang, R. Wang, S. Debbarma, S. J. Madden and B. Luther-Davies, "A broadband, quasicontinuous, mid-infrared supercontinuum generated in a chalcogenide glass waveguide," *Laser Photonics Rev.*, pp. 1-7, 2014.

[115] N. Granzow, M. Schmidt, W. Chang, L. Wang, Q. Coulombier, J. Troles, P. Toupin, I. Hartl, K. F. Lee, M. E. Fermann, L. Wondraczek and P. S. J. Russell, "Mid-infrared supercontinuum generation in $As_2S_3$ "nano-spike" step index

waveguide," *Opt. Exp.*, vol. 21, no. 9, pp. 10969-10977, 2013.

[116] W. Gao, M. E. Amraoui, M. Liao, H. Kawashima, Z. Duan, D. Deng, T. Cheng, T. Suzuki, Y. Messaddeq and Y. Ohishi, "Mid-infrared supecontinuum generation in a suspended-core $As_2S_3$ chalcogenide microstructured optical fibre," *Opt. Exp.*, vol. 21, no. 8, pp. 9573-9583, 2013.

[117] R. J. Weiblen, A. Docherty, J. Hu and C. R. Menyuk, "Calculation of the expected bandwidth for a mid-infrared supercontinuum source based on As2S3 chalcogenide photonic crystal fibres," *Opt. Exp.*, vol. 18, no. 25, pp. 26666-26674, 2010.

[118] C. Wei, X. Zhu, R. A. Norwood, F. Seng and N. Peyghambarian, "Numerical investigation on high power mid-infrared supercontinuum fibre lasers pumped at 3 μm," *Opt. Exp.*, vol. 21, no. 24, pp. 29488-29504, 2013.

[119] I. Kubat, C. R. Petersen, U. V. Mfller, A. B. Seddon, T. M. Benson, L. Brilland, D. Mechin, P. M. Moselund and O. Bang, "Thulium pumped mid-infrared 0.9-9 μm supercontinuum generation in concatenated fluoride and chalcogenide glass fibres," *Opt. Exp.*, vol. 22, no. 4, pp. 3959-3967, 2014.

[120] C. R. Petersen, U. Mfller, I. Kubat, B. Zhou, S. Dupont, J. Ramsay, T. Benson, S. Sujecki, M. Abdel-Moneim, Z. Tang, D. Furniss, A. Seddon and O. Bang, "Mid-infrared supercontinuum covering the 1.4-13.3 μm molecular fingerprint region using ultra-high NA chalcogenide step-index fibre," *Nat. Photonics*, vol. 8, pp. 830-834, 2014.

[121] U. Miller, Y. Yu, I. Kubat, C. R. Petersen, X. Gai, L. Brilland, D. Mechin, C. Caillaud, J. Troles, B. Luther-Davies and O. Bang, "Mult-imilliwatt mid-infrared supercontinuum generation in a suspended core chalcogenide fibre," *Opt. Exp.*, vol. 23, no. 3, pp. 3282-3291, 2015.

[122] A. Marandi, C. W. Rudy, V. G. Plotnichenko, E. M. Dianov, K. L. Vodopyanov and R. L. Byer, "Mid-infrared supercontinuum generation in tapered chalcogenide fiber for producing octave spanning frequency comb around 3 μm," *Opt. Exp.*, vol. 20, no. 22, pp. 24218-24225, 2012.

[123] I. Savelii, O. Mouawad, J. Fatome, B. Kibler, F. Desevedavy, G. Gadret, J. C.

Jules, P. Y. Bony, H. Kawashima, W. Gao, T. Kohoutek, T. Suzuki, Y. Ohishi and F. Smektala, "Mid-infrared 2000-nm bandwidth supercontinuum generation in suspended-core microstructured Sulphide and Tellurite optical fibres," *Opt. Exp.*, vol. 20, no. 24, pp. 27083-27093, 2012.

[124] I. Kubat, C. S. Agger, U. Moller, A. B. Seddon, Z. Tang, S. Sujecki, T. M. Benson, D. Furniss, S. Lamarini, K. Scholle, P. Fuhrberg, B. Napier, M. Farries, J. Ward, P. M. Moselund and O. Bang, "Mid-infrared supercontinuum generation to 12.5 μm in large NA chalcogenide step index fibres pumped at 4.5 μm," *Opt. Exp.*, vol. 22, no. 16, pp. 19169-19182, 2014.

[125] A. Al-Kadry, M. E. Amraoui, Y. Messaddeq and M. Rochette, "Two octaves mid-infrared supercontinuum generation in $As_2Se_3$ microwires," *Opt. Exp.*, vol. 22, no. 25, pp. 31131-31137, 2014.

[126] Y. Yu, X. Gai, T. Wang, P. Ma, R. Wang, Z. Yang, D. Choi, S. Madden and B. Luther-Davies, "Mid-infrared supercontinuum generation in chalcogenides," *Opt. Mater. Exp.*, vol. 3, no. 8, pp. 1075-1086, 2013.

[127] A. B. Salem, R. Cherif and M. Zghal, "Development Tapered As2S3 chalcogenide photonic crystal fiber for broadband mid-infrared supercontinuum generation," *Frontiers in Optics 2011/Laser Science XXVII OSA Technical Digest (Optical Society of America)*, p. FMG6, 2011.

[128] Y. Yu, X. Gai, C. Zhai, S. Qi, W. Guo, Z. Yang, R. Wang, D. Choi, S. Madden and B. Luther-Davies, "1.8-10 μm mid-infrared supercontinuum generation in a step-index chalcogenide fiber using low peak pump power," *Opt. Lett.*, vol. 40, no. 6, pp. 1081-1084, 2015.

[129] P. S. Maji and P. R.Chaudhuri, "Design of all-normal dispersion based on multi-material photonic crystal fiber in IR region for broadband supercontinuum generation," *Applied Optics*, vol. 54, no. 13, pp. 4042-4048, 2015.

[130] M. R. Karim, B. M. A. Rahman, Y. O. Azabi, A. Agrawal and G. P. Agrawal, "Ultrabroadband mid-infrared supercontinuum generation through dispersion engineering of chalcogenide microstructured fibers," *J. of the Opti. Soc. of Ame. B*, vol. 32, no. 11, pp. 2343-2351, 2015.

[131] B. J. Eggleton, B. L. Davies, K. Richardson, "Chalcogenide photonics," *Nat. Photonics,* vol. 5, pp. 141-148, 2011.

[132] A. Prasad, C. J. Zha, R. P. Wang, A. Smith, S. Madden and B. Luther-Davies, "Properties of $Ge_xAs_ySe_{1-x-y}$ glasses for all-optical signal processing," *Opt. Exp.,* vol. 16, no. 4, p. 2804–2815, 2008.

[133] J. C. Phillips, "Topology of covalent non-crystalline solids I: short range order in chalcogenide alloys," *J. Non-Cryst. Solids,* vol. 34, no. 2, pp. 153-181, 1979.

[134] K. Tanaka, "Structural phase transitions in chalcogenide glasses," *Phys. Rev. B Condens. Matter,* vol. 39, no. 2, pp. 1270-1279, 1989.

[135] M. F. Thorpe, "Continuous deformations in random networks," *J. Non-Cryst. Solids,* vol. 57, no. 3, pp. 355-370, 1983.

[136] P. Boolchand, D. G. Georgiev and a. B. Goodman, "Discovery of the intermediate phase in chalcogenide glasses," *J. Optoelect Mat.,* vol. 3, no. 3, pp. 70-720, 2001.

[137] D. A. P. Bulla, R. P. Wang, A. Prasad, A. V. Rode, S. J. Madden and B. Luther-Davies, "On the properties and stability of thermally evaporated Ge-As-Se thin films," *Appl. Phys., A Mater. Sci. Process.,* vol. 96, no. 3, pp. 615-625, 2009.

[138] F. X. Kärtner, D. J. Dougherty, H. A. Haus and E. P. Ippen, "Raman noise and soliton squeezing," *J. of the Opti. Soc. of Ame. B,* vol. 11, no. 7, pp. 1267-1276, 1994.

[139] M. Spurny, "Photonic Crystal Waveguides in Chalcogenide Glasses (Ph.D. Thesis)," University of St. Andrews, United Kingdom, 2011.

[140] X. Gai, R. P. Wang, C. Xiong, M. J. Steel, B. J. Eggleton and B. Luther-Davies, "Near-zero anomalous dispersion $Ge_{11.5}As_{24}Se_{64.5}$ glass nanowires for correlated photon pair generation: design and analysis," *Optics Express,* vol. 20, no. 2, pp. 776-786, 2012.

[141] W. Yuan, "2–10 μm mid-infrared supercontinuum generation in $As_2Se_3$ photonic crystal fiber," *Laser Phys. Lett.,* vol. 10, no. 9, p. 095107, 2013.

[142] V. V. R. K. Kumar, A. K. George, W. H. Reeves, J. C. Knight, P. S. J. Russell,

F. Omenetto and A. J. Taylor, "Extruded soft glass photonic crystal fiber for ultrabroad supercontinuum generation," *Optics Express,* vol. 10, no. 25, pp. 1520-1525, 2002.

[143] H. Ebendorff-Heidepriem, P. Petropoulos, S. Asimakis, V. Finazzi, R. Moore, K. Frampton, F. Koizumi, D. Richardson and T. Monro, "Bismuth glass holey fibers with high nonlinearity," *Optics Express,* vol. 12, no. 21, pp. 5082-5087, 2004.

[144] V. V. R. K. Kumar, A. K. George, J. C. Knight and P. S. J. Russell, "Tellurite photonic crystal fiber," *Optics Express,* vol. 11, no. 20, pp. 2641-2645, 2003.

[145] T. M. Monro, Y. D. West, D. W. Hewak, N. G. R. Broderick and D. J. Richards, "Chalcogenide holey fibers," *Electronics Letters,* vol. 36, no. 24, pp. 1998-2000, 2000.

[146] P. Sakunasinha, S. Suwanarat and S. Chiangga, "Mid-infrared supercontinuum in a $Ge_{11.5}As_{24}Se_{64.5}$ chalcogenide waveguide," in *Proc. of SPIE Vol. 9659*, Thailand, 2015.

[147] M. Sharma and S. Konar, "Three octave spanning supercontinuum by red-shifted dispersive wave in photonic crystal fibers," *J. Mod. Opt.*, vol. 63, no. 5, pp. 501-510, 2015.

[148] B. Zhang, W. Guo, Y. Yu, C. Zhai, S. Qi, A. Yang, L. Li, Z. Yang, R. Wang, D. Tang, G. Tao and B. L. Davies, "Low Loss, High NA Chalcogenide Glass Fibers for Broadband Mid-Infrared Supercontinuum Generation," *J. Am. Ceram. Soc.*, vol. 98, no. 5, pp. 1389-1392, 2015.

[149] A. Hartung, A. M. Heidt and a. H. Bartelt, "Design of all-normal dispersion microstructured optical fibers for pulse-preserving supercontinuum generation," *Opt. Express*, vol. 19, no. 8, pp. 7742-7749, 2011.

[150] A. Thai, M. Hemmer, P. K. Bates, O. Chalus and J. Biegert, "3Sub-250-mrad, passively carrier–envelope-phase-stable mid-infrared OPCPA source at high repetition rate," *Opt. Letters,* vol. 36, no. 19, pp. 3918-3920, 2011.

[151] F. Silva, D. R. Austin, A. Thai, M. Baudisch, M. Hemmer, D. Faccio, A.

Couairon and J. Biegert, "Multi-octave supercontinuum generation from mid-infrared filamentation in a bulk crystal," *Nature Communications,* vol. 3, no. 807, pp. 1-8, 2012.

[152] T. Yamashita and Y. Ohishi, "Cooperative energy transfer between Tb3+ and Yb3+ ions co-doped in borosilicate glass," *J. of Non-Crystalline Solids,* vol. 354, no. 17, pp. 1883-1890, 2008.

[153] G. Tao, S. Shabahang, E. H. Banaei, J. J. Kaufman and A. F. Abouraddy, "Multimaterial preform coextrusion for robust chalcogenide optical fibers and tapers," *Optics Letters,* vol. 37, no. 13, pp. 2751-2753, 2012.

[154] G. Tao, A. F. Abouraddy and A. M. Stolyarov, "Multimaterial fibres," *Int. J. Appl. Glass Sci,* vol. 3, no. 4, p. 349–368, 2012.

[155] F. Abouraddy, M. Bayindir, G. Benoit, S. D. Hart, K. Kuriki, N. Orf, O. Shapira, F. Sorin, B. Temelkuran and Y. Fink, "Towards multimaterial multifunctional fibres that see, hear, sense and communicate," *Nat. Mater.,* vol. 6, p. 336–347 , 2007.

[156] N. Da, L. Wondraczek, M. A. Schmidt, N. Granzow and P. S. J. Russell, "High index-contrast all-solid photonic crystal fibers by pressure-assisted melt infiltration of silica matrices," *J. Non-Cryst. Solids,* vol. 356, p. 1829–1836, 2010.

[157] N. Granzow, P. Uebel, M. A. Schmidt, A. S. Tverjanovich, L.Wondraczek and P. S. J. Russell, "Bandgap guidance in hybrid chalcogenide–silica photonic crystal fibers," *Opt. Lett.,* vol. 36, no. 13, pp. 2432-2434, 2011.

[158] C. Chaudhari, T. Suzuki and Y. Ohishi, "Design of zero chromatic dispersion chalcogenide $As_2S_3$ glass nanofibers," *J. Lightwave Technol,* vol. 27, p. 2095–2099 , 2009.

[159] D. W. Hewak, "The promise of chalcogenides," *Nat. Photonics* , vol. 5, p. 474, 2011.

[160] J. S. Sanghera, C. Florea, L. Busse, B. Shaw, F. Miklos and I. D. Aggarwal, "Reduced Fresnel losses in chalcogenide fibers by using anti-reflective surface

structures on fiber end faces," *Opt. Express*, vol. 18, p. 26760–26768 , 2010.

[161] F. Poletti, V. Finazzi, T. M. Monro, N. G. R. Broderick, V. Tse and D. J. Richardson, "Inverse design and fabrication tolerances of ultra flattened dispersion holey fibers," *Opt. Express*, vol. 13, p. 3728–3736, 2005.

[162] L. Isaenko, A. Yelisseyev, S. Lobanov, A. Titov, V. Petrov, J. J. Zondy, P. Krinitsin, A. Merkulov, V. Vedenyapin and J. Smirnova, "Growth and properties of $LiGaX_2$ (X = S, Se, Te) single crystals for nonlinear optical applications in the mid-IR," *Cryst. Res. Technol.* , vol. 38, no. 3-5, p. 379–387, 2003.

[163] V. Vedenyapin, L. Isaenko, A. Yelisseyev, S. Lobanov, A. Tyazhev, G. Marchev and V. Petrov, "New mixed $LiGa_{0.5}In_{0.5}Se_2$ nonlinear crystal for the mid-IR," *Proc. of SPIE*, vol. 7917, pp. 1-8, 2011.

# Appendix-I

## Matlab code for supercontinuum generation

Code for SCG using split-step (Fourier) method

```
clc;
clear all;
close all;
% initial parameters
n = 2^13;                % number of samples
tw = 18.5;               % width of time window
cc = 2.99792458*1e8/1e12;     % light speed [nm/ps]
wavelength = 3100;          % centre wavelength [nm]
w0 = (2.0*pi*cc)/wavelength; % centre frequency [2*pi*THz]
T = linspace (-twidth/2, twidth/2, n); % time grid
% === input pulse
power = 30000;             %  input peak power [W]
t0 = 0.0284;               % input pulse duration [ps]
A = sqrt (power)*sech (T/t0); % input field
% === fibre parameters
flength = 0.1;             % of  fibre length [m]
% Taylor series expansion coefficient [ps^2/m, ps^3/m ...]
betas = [-14.714e-3, 9.3486e-5, -12.6961e-8, 3.0737e-10, ...
       -8.3943e-13, 2.1038e-15, -3.5250e-18, 5.0524e-21, ...
       -6.8300e-24];
gamma = 2474;              % nonlinear coefficient [1/W/m]
loss = 0.68;               % loss [dB/m]
% === Raman response
fr = 0.031;                % fraction f_r by the Kramers–Kroning relation
t1 = 15.5; t2 = 230.5;
RR = (t1^2+tu2^2)/t1/t2^2*exp(-T/t2).*sin(T/t1);
RR(T<0) = 0;         % step function
```

```
%RR = RR/trapz(T,RR);  % normalise RR to unit integral
% === parameters for simulation
nsaves = 600;     % length steps number to save field at
% wave propagating field
[Z, AW, AT, W] = gnl(T, A, w0, betas, gamma, loss, ...
                    fr, RR, length, nsaves);
% === output
figure();
IW = 10*log10 (abs(AW).^2); % spectral intensity
mlIW = max(max(IW));       % max value for scaling
WL = 2*pi*cc/W; iis = (WL>15000 & WL<500); % wavelength grid
subplot(1,2,2);
pcolor(WL(iis), Z, IW(:,iis)); % pseudocolor map
caxis([mIW-40.0, mIW]);  xlim([500,15000]); shading interp;
xlabel('Wavelength / nm'); ylabel('Distance / m');

IT = 10*log10(abs(AT).^2); % temporal intensity
mIT = max(max(IT));       % max value, for scaling plot
subplot(1,2,1);
pcolor(T, Z, IT);          % pseudocolor map
caxis([mIT-40.0, mIT]);  xlim([-3,13]); shading interp;
ylabel('Distance / m') ; xlabel('Delay / ps');
```

# Appendix-II

## Matlab code for Taylor series expansion coefficient (Beta: 2,3,4……)

```
clc;
clear all;
close all;
% lambda2=[1:0.275:10]
lambda1=[1:0.2:10].*10^-6
c=3*10^8;
D=[-1181.213,-1094.882,-816.5024,-476.0627,-291.9144,-195.8021,-136.5403,-
77.40355,-45,-
20,5,20,36,42,47.77055,51.86922,54.6378,56.59749,57.73161,58.14022,58.061,57.34
801,56.28894,54.87129,53.08256,51.28548,48.8588,46.03185,45,44,42,40,38,36,34,3
2,28,25,22,20,15,10,2,-4,-12,-17]*10^-6;
w=2*pi*c./lambda1;
B2=-((D.*(lambda1.^2))./(2*pi*c))*10^24;
B3=diff(B2)./diff(w);
n=length(B2);
B3=[B3 zeros(1,n-length(B3))];
B4=diff(B3)./diff(w);
B4=[B4 zeros(1,n-length(B4))];
B5=diff(B4)./diff(w);
B5=[B5 zeros(1,n-length(B5))];
B6=diff(B5)./diff(w);
B6=[B6 zeros(1,n-length(B6))];
B7=diff(B6)./diff(w);
B7=[B7 zeros(1,n-length(B7))];
B8=diff(B7)./diff(w);
B8=[B8 zeros(1,n-length(B8))];
B9=diff(B8)./diff(w);
B9=[B9 zeros(1,n-length(B9))];
B10=diff(B9)./diff(w);
```

```
B10=[B10 zeros(1,n-length(B10))];
figure
plot(lambda1,D,'r-')
figure
plot(lambda1,B2,'k-')
figure
plot(lambda1,B3)
figure
plot(lambda1,B4)
figure
plot(lambda1,B5)
figure
plot(lambda1,B6)
figure
plot(lambda1,B7)
figure
plot(lambda1,B8)
figure
plot(lambda1,B9)
figure
plot(lambda1,B10)
 % B22=-(D.*(lambda2.^2))./(2*pi*c)
% B32=diff(B22)./diff(lambda2)
% B42=diff(B22,2)./diff(lambda2,2)
```